

**EXPERIMENTAL AND COMPUTATIONAL  
INVESTIGATION OF TRANSPORT PHENOMENA  
IN INITIATED CHEMICAL VAPOR DEPOSITION  
(iCVD) PROCESS**

**A Thesis Submitted to  
The Graduate School of Engineering and Sciences of  
Izmir Institute of Technology  
In Partial Fulfillment of the Requirements for the Degree of**

**DOCTOR OF PHILOSOPHY**

**in Chemical Engineering**

**by  
Selcan ATEŞ**

**December 2017  
İZMİR**

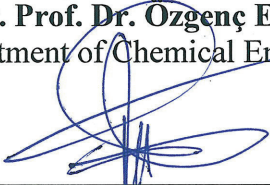
We approve the thesis of Selcan ATEŞ

**Examining Committee Members:**

---

**Assist. Prof. Dr. Özgeç EBİL**

Department of Chemical Engineering, İzmir Institute of Technology



---


**Prof. Dr. Mustafa M. DEMİR**

Department of Material Science and Engineering, İzmir Institute of Technology

---

**Prof. Dr. Mustafa DEMİRCİOĞLU**

Department of Chemical Engineering, Ege University



---

**Assoc. Prof. Dr. Güler NARİN**

Department of Chemical Engineering, Uşak University



---

**Assist. Prof. Dr. Ayben TOP**

Department of Chemical Engineering, İzmir Institute of Technology

**25 December 2017**

---

**Assist. Prof. Dr. Özgeç EBİL**

Supervisor, Department of Chemical Engineering, İzmir Institute of Technology

---

**Prof. Dr. Erol ŞEKER**

Head of the Department of Chemical Engineering

---

**Prof. Dr. Aysun SOFUOĞLU**

Dean of Graduate School of Engineering and Sciences

## ACKNOWLEDGEMENTS

It has been almost ten years in IZTECH although sometimes I feel like it was just yesterday. Through the years, I have met many people who influence me with their thoughts and behavior, and the time that I shared with them was a great experience for me that it makes a huge contribution to my personal development. During this journey, one of them is my advisor, Dr. Özgenç Ebil, who makes me feel free about the research and encourage me to do my best. He was always kind and thoughtful to me whenever I needed help, and his enthusiasm about sharing his knowledge, and experiences during his talks motivated me to look at things from new and different perspectives. Also, I would like to thank faculty members I've met in IZTECH for sharing open-minded ideas and helpful suggestions.

I am indebted to my friends; Gizem Cihanoğlu, Merve Özpirin, and Tuğçe İşler for their friendships, caring, and for sharing beautiful time during my doctorate study. Also, I would like to thank faculty stuffs; Ahmet Kurul, Ahmet Köken, and Nazil Karaca for their endless support in solving problems with the best options.

Whenever I have to struggle in difficult times, I know that they are always ready to share. So, I am indebted to my beautiful family, my mother Birsen Ateş and my father Yener Ateş, for their endless love and support. Nilüfer, Barış, and Neslihan; thank you all for your cares, suggestions and helps.

Lastly, I would like to express that all of those people, knowledge in years, opportunities, happiness, struggles, and tears in eyes are precious gifts from Allah, and all praise is to Allah, who let me to experience all these beautiful moments and who taught man that which he knew not.

## ABSTRACT

### EXPERIMENTAL AND COMPUTATIONAL INVESTIGATION OF TRANSPORT PHENOMENA IN INITIATED CHEMICAL VAPOR DEPOSITION (iCVD) PROCESS

As a polymer thin-film deposition technique, initiated CVD (iCVD) is a heterogeneous process involving gas phase precursors and solid film formation on a solid/liquid substrates at different temperature regions. Obtaining fine-tuned film properties over different substrate geometries at different process conditions is a challenging tasks and requires experimental trials. The major goal of this study is to develop a computational model which describes all relevant transport phenomena occurring in iCVD process, and which is capable to predict the polymer film thickness at different deposition conditions for flat and/or non-flat substrates in a 3D reactor geometry.

A Finite Element Analysis (FEA)-based 3D computational model, which can be applied to a variety number of iCVD reactor and substrate geometries, has been developed in the study. To validate the model, reported experimental conditions of 1H,1H,2H,2H-perfluorodecyl acrylate (PFDA) deposition with *t*-butyl peroxide (TBPO) initiator, and butyl acrylate (BA) deposition with *t*-amyl peroxide (TAPO) initiator, are applied to the model, respectively. The simulation results of both deposition processes show good agreement with experimental results reported in literature. Presented model successfully describes the relevant transport phenomena, and provides a priori predictions on polymerization rate, and film thickness on complex substrate geometries for a polymerization reaction with known kinetic data.

For further studies, presented model can be modified or used as an approach for modeling of other types of CVD systems as well as facilitating process scale-up. The model can also extract valuable polymerization kinetics data provided that a sufficient number of experiments are performed at a specified substrate temperature, and process parameters and measured final film thicknesses are entered to the model.



## ÖZET

### BAŞLATILMIŞ KİMYASAL BUHAR BİRİKTİRME PROSESİNDE TAŞINIM İŞLEMLERİNİN DENEYSEL VE HESAPLAMALI İNCELEMESİ

Polimer ince-film biriktirme tekniği olarak; başlatılmış KBB (iCVD) farklı sıcaklık bölgelerinde gaz fazında kimyasallar ve katı/sıvı alttaş üzerinde katı polimer üretimini içeren heterojen bir süreçtir. Farklı yüzey geometrilerinde ve proses koşullarında kontrollü bir şekilde film özellikleri elde etmek zorlayıcı ve deneysel çalışmalar gerektiren bir iştir. Bu çalışmanın temel amacı başlatılmış-KBB prosesinde gerçekleşen tüm taşınım işlemlerini tanımlayan ve farklı biriktirme koşullarında düz ve/veya düz olmayan alttaşlar için polimer film kalınlığını üç boyutlu reaktör geometrisinde tahmin etmeyi sağlayan hesaplamalı model geliştirmektir.

Bu çalışmada farklı iCVD reaktör ve alttaş geometrilerine uygulanabilir olan, Sonlu Elemanlar Metodu (SEM) tabanlı, 3 boyutlu hesaplamalı model geliştirilmiştir. Modeli doğrulamak amacıyla, sırasıyla; yayınlanmış 1H,1H,2H,2H-perfluorodecyl akrilat'ın (PFDA) *t*-butyl peroksit (TBPO) ile olan biriktirmesi, ve butyl akrilat'ın (BA) *t*-amyl peroksit (TAPO) ile olan biriktirmesinin deneysel koşulları modele uygulanmıştır. Her iki depozisyon prosesinin simülasyon sonuçları literatürde bildirilen deneysel sonuçlarla oldukça uyum göstermiştir. Sunulan model Başlatılmış-KBB (iCVD) sürecinde gerçekleşen taşınım işlemlerini başarılı bir şekilde açıklamaktadır ve kinetik verileri bilinen polimerizasyon reaksiyonları için kompleks alttaş üzerindeki polimerleşme hızının ve film kalınlık profilinin önceden belirlenebilmesine imkan sağlamaktadır.

İleriki çalışmalar için, sunulan model modifiye edilebilir ya da büyük prosesler için olanak sağlamanın yanı sıra diğer KBB (CVD) sistemlerinin modellenmesinde bir yöntem olarak kullanılabilir. Bu model ayrıca sabit alttaş sıcaklığında gerçekleştirilecek yeterli sayıda deneysel çalışmalar sonucu üretilen polimer filmlerin kalınlıklarının ölçülmesiyle oldukça değerli polimerizasyon kinetik verilerinin elde edilmesinde de kullanılabilir.

# TABLE OF CONTENTS

LIST OF FIGURES.....	viii
LIST OF TABLES.....	xi
CHAPTER 1. INTRODUCTION.....	1
1.1. Polymerization Methods.....	2
1.1. Initiated Chemical Vapor Deposition (iCVD) Process.....	4
1.2. Reaction Mechanism for iCVD.....	5
CHAPTER 2. LITERATURE REVIEW.....	10
2.1. Modeling Studies in CVD system.....	10
2.2. Effect of Process Parameters and Kinetics on Film Growth in iCVD...	12
2.3. Modeling Studies of iCVD process.....	15
2.4. Kinetic Studies for Determination of Polymerization Rate Constants...	16
CHAPTER 3. MODELING OF iCVD.....	18
3.1. Model Requirements for iCVD Process .....	18
3.2. Model Development.....	18
3.2.1. Model Simplifications and Transport Equations .....	20
3.2.2. Boundary Conditions .....	24
3.2.2.1. Fluid Flow Boundary Conditions.....	25
3.2.2.2. Energy Boundary Conditions.....	26
3.2.2.3. Mass Transport Boundary Conditions .....	27
3.2.2.4. Surface Polymerization Conditions .....	28
3.2.2.5. Properties of Gas Mixtures .....	30
3.3. Numerical Solution Methods for Solving of Model Equations .....	31
3.4. Implementation of the Model .....	32
3.4.1. Model Implementation in a Cylindrical Reactor Geometry .....	32

3.4.1.1. Poly (1H,1H,2H,2H-perfluorodecyl Acrylate) Deposition Modeling.....	33
3.4.1.2. n-Butyl Acrylate Deposition Modeling .....	36
3.4.2. Model Implementation in a Square Type Reactor Geometry .....	39
3.4.2.1. iCVD Process.....	41
CHAPTER 4. RESULTS AND DISCUSSION .....	43
4.1. Model Implementation in Cylindrical Type of Reactor Geometry.....	43
4.1.1. Model Validation for PFDA polymerization.....	44
4.1.2. Model Validation for nBA polymerization.....	57
4.2. Model Implementation in Square Type of Reactor Geometry.....	68
4.3. The Effect of Process Parameters on Deposition Rate and Film Uniformity .....	71
4.3.1. The Effect of $P_M/P_{sat}$ .....	71
4.3.2. The Effect of Reactor Pressure .....	72
4.3.3. The Effect of Initiator Type .....	74
4.3.4. The Effect of Filament Array.....	77
4.3.5. The Effect of Substrate Geometry .....	79
CHAPTER 5. CONCLUSION.....	82
REFERENCES .....	84
APPENDIX A. MODEL DETAILS.....	87

## LIST OF FIGURES

<u>Figure</u>	<u>Page</u>
Figure 1.1. Schematic representation of a typical iCVD system.....	5
Figure 3.1. Illustration of modeling approach .....	19
Figure 3.2. Cylindrical and square type iCVD reactor geometries used in the study .....	25
Figure 3.3. Representation of (a) front and (b) top view of cylindrical iCVD reactor geometry.....	33
Figure 3.4. Square type iCVD reactor geometry used in the study .....	39
Figure 3.5. Custom-built square type of iCVD reactor used for polymerization of nBA with TBPO initiator.....	42
Figure 4.1. Comparison of experimental and predicted deposition rates at $D_{ik}: 5e-5 \text{ m}^2/\text{s}$ with respect to $P_M/P_{sat.}$ with respect to $P_M/P_{sat.}$ .....	46
Figure 4.2. Predicted film deposition rate (nm/min) on substrate surface at process conditions of P4.....	48
Figure 4.3. Predicted deposition rates at midline of the substrate surface. ....	48
Figure 4.4. Predicted surface average rate of polymerization ( $R_p$ ), and deposition rate (DR) at process conditions given in Table 4.1.....	49
Figure 4.5. From top to bottom: surface monomer $[M]$ , active polymer $[M.]$ , and surface radical $[R.]$ concentrations at midline on substrate surface for all deposition conditions given in Table 4.1.....	50
Figure 4.6. Model prediction of velocity distribution (SI unit: m/s) for P2 inside iCVD reactor (top), and detailed view of velocity distribution at the midline of the reactor (bottom).....	52
Figure 4.7. Model prediction of temperature distribution (SI unit: K) for P2 in iCVD reactor (top), and detailed view of temperature distribution at the midline of the reactor (bottom).....	52
Figure 4.8. Predicted mole fraction variations of (a) monomer, (b) initiator, and (c) radical species along the flow direction for P2. ....	54
Figure 4.9. Representation of midline at a distance of 1.5 cm above the surface .....	55
Figure 4.10. Predicted mole fractions of the species through the midline at a distance of 1.5 cm above the surface for P1-P6.....	56

Figure 4.11. Comparison of reported and calculated deposition rates for nBA polymerization at different $P_M/P_{sat}$ .....	59
Figure 4.12. Model prediction of deposition rate (SI unit: nm/min) on substrate surface for B4.....	59
Figure 4.13. Predicted deposition rates for B1-B7 through at midline on substrate surface.....	60
Figure 4.14. Surface-averaged values of predicted $R_p$ and DR at different $F_M/F_{Total}$ for nBA polymerization.....	61
Figure 4.15. From top to bottom: adsorbed monomer concentration [M], polymer radical concentration, [M.], and primary radical concentration, [R.], on substrate surface for B1-B7 .....	62
Figure 4.16. (a) Velocity (SI unit: m/s), and (b) temperature (SI unit: K) profiles along the flow direction for B4 with bottom profiles representing the midline of the reactor geometry.....	63
Figure 4.17. Predicted mole fraction distributions of (a) monomer, (b) initiator, (c) radical, and (d) carrier gas along the flow direction for B4.....	65
Figure 4.18. Radical mole fraction distributions at midline for (a) B2 (b) B7.....	65
Figure 4.19. Predicted mole fractions of the species 1.5 cm above the substrate at the midline for deposition conditions listed in Table 4.3.....	67
Figure 4.20. Model prediction of film deposition rate (nm/min) on substrate surface for E3.....	69
Figure 4.21. From left to right, velocity (SI unit: m/s) and temperature (SI unit: K) profiles along flow direction for E3. ....	69
Figure 4.22. Predicted mole fractions of monomer (top), initiator (middle), and radical (bottom) species along the flow direction for E3.....	70
Figure 4.23. Comparison of experimentally measured and predicted deposition rates with respect to $P_M/P_{sat}$ . ....	72
Figure 4.24. Change of deposition rate in flow direction with respect to total pressure for B4.....	73
Figure 4.25. Partial pressures of monomer, initiator, radical, and argon through the midline 1 cm above the substrate surface .....	74
Figure 4.26. Mole fraction distributions of radical species when a) TAPO, and b) TBPO initiators are used.....	76

Figure 4.27. Species mole fractions 1.5 cm above the bottom surface of the reactor when a) TAPO b) TBPO initiators are used.....	76
Figure 4.28. Comparison of deposition rate for nBA polymerization with different initiator species.....	77
Figure 4.29. Predicted mole fraction variation of radical species for 14 filaments (top), 4 filaments (middle) and 1 filament (bottom).....	78
Figure 4.30. Comparison of deposition rates for nBA polymerization at different filament numbers.....	79
Figure 4.31. Three dimensional substrate geometries. a) rectangular shape b) ellipsoid shape.....	80
Figure 4.32. Deposition rates (nm/min) on substrates with (a) rectangular prism, and (b) ellipsoidal geometries showing uniform film thickness can be achieved for complex geometries.....	80

## LIST OF TABLES

<b><u>Table</u></b>	<b><u>Page</u></b>
Table 1.1. Thermally decomposing initiators and decomposition temperatures .....	3
Table 1.2. Free radical polymerization mechanism in iCVD process.....	6
Table 3.1. Selected parameters and variables for PFDA polymerization used in the model .....	34
Table 3.2. Flow rates of PFDA monomer at a fixed initiator flow rate of 0.82 sccm.....	35
Table 3.3. Kinetic parameters for PFDA polymerization at 44 °C .....	35
Table 3.4. Selected parameters and variables for nBA polymerization used in the model.....	37
Table 3.5. Monomer (BA), initiator (TAPO) and carrier gas flow rates for nBA polymerization.....	38
Table 3.6. Kinetic parameters for nBA polymerization at 23°C .....	38
Table 3.7. Selected parameters and variables for nBA polymerization with TBPO initiator.....	40
Table 3.8. Flow rates of monomer and initiator for nBA polymerization.....	41
Table 4.1. Reported process conditions and experimental deposition rates of PFDA polymerization in iCVD process at constant initiator flow rate of 0.82 sccm.....	44
Table 4.2. Comparison of experimental results of deposition rates with model predictions at different Maxwell-Stefan diffusivities .....	45
Table 4.3. Reported process conditions of nBA polymerization in iCVD process.....	57
Table 4.4. Comparison of experimentally found deposition rates with the model predictions for nBA .....	68
Table 4.5. Initiator species and primary radicals.....	75

# CHAPTER 1

## INTRODUCTION

Surface functionalization and thin film coatings of polymers have attracted a great deal of attention in recent years due to their ability to modify the desired surface without losing structural properties of bulk and easily integration into various size of flexible devices. With the rapid change of technology, to fulfill the requirements, new products and devices used in industry and households are getting smaller and become more complex, which, therefore, make polymers an inevitable unit of producing features with high-quality surface properties. With the advance of thin-film technology, polymer films with different features have been widely used and become one of the major components of biotechnology, medical, optical coatings, electronics, energy related and semiconductor industries (Ozaydin-Ince et al., 2012). For fabricating polymer thin films, liquid-based techniques, such as spraying, spin-coating, dip-coating, and ink-jet printing have been predominantly applied in industry due to the ease of scaling up and low cost of process. However, after polymer synthesis, these types of processes generally require some additional treatment with solvents, which are toxic to environment and human health. Solvent usage can also dissolve, make swell, and degrade fragile surfaces such as textiles, papers and introduces impurities into the system leading defective film formation (Alf et al., 2010). Additionally, challenges which are resulted from de-wetting and surface tension can lead to non-uniform coatings in micro- and nanometer sized structures where the coating solution accumulates at the bottom of the features and leaves the edges uncoated. All these challenges limit the application of solvent in polymer film manufacturing, in particular, high-purity electronic and noncytotoxic biomedical applications. Therefore, vapor-phase process can be a reliable alternative method to avoid difficulties arising from liquid-phase techniques in polymer film synthesis and it needs to be employed when delicate substrates and/or complex geometries are required to be coated.

Chemical vapor deposition (CVD) is a frequently employed, single-step, solvent-free, and all-dry vacuum process where the precursors are introduced into the system in vapor phase and conformal coating of complex geometries are achieved (Yagüe et al., 2013). It has been commonly used deposition technique, particularly in semiconductor



industry in which high substrate temperature and high powers required to deposit inorganic thin films. On the other hand, deposition of polymer films is a gentle process that is; such deposition conditions of inorganics are not compatible with that of polymers leading to formation of undesirable crosslinking and polymer film damaging. By advancing in solution chemists, CVD reactants and reactor designs have been modified to achieve low temperature and low energy input polymer depositions which, therefore, make CVD commonly used technique for polymer thin film coatings.

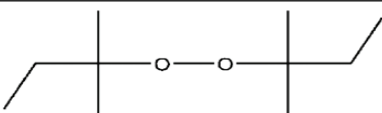
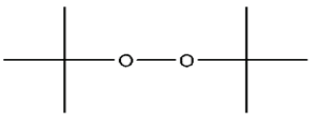
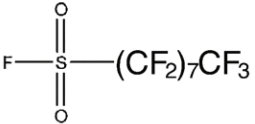
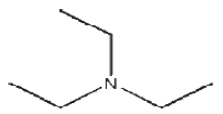
## **1.1. Polymerization Methods**

Polymers produced by CVD techniques can be classified according to the polymerization mechanism as step-growth and chain-growth polymers. In step-growth polymerization, increases in chain length are achieved sequentially through pairwise reactions between monomers, dimers and higher oligomers. One of the common step-growth polymerization technique is molecular layer deposition (MLD) in which the reactants are molecular fragments and are introduced to the system alternately, allowing the film to be grown layer by layer until the target thickness is reached. On the other hand, chain-growth polymerization occurs fast with the breaking of double-bond through various forms of initiation (David Dorschner, 2010). Free-radical polymerization is a common polymerization method in which chains with reactive free-radical species are successively added to form the polymer. The reaction mechanism consists of three main steps. The first step of the polymerization is the initiation, which increases the number of highly reactive free radicals. These radicals, which can be created using an initiator; light, heat or redox reaction, then react with the monomers creating free-radical active sites. The second step is the propagation, where the polymer chains grow by the addition of monomer molecules to the free-radical active sites. The third and the final step is the termination which can occur via several mechanisms. One possibility is that the active sites of two chains or the active site of a chain and a free radical can meet and react which terminates the chain growth. Another possibility is that the active chain site can react with a non-reactive molecule (Ozaydin-Ince et al., 2012; Im and Gleason, 2011).

One of the common CVD techniques based on chain-growth polymerization is the plasma-enhanced CVD (PECVD) in which energetic plasma electrons are used to break down the monomer bonds and to create the active sites. However, electron bombardment

results in undesired bond dissociation and formation of unwanted side reactions such as excessive crosslinking or fragmentation which lead to damage or loss of the functional groups of the monomer (Sreenivasan and Gleason, 2009; Tenhaeff and Gleason, 2008). Photo-initiated CVD (piCVD) is another CVD technique where the monomer radicals are initiated using UV radiation (Baxamusa et al., 2008). Although polymerization rates are significantly lower than the PECVD, it is a milder process which results in improved functional retention. Instead of plasma or photons, thermal energy can also be used to breakdown the monomer to initiate the polymerization mechanism. In Hot-wire CVD (HWCVD), resistively heated filaments breakdown the monomer at a temperature of higher than 800 °C in order to initiate the polymerization. As a subset of HWCVD, initiated chemical vapor deposition (iCVD) also uses the thermal energy of hot filaments, but, the key distinction of iCVD process is to employ initiating species, majority of which decomposes thermally between 200-400 °C at the vicinity of resistively heated filaments within the vacuum chamber. Among the initiator chemicals, tert-butyl peroxide (TBPO), tert-amyl peroxide (TAPO), perfluorooctane sulfonyl fluoride (PFOS), tert-butyl peroxybenzoate (TBPOB), and triethylamine (TEA) are the most commonly employed, and thermally decomposed initiators of which chemical structure and decomposition conditions are presented in Table 1.1.

Table 1.1. Thermally decomposing initiators and decomposition temperatures.  
(Source: Tenhaeff and Gleason, 2008)

Initiator Type	Chemical Structure	Dissociation Temperature
Tert amyl peroxide (TAPO)		150-250 °C
Tert-butyl peroxide (TBPO)		200-300 °C
Perfluorooctane sulfonyl fluoride (PFOS)		450-550 °C
Triethylamine (TEA)		450-550 °C

## 1.2. Initiated Chemical Vapor Deposition (iCVD) Process

The iCVD is a versatile method and has extended capabilities to produce well-defined polymers as thin films and coatings with high deposition rates through the use of an initiator, and provides full functional retention of deposited polymers.

Typical iCVD process mainly involves precursors, vapor delivery equipment, reaction chamber, temperature, pressure, and exhaust control units as shown in Figure 1.1. The iCVD is a solventless and all-dry vacuum process that uses the vapor pressures of the liquid precursors for film deposition. Most of the cases, monomer(s) cannot meet the required vapor pressure at room temperature. Therefore, they need to be vaporized for delivery to the reaction chamber and this can be handled through the heating of the liquid container to increase their vapor pressures. Flow of vaporized precursors are metered accurately using mass flow controllers and delivered into the chamber through the heated delivery lines of which temperature are controlled via PID temperature controllers. Reaction chambers may have different configurations such as pancake and square type of geometry, and they generally involve an array of filament which is positioned at a distance from substrate surface to be coated. Inside the reaction chamber, there are two different temperature regions which are the heated filament wires and the cooled substrate area. Temperature of hot filament wires is maintained typically 200-400 °C through the use of a power supply and the temperature of the substrate is maintained at 0-30 °C via recirculating chiller having backside contact with a stage in order to promote adsorption. Inside the chamber, polymerization occurs under vacuum conditions, which is generally kept at 0.1-1 Torr, and adjusted through the downstream throttle valve in a feedback loop with a pressure gauge and controller, and manual valve.

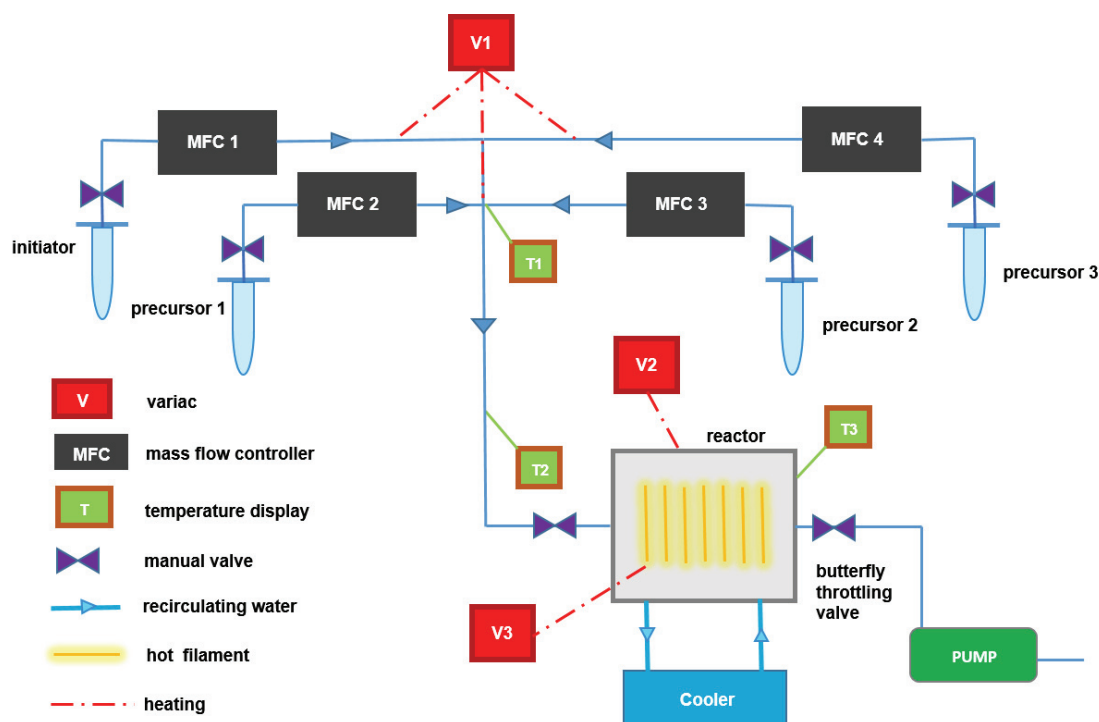


Figure 1.1. Schematic representation of a typical iCVD system.

### 1.3. Reaction Mechanism for iCVD

iCVD is a versatile method that it combines the solution phase polymerization and vapor phase film deposition in a single step. It is a common way to produce polymers identical to those obtained from liquid-phase polymerization (Lau and Gleason, 2006a, 2006b; Im and Gleason, 2011). Thus, it enables to produce conformal coating of polymer films at nanometer scale without using any solvent. The reaction mechanism and kinetics of iCVD follow the free-radical polymerization which is a widely studied and translated to the industrial applications due to their tolerance for low reactant purities, and its capability to polymerize almost any chemical with a vinyl group. For traditional free-radical polymerization, all of the mechanistic steps occur in a single temperature and single solution phase. However, since iCVD involves both gas phase and heterogeneous reactions taking place at different temperature regions, free radical polymerization occurs in a heterogeneous and solventless environment, and approaches similar way with the solution phase chain-growth polymerization stages involving initiation, propagation, and termination reactions (Coclite et al., 2013). In brief explanation, vapor phase of monomer and initiator species are first delivered into the reactor chamber which is held at mild

reactor pressure. Decomposition step, which involves the creation of a free-radical, occurs in the vapor phase by thermal dissociation of initiators to form free radicals. These radicals then transport to the surface and react with an adsorbed monomer molecule to initiate the free-radical polymerization reaction by creating one-mer ready to grow into a polymer chain (Tenhaeff and Gleason, 2008). By rapid addition of monomers to this active polymer, propagation step occurs and active chain grows until the chain is terminated by another free radical, whether it is another chain end or a dissociated initiator molecule. Described reaction mechanism for iCVD process is shown in Table 1.2 where the  $k_d$ ,  $k_i$ ,  $k_p$ ,  $k_t$ ,  $k_t'$ ,  $k_t''$  are the reaction rate coefficients of decomposition, initiation, propagation, termination, primary radical termination, and primary radical recombination, respectively.

Table 1.2. Free radical polymerization mechanism in iCVD process.  
(Source: Lau and Gleason, 2006b)

Initiator decomposition	$I (gas) \xrightarrow{k_d} 2R (gas)$
Primary radical adsorption	$R (gas) \xrightarrow{k_{ad,R}} R \cdot (ad)$
Monomer adsorption	$M (gas) \xrightarrow{k_{ad,M}} M (ad)$
Initiation	$R \cdot (ad) + M (ad) \xrightarrow{k_i} M_1 \cdot (ad)$
Propagation	$M_n \cdot (ad) + M (ad) \xrightarrow{k_p} M_{n+1} \cdot (ad)$
Termination	$M_n \cdot (ad) + M_m \cdot (ad) \xrightarrow{k_t} M_{n+m} (ad)$ and $M_n (ad) + M_m (ad)$
Primary radical termination	$M_n \cdot (ad) + R \cdot (ad) \xrightarrow{k_t'} M_n (ad)$
Primary radical recombination	$R \cdot (ad) + R \cdot (ad) \xrightarrow{k_t''} M_m (ad)$

As stated earlier, polymerization on the surface is initiated by the radicals which are formed by the thermal decomposition of the initiator species in iCVD process. Thus, to increase the deposition rate on the surface, increasing filament temperature results in an increase in the rate of radical formation in which the rate constant ( $k_d$ ) for the decomposition of the initiator can be described as represented in Eq. (1.1).

$$k_d \approx \exp\left[-\frac{E_d}{RT_{fil}}\right] \quad (1.1)$$

In the equation above,  $E_d$  is the activation energy for the decomposition reaction and  $T_{fil}$  is the filament temperature (Ozaydin-Ince and Gleason, 2009). In iCVD process, surface polymerization follows the Eley-Rideal adsorption mechanism in which the rate of polymerization or deposition reaction depends on both the concentration of adsorbed monomer species on the surface and gas phase radical concentration (Ozaydin-Ince et al., 2012).

Monomer surface coverage depends on the vapor phase monomer concentration and can be predicted considering the dimensionless ratio of a monomer's partial pressure to its saturation pressure ( $P_M/P_{sat}$ ) through the limiting form of Brunauer-Emmett-Teller (BET) adsorption isotherm;

$$V_{ad} = \frac{V_{ml}c(P_M/P_{sat})}{(1 - P_M/P_{sat})[1 - (1 - c)(P_M/P_{sat})]} \quad (1.2)$$

where  $V_{ad}$  is the total adsorbed volume,  $V_{ml}$  is the monolayer adsorbed volume, and  $c$  is the constant which is typically used as a fitting parameter and can also be obtained using;

$$c \approx \exp\left(\frac{\Delta H_{des} - \Delta H_{vap}}{RT}\right) \quad (1.3)$$

where  $\Delta H_{des}$  is the heat of desorption of a monolayer, and the  $\Delta H_{vap}$  is the heat of vaporization. According to adsorption isotherm studies of vinyl monomers, monolayer coverage is reached for  $P_M/P_{sat} \sim 0.4$ , while condensation of a liquid corresponds to a value of unity for  $P_M/P_{sat}$  (Asatekin et al., 2010). When  $P_M/P_{sat}$  is much less than unity, monomer surface concentration becomes proportional to  $P_M/P_{sat}$ . Therefore,  $V_{ad}$  becomes,

$$V_{ad|P_M/P_{sat} \rightarrow 0} = V_{ml}c(P_M/P_{sat}) \quad (1.4)$$

The surface adsorbed monomer concentration, therefore, can be described as represented in Eq. (1.5) where  $\rho_M$  is the density, and  $MW_M$  is the molecular weight of the monomer.

$$[M] = \frac{\rho_M}{MW_M} \frac{V_{ad}}{V_{ml}} \quad (1.5)$$

By inserting Eq. (1.4) to Eq. (1.5), the final equation which describes the surface monomer concentration becomes;

$$[M] = \frac{\rho_M}{MW_M} c \frac{P_M}{P_{sat}} \quad (1.6)$$

Gas phase monomer partial pressure ( $P_M$ ) can be written in terms of flow rate of precursors introduced to system as described in Eq. (1.7).

$$P_M = \frac{F_M}{F_{total}} P_{total} \quad (1.7)$$

Therefore, Eq. (1.6) becomes as;

$$[M] = \frac{\rho_M}{MW_M} c \frac{F_M}{F_{total}} \frac{P_{total}}{P_{sat}} \quad (1.8)$$

Eq. (1.8) states that adsorbed monomer concentration is a function of gas phase monomer material properties, flow rates of precursors, reactor and monomer saturation pressures. It is also related with  $c$ , the BET constant, which is a function of the surface temperature where the deposition takes place.

There are many parameters affecting iCVD process conditions and polymerization rate, and most of which are difficult to control externally. It is a complex process that involves fluid flow of gaseous precursors delivering through different temperature regions inside the chamber. As precursors moving along the reactor, their velocity and fluid properties will also change spatially with respect to temperature, and reactor pressure. In addition, monomer and initiator type will also affect the deposition behavior and film uniformity since different materials have different fluid properties and transport features. Moreover, in reactor chamber, initiator species thermally decompose (as defined in Eq. (1.1)) to form active radical intermediates over the hot filament regions which in turn leads to concentration gradient of species in reactor chamber. Mass transport of multicomponent gaseous species to the substrate surface occurs according to

each species' diffusional behavior, and to the distance between filament array and substrate surface. As a final step, over the surface, free radical polymerization reactions, following the adsorption of monomer and radical species, will take place on the cooled substrate surface with respect to reaction rate coefficient of free-radical polymerization steps. Therefore, iCVD is multi-parameter process involving coupled momentum and heat transfer, multi-component mass transfer, reaction, and adsorption phenomena occurring inside the vacuum chamber. Thus, to understand the deposition characteristics of a coated film, effect of all these parameters and transport phenomena need to be investigated in a computational environment supported by experimental data.

In this thesis, our main goal is to develop a computational model to understand the transport phenomena occurring inside the iCVD process and to determine optimum deposition conditions for uniform film coatings. It is believed that developing such model will assist to predict film thickness and uniformity without carrying out time-consuming trial and error experiments which, in turn, minimize the expensive chemical usage and waste of money. To be able to do this, a mathematical model is developed, then the accuracy of the model is checked for 1H,1H,2H,2H- perfluorodecyl acrylate (PFDA) and n- butyl acrylate (BA) monomers via comparing model outputs with the experimental results reported in literature.

This thesis contains five chapters. In Chapter 2, both mathematical and computational modeling studies on CVD and iCVD process, and deposition parameters affecting the film thickness are investigated in detail. In Chapter 3, a mathematical model for iCVD system is developed describing specific boundary conditions. Model implementation is also used in different reactor geometries and different process conditions. In Chapter 4, model accuracy is compared and confirmed with the experimental results published in literature, and governing transport equations and the reactions are investigated and discussed in detail. Finally, the conclusions and some recommendations are listed in Chapter 5.



## CHAPTER 2

### LITERATURE REVIEW

#### 2.1. Modeling Studies in CVD system

Chemical vapor deposition has been received broad attention both in industry and academia since it enables to synthesis of high-purity, defect-free films with high growth rates, and it offers good control of film structure, and excellent uniformity of wide variety of materials. The deposition of thin films with CVD is a process of growing importance, particularly in semiconductor industry due to the ability to be scaled-up and to meet the requirements such as the quality of deposited film, thickness, and uniformity, e.g., although dimensions of microelectronic devices decreases and diameters of wafers increases. Thus, to understand the effect of process parameters and to design the equipment for obtaining their better performance, considerable amount of knowledge on physical and chemical parameters on CVD of inorganics is available thanks to accurate predictions of theoretical and numerical models, and many successful experimental investigations. Among the inorganics, silicon carbide, silicon oxide, GaAs, and tungsten have been widely studied through numerical and computational modeling and detailed CVD models have been developed by studying multiple transport mechanisms in different type of CVD reactors.

In the study carried out by Veneroni et al. (2005), epitaxial silicon carbide (SiC) growth rate and stoichiometry were investigated as a function of various parameters in a horizontal hot wall type reactor models (1D-3D) with different complexity using finite element method. Since CVD processes involve material transport physics, gas phase and surface chemical reactions, it can still be quite difficult to achieve an effective model, such that, in the study they also stated that obtaining reliable kinetic data for both gas phase and the surface were essential for the accurate prediction of growth rate.

In a different study carried out by Uzuafa et al. (1999), a comprehensive model was developed for the deposition of hydrogenated amorphous silicon films (a-Si:H) in a laser-induced chemical vapor deposition (LICVD) method. A simple surface reaction mechanism considering gas-phase and solid surface reactions was proposed in the study.

Additionally, the model considered gas-phase flow, convective transport effect, and reaction rates on the solid wafer and the boundary layer equations were used to calculate flow and temperature profiles. For the concentration distribution of all important intermediate species, finite-difference scheme was employed to solve two dimensional concentration profiles and finally they noted that  $\text{Si}_2\text{H}_4$  had a significant contribution to the deposition rate while disilane not.

In addition to the studies focused on the reaction mechanism and kinetics, there have been a lot of reports about modeling studies on CVD process used to simulate the distribution of temperature, gas phase flow rate, and concentration distribution for different type of CVD reactors. Among the studies, Li et al. (2015) investigated the temperature, gas flow, and gas component factors which affect the final product in a self-designed CVD process. They simulated and analyzed the influence of these factors on SiC nanowires deposition on the substrate using Fluent software based on Computational Fluid Dynamics (CFD) principle. Simulated results were also confirmed by the experimental studies which therefore providing a useful theoretical basis for optimizing process parameters and reactor design for the deposition of SiC nanowires. Similar study was also carried out for the modeling of fiber-reinforced silicon carbide composites (B M Allen, 2014). The study was objected to build a series of models that combine macroscopic flow and chemistry with microscopic geometry changes using Comsol Multiphysics simulation program based on the finite element methods. The resulting simulations obtained from the model in which various parameters were given as input indicated that fluid pressure was a major factor of determining how uniform film was. In addition, they noted that even with laminar flow, vortices of low pressure could form leading to uneven reaction rates and species concentration on the substrate which, therefore, affect the uniformity of SiC deposition.

Most CVD processes are operated under reduced pressure environment to achieve uniformity of the deposits. However, a type of CVD which is called as atmospheric pressure CVD (APCVD) has also been used even though it does not meet the uniformity requirements of some applications and growth rate is often small. In a study carried out by Vanka et al. (2004), to overcome the negative effects of atmospheric pressure operation, and to produce high growth rate of films, various effect of geometrical parameters on growth rate and uniformity were investigated in a jet impingement chemical vapor deposition reactor operated at atmospheric pressure. In the study, they used previously validated two-dimensional model to numerically solve the governing

equations and the spatial terms in the governing equations were discretized using second-order finite volume method. Their results showed that uniform deposits at atmospheric pressure could be achieved for appropriate choice of substrate rotation rate, inlet flow rate, and reactor dimensionless length.

Hot-wire chemical vapor deposition (HWCVD), on the other hand, is one of the commonly employed CVD technique for the deposition of inorganics and various mathematical models have been reported in the literature. A two-dimensional computational model was reported by Olivias-Martinez et al. (2007) for HWCVD process to produce diamond film. Since production of diamond film depends on many factors including substrate material, temperature, and gas-phase compositions, a model enabling to couple and solve the overall momentum, energy, and mass equations was presented. The model also incorporated the simplified reaction mechanism which consists of twelve chemical reactions involving nine species. In addition, they also investigated the shape and dimensions of the reactor as well as the number of filaments, and substrate geometry. They concluded that increasing the filament number increased both the  $\text{CH}_3$  concentration and growth rate of diamond film.

As a sub-set of HWCVD, initiated chemical vapor deposition (iCVD) process also involves fluid flow, heat transfer, multicomponent species transfer, and reactions occurring in gas-phase and solid surfaces. It is a complex process that deposition kinetics of polymers as well as the transport phenomena occurring inside the reactor chamber need to be investigated in detail to understand the effect of process parameters on deposited film thickness.

## **2.2. Effect of Process Parameters and Kinetics on Film Growth in iCVD**

The effect of process parameters including precursor flow rates, substrate temperature, reactor pressure, and filament temperature, on deposition kinetics have been vastly investigated in literature for good control of film properties and understanding the deposition kinetics. In industrial applications, analyzing the effect of these various factors are essential, particularly, to have high deposition rates leading efficient consumption of the precursors in the manufacturing process. Therefore, understanding the deposition mechanism and the effects of the process parameters are necessary to obtain high film

growth rate and to optimize the iCVD process for producing desired film coating with good conformality over the structure surface.

As stated before, iCVD uses free radical initiating species to start the polymerization reaction over the surface. There are commonly used types of initiator species in literature which are activated via heat, UV light, ion or electron beam to decompose to form the active radicals (Im and Gleason, 2011). Therefore, selecting suitable initiator type for iCVD reactor is essential to obtain the desired film deposition with higher growth rate in the process. The effect of initiator type was studied by Xu and Gleason (2011) for pCHMA thin film synthesis. In the study, they used *tert*-butyl peroxybenzoate (TBPOB) as initiator, of which vapor pressure is only 0.00337 Torr at room temperature, and compared the deposition results with that of the film synthesis with TBPO. According to the study, using TBPOB instead of TBPO increased the film growth rate by a factor of up to seven and lowered the filament temperature from 257 to 170 °C yielding higher deposition rates at the same process conditions. This is due to having higher sticking probability of benzoate radical, generated from thermal decomposition of TBPOB, to the surface compared to the *t*-butoxy radical.

Since decomposition reaction of the initiator species occurs on the hot filament wires, the choice of filament wire materials can also influence the deposition rate. In the study carried out by Cruden et al. (2002), the effect of different filament types was investigated and results showed that Nichrome (80% Ni/20% Cr) yields much higher deposition rate compared to alumina. Additionally, filament temperature also plays a critical role in iCVD deposition kinetics for thermally decomposed initiators due to the type of radical formation depends on the filament temperature (Ozaydin-Ince and Gleason, 2009). In the study carried out by Ozaydin-Ince and Gleason (2009), they studied the effect of filament temperature on deposition rate using TBPO initiator. In addition, they investigated the thermal decomposition of TBPO and radical formation at different filament temperatures using gas phase FTIR. In the study, it is stated that decomposition of TBPO leads to formation of methyl radicals as well as *t*-butoxy radical in liquid phase polymerization (Ozaydin-Ince and Gleason, 2009). According to their study, at filament temperatures below 250 °C and above 270 °C, they observed that the primary type of radical that was formed was the *t*-butoxy species since methyl radicals were much volatile which limits the surface concentration of radicals to participate in starting polymerization on the surface. On the other hand, in the case of *tert*-amyl peroxide (TAPO) initiator, Lau and Gleason (2006b) revealed that it initially forms the

*tert*-amyl peroxy radical, but then, these peroxy radical rapidly undergoes  $\beta$ -scission to yield acetone and ethyl radicals for TAPO initiator (Nakamura et al., 1996).

Filament temperature does not influence the  $P_M/P_{sat}$ , but it influences the concentration of the radicals on the surface which in turn affects the deposition rate of the film. In the study, they also investigated the effect of filament temperature on EDGA deposition rate by changing filament temperature in the range of 170-320 °C at a fixed substrate temperature and observed two different regime for all flowrates. It was observed that at lower filament temperature, the film growth rate strongly depends on the filament temperature, which is the characteristic of a reaction-kinetics-limited process that deposition kinetic is limited by the formation of the radical not by the monomer vapor concentration. On the other hand, at high filament temperature, deposition rate less dependent on the filament temperature, which is the characteristic of mass transfer-regime, that is, filament temperature is high enough to decompose the initiators so the deposition rate depends on the arrival of the formed radical species onto the substrate surface from gas phase to the substrate. Therefore, in order to obtain the high growth rate, it is revealed that monomer flow rate could be increased in the process. O'Shaughnessy et al. (2006) also searched for the effect of filament temperature as well as substrate temperature on deposition kinetics of V3D3 polymerization with TBPO initiator, and they observed similar two distinct regimes in the Arrhenius plot of deposition rate with filament temperature in which high temperature region limited by mass transfer.

In iCVD process, initiator and monomer species are introduced into the chamber as vapor phase and based on the knowledge of vapor pressure of the monomers, operating conditions for desired film thickness can be predicted at a specified substrate temperature (Im and Gleason, 2011). The saturation pressure of a monomer is used for the prediction of monomer volatility, which means that at equal monomer gas pressures, heavier monomer gets adsorbed onto the surface more than that of light monomer does. In the study carried out by Lau and Gleason (2006a), they investigated the effect of monomer-saturated vapor pressure using a homologous series of alkyl acrylate (ethyl to hexyl acrylate) on the deposition rate. It was observed that at the same deposition conditions, using heavier monomer lead to increase deposition rate due to more favorable monomer adsorption. In the study, they also examined the effect of filament temperature for the three set of  $P_M/P_{sat}$  ratio and observed closer activation energies suggesting that deposition rate was limited by the mass transfer of the radical species.

Among the process parameters, substrate temperature has a strong influence on deposition rate since adsorption-desorption mechanisms of the precursors and polymerization reactions take place on the substrate surface. For most of the inorganics and some CVD polymers, increasing substrate temperature accelerates kinetics of the surface reactions which therefore results in enhanced deposition rates. On the other hand, studies demonstrated that there is an inverse relationship between substrate temperature and deposition rate for iCVD polymers indicating that an Arrhenius type relation exist between the temperature and the deposition rate (Ozaydin-Ince et al., 2012). In the experimental study of their investigation, Lau and Gleason (2006a) conducted a series of experiments to see explicitly the effect of substrate temperature by choosing ethyl acrylate as the monomer and fixing the other process parameters constant. The result of an Arrhenius plot of deposition rate with substrate temperature yields an averaged apparent  $E_a$  of  $-79.4 \text{ kJ mol}^{-1}$  which means that decreasing substrate temperature leads to an increase in deposition kinetics.

There are also other studies in literature investigating the mentioned parameters for different monomer type and different reaction conditions. Among them, Chan and Gleason (2006) studied the growth rate of glycidyl methacrylate (GMA) and cyclohexyl methacrylate (CHMA) monomers' polymerization using TBPO initiator. They investigated the effect of monomer surface concentration on deposition rate and the number-average weights of polymers by changing precursors flow rate at different substrate temperatures. Similar attempt was also carried out by Janakiraman et al. (2015) for the deposition of poly (vinylpyrrolidone) (PVP) and poly (4-vinylpyridine) (P4VP) in order to understand their kinetics and to provide a basis for their dye sensitized solar cells applications. In the study, effect of  $P_M/P_{sat}$ , reactor pressure, and substrate temperature on deposition rate were investigated for each type of monomer and it was found that polymerization rate increased with increasing pressure and decreasing with increasing substrate temperature.

### **2.3. Modeling Studies of iCVD process**

Besides the externally controlled process parameters, both transport and reaction rate knowledge are necessary for the successful scale-up of iCVD. Although Arrhenius relationships of deposition rate are generally formed with various process parameters,

care must be given to understand the underlying factors such as gas phase and surface concentrations of species, and rate coefficients of adsorption and decomposition reactions. Therefore, modeling studies which are supported with kinetic studies will assist to better understand of the iCVD deposition onto substrate with more complex geometries and to optimize the reactor conditions for desired film thickness.

Although studies based on various numerical methods for solution-based free radical polymerization exist, there are limited attempts for iCVD process due to the presence of both gaseous and heterogeneous phase reactions in process, and the absence of chemical kinetic data unlike well-studied inorganic materials commonly used in established semiconductor industry.

An attempt on computational modeling of iCVD process was presented by Josef Brecka (2009). In the study, ethylene glycol diacrylate (EGDA) film deposition with tert-butyl peroxide (TBPO) was used to validate the computational model predictions with experimental data. Presented model in the study was built under Comsol Multiphysics computational software environment which enabled to couple fluid flow, heat transfer, and species composition. Although transport phenomena occurring inside the iCVD chamber was successfully simulated, the deposition rate on the substrate could not be achieved in the model due to the unknown kinetic parameters of free radical polymerization reactions of EGDA monomer. This study clearly indicates that to obtain an accurate modeling of iCVD process, kinetic parameters obtained from experiments and/or derived from modeling studies are extremely important.

## **2.4. Kinetic Studies for Determination of Polymerization Rate Constants**

A detailed study on kinetic parameters of iCVD polymers were for the first time studied by Lau and Gleason (2006b) in a two-part investigation. As mentioned before, in the experimental part of the study, they carried out a series of experiments on deposition of homologous series of n-alkyl acrylates (n=2-6) initiated with TAPO, and they investigated the effects of surface monomer concentrations on deposition rate and molecular weight of the polymer. Following up the experimental study, in the kinetic study, the aim was to develop a mechanistic model for describing the kinetic behavior of acrylate monomers. They proposed a reaction mechanism including a series of steps involving decomposition, adsorption, and surface polymerization reactions as previously

shown in Table 1.2. In bulk-phase radical polymerization, primary radical and polymer radical concentrations on the surface were assumed to be constant. Therefore, using similar pseudo steady state approximation analogous to bulk phase, rate of polymerization and also kinetic chain length were derived implicitly. Using n-BA as the monomer together with TAPO initiator, they conducted a series of experiments to obtain deposition rate and molecular weight as a function of  $P_M/P_{sat}$  at a fixed surface temperature of 23 °C. Using argon patch flow, a constant total flow rate (3.7 sccm) was maintained to obtain constant residence time, and also experiments were conducted at constant reactor pressure, filament and surface temperature, that is, the experimental kinetic data would solely be affected by the adsorbed monomer concentration, not by the other parameters. They obtained increasing deposition rate with increasing surface monomer concentration. Then, assuming reactions occur within a monolayer thickness, they derived monolayer volume and film thickness using QCM adsorption data together with fitting the data to the BET equation. For the kinetic model, using a multi-response parameter estimation procedure, experimental data were fitted to the model and they derived surface initiation, propagation, and termination rate constants. According to the results, estimated parameters matched well with experimental data and with the value obtained from liquid phase free radical polymerization. Therefore, it is a strong evidence that iCVD polymerization kinetics closely follows that of their liquid phase counterpart (Lau and Gleason, 2006a, 2006b). Similar kinetic study based on the multi-response parameter estimation procedure was applied for 1H,1H,2H,2H-perfluorodecyl acrylate (PFDA) polymerization with TBPO by Gupta and Gleason (2006). Surface polymerization rate coefficients were determined at 44 °C of substrate temperature, and good agreement between experimental and kinetic data was observed for the iCVD of PFDA at given deposition conditions.



## CHAPTER 3

### MODELING OF iCVD

#### 3.1. Model Requirements for iCVD Process

New developments in technology lead to growth in the necessary investment of time and the money to fulfill the demands with required features particularly in microelectronic industry to manufacture the integrated circuits. Most of the time, to meet the demands on homogeneous and uniform film coating of devices, an empirical way, which is mainly relying on the feelings of an experienced engineer, is used as an approach. Such trial and error approaches are not capable to fine tuning of film properties associated with the size and structure of the devices, and require experimental trials which, therefore, consume time, sources, and money. Therefore, to understand the effects of process parameters on final film properties, a comprehensive analysis should include fluid flow, heat and multicomponent mass transport, gas phase and surface reaction kinetics, and thermodynamics phenomena describing iCVD process. Although, a number of computational models involving partial differential equations described above-mentioned phenomena in details, the model accuracy depends on the availability of data related to chemical and physical properties of species and reaction kinetics. A substantial knowledge exists for commonly used CVD materials, especially thanks to mature semiconductor industry. Unfortunately, such knowledge is rather weak for most iCVD compatible materials. What is needed is a realistic computational model including all these phenomena for accurate prediction of final film properties for a given set of process parameters and conditions.

#### 3.2. Model Development

In order to develop a successful model for iCVD, proposed model needs to be capable of coupling and utilizing multidisciplinary approach such as transport physics of ideal gases, gas phase and surface reaction, and computational fluid dynamics since iCVD involves;

- Fluid flow of gaseous species at different temperature regions,
- Thermal decomposition of initiator molecules to produce reactive intermediates at the vicinity of heated filaments,
- Mass transport of multi-component gaseous species to the substrate,
- Adsorption of species and polymerization reactions on the cooled surface.

Based on the knowledge, a general model describing the iCVD process can consist of several blocks as illustrated in Figure 3.1. In the model, process parameters which describes the iCVD process, generally involves details about the reactor geometry and its dimensions as well as the process conditions, such as precursor flow rates, temperature set points, reactor pressure, and kinetic coefficients of the reactions. With the help of coupled conservation of mass, momentum, and energy equations with the appropriate boundary conditions, transport of the species in the reactor can be described in the model. According to the model predictions, one can able to obtain the gas flow, temperature and composition distributions of the species at described reactor conditions, and determine the deposition rate and uniformity of the deposited film over the substrate surface as the model outputs. However, for the actual modeling of the deposition process, knowledge of the chemical mechanisms and polymerization rate constants need to be defined.

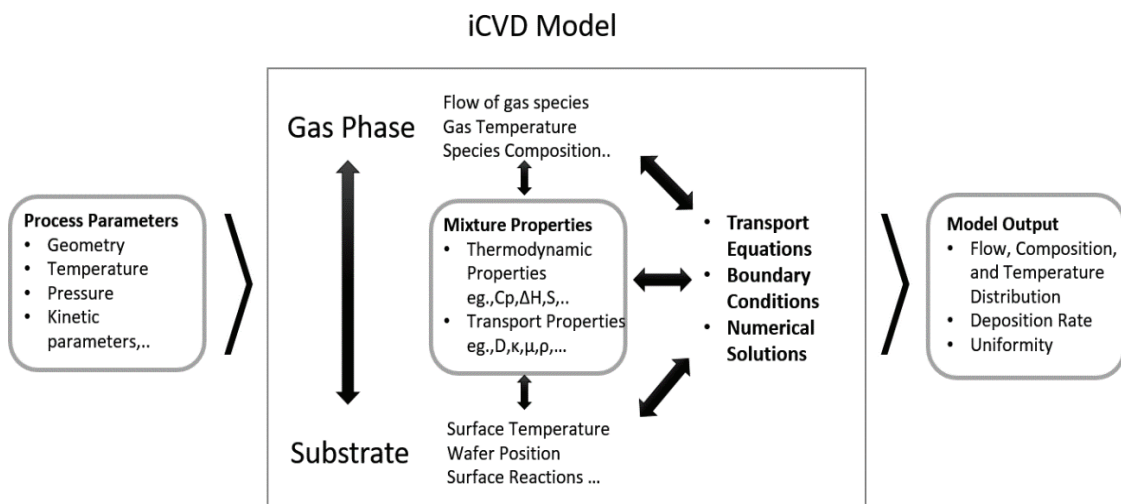


Figure 3.1. Illustration of modeling approach.

### 3.2.1. Model Simplifications and Transport Equations

Reasonable assumptions are necessary to reduce the complexity of solving coupled non-linear equations numerically and to reduce the effort and time in the computational analyzing of the system. This assumptions generally justified for the CVD process conditions which do not essentially limit the accuracy and the applicability of the model.

The presented model here assumes that the iCVD process operates at steady-state conditions and gases treat as ideal gases, behaving in accordance with ideal gas law and Newton's law of viscosity at a described pressure and temperature conditions. The gas flow is assumed to be laminar. Therefore, single-phase, compressible fluid flow in iCVD reactor is described by conservation of mass and conservation of momentum equations through the following equations;

$$\nabla \cdot (\rho \mathbf{u}) = 0 \quad (3.1)$$

$$\rho(\mathbf{u} \cdot \nabla) \mathbf{u} = \nabla \cdot \left[ -p\mathbf{I} + \mu(\nabla \mathbf{u} + (\nabla \mathbf{u})^T) - \frac{2}{3}\mu(\nabla \cdot \mathbf{u})\mathbf{I} \right] + \mathbf{F} \quad (3.2)$$

where  $\rho$  (SI unit: kg/m<sup>3</sup>) is the density,  $\mathbf{u}$  (SI unit: m/s) is the velocity vector,  $p$  (SI unit: Pa) is the pressure,  $\mu$  (SI unit: Pa.s) is the dynamic viscosity of ideal gas mixture and  $\mathbf{F}$  (SI unit: N/m<sup>3</sup>) is the volume force vector. Since no large velocity gradient appears and low Mach number flows in CVD processes, viscous heating and the effect of pressure variations on the temperature can be neglected, respectively. Therefore, by ignoring these terms, those equations are coupled to heat equation expressed by;

$$\rho c_p \mathbf{u} \cdot \nabla T = \nabla \cdot (k \nabla T) + Q_h \quad (3.3)$$

where  $c_p$  (SI unit: J/(kg.K)) is the specific heat capacity of the fluid at constant pressure,  $T$  (SI unit: K) is the temperature,  $k$  (SI unit: W/(m.K)) is the thermal conductivity, and  $Q_h$  defines heat sources other than viscous heating. The total heat flux vector is calculated by Eq. (3.4),

$$\rho \mathbf{u}U - k\nabla T + \mathbf{q}_r \quad (3.4)$$

where  $U$  is the internal energy and  $\mathbf{q}_r$  is the radiative heat flux. To reduce the complexity and due to relatively low temperatures,  $\mathbf{q}_r$  term is neglected in the model.  $U$  term is related to the enthalpy,  $H$ , and calculated by the following equation;

$$H = U + \frac{p}{\rho} \quad (3.5)$$

Fluid properties;  $\rho$ ,  $\mu$ ,  $c_p$ , and  $k$ , in above equations, are not only functions of the temperature and pressure, but also function of the composition of the gas mixture. Therefore, general flow and energy equations are coupled to the species concentration equations to describe mixture properties as a function of velocity, temperature, and mass fractions.

iCVD involves transport of multi-component gaseous species and Eq. (3.6) describes the mass transport for an individual species in the model;

$$\nabla \cdot \mathbf{j}_i + \rho(\mathbf{u} \cdot \nabla)w_i = R_i \quad (3.6)$$

where  $\rho$  (SI unit: kg/m<sup>3</sup>) denotes the mixture density and  $\mathbf{u}$  (SI unit: m/s) the mass averaged velocity of the mixture. The remaining variables are specific for each of the species, where  $w_i$  is the mass fraction of the  $i$ th species ( $i=1, \dots, Q$ ),  $\mathbf{j}_i$  (SI unit: kg/(m<sup>2</sup>.s)) is the mass flux relative to the mass averaged velocity vector, and  $R_i$  (SI unit: kg/(m<sup>3</sup>.s)) is the rate expression describing production or consumption of the  $i$ th species. Sum of the transport equations of all species gives Eq. (3.7) for the conservation of mass;

$$\nabla \cdot (\rho \mathbf{u}) = 0 \quad (3.7)$$

assuming that;

$$\sum_{i=1}^Q w_i = 1, \sum_{i=1}^Q \mathbf{j}_i = 0, \sum_{i=1}^Q R_i = 0 \quad (3.8)$$

Therefore, using mass conservation equations, the species transport for an individual species,  $i$  is solved in Eq. (3.6) described above. In a  $Q$  component gas mixture, there are  $Q - 1$  independent species concentration equations of the form of above equation. To compute the mass fraction of the remaining species, model uses the definition that the sum of the mass fractions is equal to 1:

$$w_k = 1 - \sum_{i=2}^Q w_i \quad (3.9)$$

Since the gas mixture consists of more than three species in iCVD process, model employs the Maxwell-Stefan diffusion model in which mass flux relative to the mass average velocity,  $\mathbf{j}_i$ , is described (Curtiss and Bird, 1999) as;

$$\mathbf{j}_i = - \left( \rho w_i \sum_{k=1}^Q D_{ik} \mathbf{d}_k + D_i^T \nabla \ln T \right) \quad (3.10)$$

where  $D_{ik}$  (SI unit:  $\text{m}^2/\text{s}$ ) is the multicomponent Fick diffusivities,  $\mathbf{d}_k$  (SI unit:  $1/\text{m}$ ) is the diffusional driving force acting on species  $k$ ,  $w_i$  is the mass fraction of each component,  $T$  is the temperature, and  $D_i^T$  is the thermal diffusion coefficient. For an ideal gas mixture, diffusional driving force is defined by Eq. (3.11) (Curtiss and Bird, 1999) which is;

$$\mathbf{d}_k = \frac{1}{cRT} [\nabla p_k - w_k \nabla p - \rho_k \mathbf{g}_k + w_k \sum_{l=1}^Q \rho_l \mathbf{g}_l] \quad (3.11)$$

where  $c$  (SI unit:  $\text{mole}/\text{m}^3$ ) is the total molar concentration,  $R$  is the universal gas constant ( $8.314 \text{ J}/(\text{mole}\cdot\text{K})$ ),  $p$  (SI unit: Pa) is the total pressure,  $p_k$  (SI unit: Pa) is the partial pressure,  $\rho_k$  (SI unit:  $\text{kg}/\text{m}^3$ ) is the density of species  $k$ , and  $\mathbf{g}_k$  (SI unit:  $\text{m}/\text{s}^2$ ) is an external force (per unit mass) acting on species  $k$ . The last two term in Eq. (3.11) is omitted due to the absence of external force (such as gravity) in the model. When we look at the above equations, it can be seen that the total diffusive flux for the species depends on the gradients of all species concentration, temperature, and pressure. Applying the ideal gas law,  $p = c.R.T$ , and the definition of the partial pressures,  $p_k = x_k p$ , diffusional driving force described in Eq. (3.11) can be written as;

$$\mathbf{d}_k = \nabla x_k + \frac{1}{p} [(x_k - w_k) \nabla p] \quad (3.12)$$

The mole fraction,  $x_k$ , is prescribed as;

$$x_k = \frac{w_k}{M_k} M \quad (3.13)$$

and the mean molar mass,  $M$  (SI unit: kg/mole) is expressed by;

$$\frac{1}{M} = \sum_{i=1}^Q \frac{w_i}{M_i} \quad (3.14)$$

Therefore, when Maxwell-Stefan diffusion model is applied, final form of multicomponent mass transport equation becomes as expressed in Eq. (3.15).

$$\rho(\mathbf{u} \cdot \nabla) w_i = \nabla \cdot \left( \rho w_i \sum_{k=1}^Q D_{ik} \mathbf{d}_k + D_i^T \frac{\nabla T}{T} \right) + R_i \quad (3.15)$$

Multicomponent Fick diffusivities,  $D_{ik}$ , in above equation are solved for each of the components by applying multicomponent Fick diffusivity matrix (Bird et al., 2007). Eq. (3.15) also involves the thermal diffusion coefficient,  $D_i^T$ , but thermal diffusion effect (or Soret effect) is generally applicable for the conditions of large temperature gradient exist, and causes the large or heavy gas molecules to concentrate in the cold regions of the reactor, while small or light molecules concentrate in the hottest region of the reactor chamber (Kleijn and Werner, 1993). This effect may be a significant factor for some types of CVD systems, but compared to the ordinary diffusion, thermal diffusion effect is assumed to be very small and can be neglected for our iCVD conditions. Therefore, thermal diffusion effect is neglected in the model by taking multicomponent thermal diffusion coefficient,  $D_i^T$ , zero for each of the components.

Last thing about the mass conservation equation, represented by Eq. (3.6), is the  $R_i$  term which represents the creation and the destruction of the  $i$ th species. Consider a general reaction belonging to a set of  $j$  reactions and involving  $i$  species. In iCVD process,

an irreversible decomposition reaction of initiator can be described at the vicinity of the heated filaments by such a reaction;

$$r_j = k_j^f \prod_{i=1}^Q c_i^{-v_{ij}} \quad (3.16)$$

where  $r_j$  (SI unit: mole/(m<sup>3</sup>.s)) is the reaction rate,  $k_j^f$  is the forward rate constant, which is strongly depend on the temperature,  $c_i$  ( $= px_i/RT$ ) is the molar concentration (SI unit: mole/m<sup>3</sup>) of the  $i$ th species,  $x_i$  is the mole fraction of the  $i$ th species, and  $p$  is the total pressure,  $v_{ij}$ , is the stoichiometric coefficient which is defined as being negative for reactants and positive for products. In addition to the concentration dependence, reaction rate constant,  $k_j^f$ , can also be defined in terms of Arrhenius expression as;

$$k(T) = A \exp\left(\frac{-E_A}{RT}\right) \quad (3.17)$$

where  $A$  is the pre-exponential factor,  $E_A$  is the activation energy, and  $R$  is the general gas constant.

### 3.2.2. Boundary Conditions

Describing a set of boundary conditions for the transport equations given in section 3.2.1 is necessary to develop a model for iCVD system. To determine the velocity, heat transfer, and the concentration distribution of the species, defining accurate process parameters for the reactor boundaries leads to successful coupling of complex physical phenomena. Thus, it helps to define better predictions for the process optimization. Here, Figure 3.2 represents the iCVD reactor schemes used in the study to check the validity of the model with experimental studies. Boundary conditions involving inlet and outlet openings, heated filament array, cooled surface area, and substrate surface are demonstrated for each reactors to figure out the specified conditions for the boundaries. For simplification, auxiliary side ports such as thermocouple and power feedthroughs

were ignored in the model. Details about the reactor geometry and dimensions will be defined in the following sections.

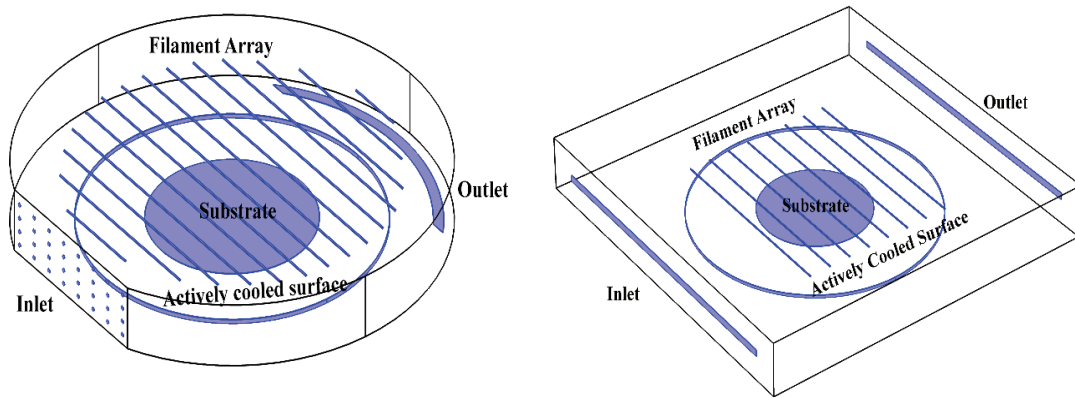


Figure 3.2. Cylindrical and square type iCVD reactor geometries used in the study.

### 3.2.2.1. Fluid Flow Boundary Conditions

On the walls, remaining from the described boundaries, no-slip boundary condition is applied where the fluid velocity is zero.

$$\mathbf{u} = 0 \text{ (no-slip wall)} \quad (3.18)$$

The reactor initial condition and outlet boundary condition are specified with respect to the pressure where;

$$p = P_{total} \text{ (reactor pressure)} \quad (3.19)$$

In iCVD system, flow rates are generally described in unit of “sccm” which stands for the unit of *standard cubic of centimeters per minute*. In our model, to describe the inflow velocity, total flow rate of species,  $F_{total}$ , which involves the flow of monomer, initiator, radical, and inert gas (in the case of patch flow used conditions), is specified as a standard volumetric flow rate in the inflow of the reactor according to the following equation.

$$-\int_{\Omega} \frac{\rho}{\rho_{st}} (\mathbf{u} \cdot \mathbf{n}) dS = Q_{sv} \quad (3.20)$$



In the equation,  $Q_{sv}$  is the standard flow rate, and  $\rho$  is the fluid density at a described temperature. The standard density,  $\rho_{st}$ , is defined by the following equation;

$$\rho_{st} = \frac{p_{st}M_n}{RT_{st}} \quad (3.21)$$

where  $M_n$  is the mean molar mass of the fluid,  $p_{st}$  is the standard pressure,  $R$  is the universal gas constant and  $T_{st}$  is the standard temperature. Therefore, the boundary conditions for the velocity vector at the inlet boundary are given by;

$$-\mathbf{n} \cdot \mathbf{u} = u_{in} \quad (3.22)$$

$$\mathbf{n} \times \mathbf{u} = \mathbf{0} \quad (3.23)$$

with  $\mathbf{n}$ , a unit vector normal to the inflow opening.

### 3.2.2.2. Energy Boundary Conditions

In most of the case, using fixed isothermal boundary condition for describing the temperature boundary conditions is a practical way to solve the complexity of the problem although it is not always possible to obtain isothermal conditions in the real experimental studies as in the case of reactor side walls. Thus, as a result of heat transfer with their surroundings, temperature distribution can be modeled in detail by taking consideration of heat conduction with respect to material type; conductive, radiative and convective heat transfer between reactor gases, walls and surroundings. Here, in this model, to simplify the energy related equations, isothermal temperature ( $T = T_0$ ) boundary condition is prescribed for the inflow, substrate surface, filaments, and the reactor walls for a given geometry through the equations of (3.24)-(3.27). It is worth to mention that substrate, which is placed on the actively cooled surface, is assumed to be contact well with the cooled surface. Therefore, substrate temperature equals to temperature of actively cooled surface area.

$$T = T_{inlet} \text{ (Temperature at the inlet boundary)} \quad (3.24)$$

$$T = T_{filament} \text{ (Temperature of filament wires)} \quad (3.25)$$

$$T = T_{substrate} \text{ (Temperature of substrate surface)} \quad (3.26)$$

$$T = T_{wall} \text{ (Temperature of reactor wall)} \quad (3.27)$$

Thermal insulation, where the no heat flux across the boundary given by;

$$\mathbf{n} \cdot (k\nabla T) = 0 \quad (3.28)$$

is applied for the top of reactor surface and for the bottom surface around the actively cooled area. At outlet boundary, Eq. (3.29) is applied;

$$-\mathbf{n} \cdot \mathbf{q} = 0 \quad (3.29)$$

which states that the only heat transfer over a boundary is by convection.

### 3.2.2.3. Mass Transport Boundary Conditions

Initial and inlet boundary conditions are described using mass fractions of species. In the model, inert gas (if exists) is used for the constraint element and mass fraction of the remaining species is calculated by;

$$w_1 = 1 - \sum_{i=2}^Q w_i \quad (3.30)$$

Inward mass flux is defined over the filaments for decomposition reactions of initiator by;

$$-\mathbf{n} \cdot (\rho w_i \mathbf{u} + \mathbf{j}_i) = N_{0,i} \quad (3.31)$$

Outflow boundary is defined by;

$$-\mathbf{n} \cdot \rho \mathbf{w}_i \sum_k D_{ik} \mathbf{d}_{ik} = 0 \quad (3.32)$$

### 3.2.2.4. Surface Polymerization Conditions

Before describing the surface boundary conditions in the model, it is useful to remember that surface reactions in iCVD polymerization are analogous to the radical polymerization steps in bulk phase (Lau and Gleason, 2006a, 2006b) which makes kinetic equations below applicable to the iCVD polymerization,

$$R_p = k_p [M][M.] \quad (3.33)$$

$$R_i = k_i [M][R.] \quad (3.34)$$

$$v_i = \frac{R_p}{R_i} = \frac{k_p [M][M.]}{k_i [M][R.]} \quad (3.35)$$

where the expressions of rate of polymerization,  $R_p$ , the rate of initiation,  $R_i$ , and kinetic chain length,  $v_i$ , are specified in terms of monomer surface concentration,  $[M]$ , the polymer radical concentration,  $[M.]$ , and the primary radical concentration,  $[R.]$  on the surface. In the equations above,  $[M]$ , adsorbed monomer concentration term is calculated using Eq. (3.36) of which derivation is demonstrated in previous chapter in detail. In the equation, terms  $\rho_M$  and  $MW_M$  are the density and the molecular weight of the monomer, respectively;  $c$  term is the BET constant, which is obtained from BET equation fitted to QCM adsorption measurements;  $P_{sat}$ , is the saturation pressure of the monomer, and  $P_M$ , is the monomer partial pressure varying through the reactor inlet and outlet boundaries as a function of flow rate, composition, temperature, and pressure of the gas mixture.

$$[M] = \frac{\rho_M}{MW_M} \cdot c \cdot \frac{P_M(x, y, z)}{P_{sat}} \quad (3.36)$$

In order to derive the overall rate of polymerization implicitly, making a pseudo steady state approximation on the active radical intermediates is a common way used in the literature since it is almost impossible to measure radical concentrations on the substrate surface experimentally (Lau and Gleason, 2006b). In previous literature studies, this circumstance is overcome by defining ‘r’ parameter which represents the rate of appearance of primary radical adsorbed on the surface that eventually get consumed by surface initiation, primary radical termination, and primary radical recombination reactions. Detailed reaction mechanism and underlying assumptions can be found in literature (Lau and Gleason, 2006b; Odian, 2004).

Unlike the studies, in the presented model, the numerical value of any described parameter and/or variable, which is evaluated in the coupled governing equations, can be obtained at any point of x, y, z directions in reactor geometry and can be simulated using a computational program. Since model gives the numerical value of gas phase monomer and radical concentrations, it is assumed that all radical species, get diffused and just present above the prescribed substrate surface are consumed by initiation, primary radical termination and recombination surface reactions as expressed in Eq. (3.37). Therefore, to find the unknown parameters of [R.] and [M.], expressions for [R.] and [M.] represented by Eq. (3.37) and Eq. (3.38) can be solved simultaneously for the surface boundary, which is the cooled substrate surface placed in the middle of actively cooled surface area.

[R.] balance:

$$k_d[R]_{gas} = \underbrace{k_i[M][R.]}_{initiation} + \underbrace{k'_t[M.][R.]}_{radical\ combination} + \underbrace{2k''_t[R.]^2}_{radical\ recombination} \quad (3.37)$$

[M.] balance:

$$\underbrace{k_i[M][R.]}_{initiation} = \underbrace{2k_t[M.]^2}_{termination} + \underbrace{k'_t[R.][M.]}_{radical\ combination} \quad (3.38)$$

Calculated [M.] value is then substituted in Eq. (3.33) to obtain the rate of polymerization,  $R_p$ , or in other words, to find the rate of consumption of monomer the concentration on the surface. Defining  $R_p$  term also leads to find deposition rate (DR) over the surface as expressed in Eq. (3.39).

$$DR = \frac{R_p h_{ml} MW_M}{\rho_p} \quad (3.39)$$

In the equation above,  $R_p$  (SI unit: mole/(L.s)) is the rate of polymerization,  $h_{ml}$  (SI unit: cm) is the monolayer thickness derived from BET equation,  $MW_M$  (SI unit: g/mole) is the molecular weight of monomer,  $\rho_p$  (SI unit: g/cm<sup>3</sup>) is the polymer density.

### 3.2.2.5. Properties of Gas Mixtures

Gas mixture properties, where  $\rho$  (SI unit: g/cm<sup>3</sup>) is the mixture density,  $k$  (SI unit: W/(m.K)) is the thermal conductivity,  $\mu$  (SI unit: Pa.s) is the dynamic viscosity, and  $c_p$  (SI unit: J/(kg.K)) is the heat capacity at constant pressure are calculated using concentrations ( $c_i$ ) and molar mass ( $M_i$ ) of species according to the expressions given below.

$$\rho = \sum_i c_i M_i \quad (3.40)$$

$$k = 0.5 \left( \sum_i x_i k_i + \left( \sum_i x_i / k_i \right)^{-1} \right) \quad (3.41)$$

$$\mu = \sum_i^n \frac{\mu_i}{1 + \frac{1}{x_i} \sum_{j=1, j \neq i}^n x_j \varphi_{ij}} \quad (3.42)$$

$$\varphi_{ij} = \frac{[1 + (\mu_i/\mu_j)^{0.5} (M_i/M_j)^{0.25}]^2}{(4\sqrt{2})[1 + M_i/M_j]^{0.5}} \quad (3.43)$$

$$c_p = \sum w_i \frac{c_{p,i}}{M_i} \quad (3.44)$$

### **3.3. Numerical Solution Methods for Solving of Model Equations**

Model described in the previous sections consists of many coupled non-linear equations with boundary conditions, which are very difficult to solve analytically in general. In modeling and computational investigations, models are built to be solved with either non-effective analytical methods as in the case of empirical models or with numerical solutions. Fortunately, thanks to developing computational analysis, applying numerical methods to find approximate solutions of the equations is approved as a practical solution to solve the complex problems. Depending on the complexity of the equations described for the boundaries and the number of iterations, solution time and the accuracy of the prediction can be changed in the numerical solution. There are three common classes of numerical methods which has been generally applied to solve computational fluid dynamic problems appearing in CVD modeling. These are the: (1) Finite Element Method (FEM), (2) Finite Difference Method (FDM), and (3) Finite Volume Method (FVM). All these methods can be applied in a computational programs by a code compiler as in the case of Matlab program, or by building a model via specifying its domains, boundaries, parameters, and allowing to select physics as in the case of Comsol Multiphysics simulation program. Such computational programs make modeling simple for those of models involving complex equations and geometries by eliminating code writing. In a computational program, model development generally begins with forming a spatial dimensions of geometry to describe the boundary conditions, and then improved by describing parameters and physics until the model reaches a sufficient accurate predictions with experimental results.

Here presented model uses finite element analysis to solve the coupled non-linear equations based on sub-division of the continuous domains into finite size, but not necessarily to uniform elements. The entire geometry is divided into several regions; each region having a different element size based on the complexity of the geometry, and the boundary conditions used for that particular region. For every mesh of the elements, integral form of described governing equations are solved together to give an approximation.

### **3.4. Implementation of the Model**

To validate the model, reported experimental conditions of 1H,1H,2H,2H-perfluorodecyl acrylate (PFDA) deposition with *t*-butyl peroxide (TBPO) initiator (Gupta and Gleason, 2006), and butyl acrylate (BA) deposition with *t*-amyl peroxide (TAPO) initiator (Lau and Gleason, 2006b), are applied to the model, respectively. Both of the studies involve rate coefficients of surface polymerization reactions at a constant substrate temperature as well as confirmed deposition rate results at specified experimental conditions. Thus, accuracy of the model is supposed to be proved by comparing the model outputs with reported results for the same geometry and experimental conditions. In addition, using different kind of iCVD reactor and applying different experimental conditions, applicability of the model is also controlled in the presented study.

#### **3.4.1. Model Implementation in a Cylindrical Reactor Geometry**

A three-dimensional cylindrical reactor geometry which has been typically used in literature (Gupta and Gleason, 2006; Lau and Gleason, 2006a, 2006b), is accommodated to validate the model as illustrated in Figure 3.3. Dimensions of reactor geometry, filament number, and the distance between cooled surface and hot filaments are prescribed in the model according to data given in the following subjected studies. Since there is not any clear statement about the inlet and outlet boundaries; in the model, the gas mixture is considered to flow into the reactor through a showerhead consisting of an array of 32 circular openings with a radius of 0.1 cm, and leaves the reactor from a semi-circle shape opening which is placed at the bottom of the reactor. In addition, for simplification auxiliary side ports such as thermocouple and power feedthroughs are neglected and not shown in the simulated geometry.

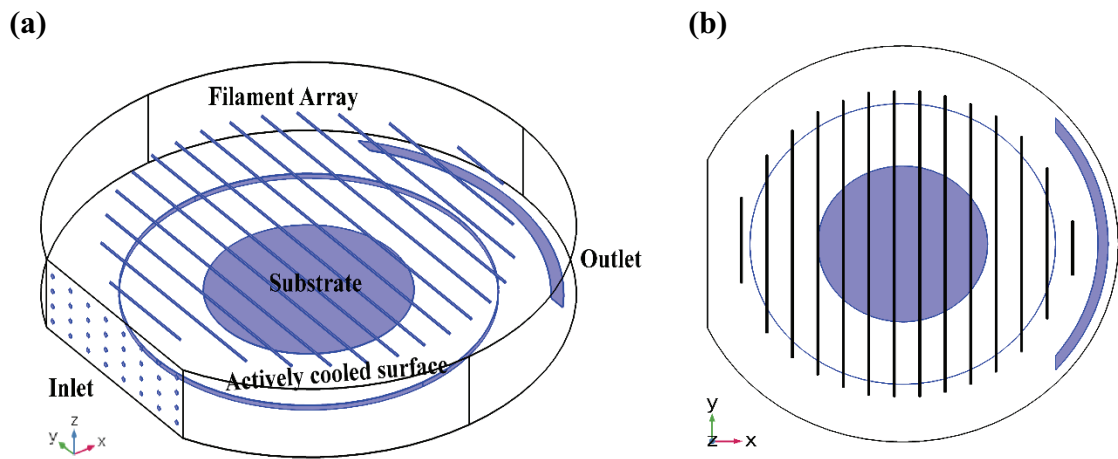


Figure 3.3. Representation of (a) front and (b) top view of cylindrical iCVD reactor geometry.

### 3.4.1.1. Poly (1H,1H,2H,2H-perfluorodecyl Acrylate) Deposition Modeling

1H,1H,2H,2H-perfluorodecyl acrylate (PFDA) deposition modeling of iCVD process is validated by using the same geometrical and experimental conditions of the reported study (Gupta and Gleason, 2006). The cylindrical reactor geometry with a diameter of 24 cm and height of 3.3 cm is used in the model. Although details are not mentioned in the study, an array of filaments consisting of 14 filaments with a diameter of 0.1 cm, spaced 1.5 cm apart and suspended over cooled surface at a distance of 2.9 cm is used in the model. At the bottom of the reactor, a circular area with a diameter of 18 cm is actively cooled and a 100-mm-diameter of wafer to be coated is placed upon it where the temperature is kept constant at 44 °C. In the model; 1H,1H,2H,2H-perfluorodecyl acrylate (PFDA) is used as a monomer together with tert-butyl peroxide (TBPO) initiator. At filament temperature of 300 °C, t-butoxy radical is prescribed as a primary radical species as previously explained in Chapter 2. Table 3.1 represents the process conditions and model parameters which are used in the simulations. The values of monomer and polymer densities are assumed as in the table given below since there is no clear statement about their exact values in the report.



Table 3.1. Selected parameters and variables for PFDA polymerization used in the model.

<b>Parameters</b>	<b>Value</b>	<b>Description</b>
F_monomer	0.67 (sccm)	Monomer flow rate
F_initiator	0.82 (sccm)	Initiator flow rate
MW_monomer	518.17 (g/mol)	Molecular weight of monomer
MW_initiator	146.23 (g/mol)	Molecular weight of initiator
MW_radical	76.115 (g/mol)	Molecular weight of radical
$\rho_{\text{monomer}}$	1 (g/cm <sup>3</sup> )	Monomer density
$\rho_{\text{polymer}}$	1.2 (g/cm <sup>3</sup> )	Polymer density
P_total	0.10 (Torr)	Reactor total pressure
P_sat	0.16 (Torr) @ 44 °C	Saturation pressure of monomer
T_substrate	44 °C	Substrate temperature
T_filament	300 °C	Filament temperature
T_inflow	80 °C	Inflow temperature
T_wall	55 °C	Reactor wall temperature
R_filament	0.05 (cm)	Radius of a filament
R_surface	5 (cm)	Radius of wafer

In order to compare the deposition rate results, flow rate combinations of monomer and initiator species shown in Table 3.2, are used in the model. Deposition conditions were fixed at 0.1 Torr reactor pressure, and 44 °C substrate temperature for each of experimental runs of which kinetic data are represented in Table 3.3 for PFDA film deposition.

Table 3.2. Flow rates of PFDA monomer at a fixed initiator flow rate of 0.82 sccm.

Run number	F_monomer (sccm)
P1	0.67
P2	0.52
P3	0.42
P4	0.35
P5	0.31
P6	0.26
P7	0.13

Table 3.3. Kinetic parameters for PFDA polymerization at 44 °C.  
(Source: Gupta and Gleason, 2006)

Parameters	Value	Description
$k_i$	7494 (L/mol.s)	Initiation rate constant
$k_p$	11418 (L/mol.s)	Propagation rate constant
$k_t$	$2.3 \times 10^4$ (L/mol.s)	Termination rate constant
$k'_t$	$10.66 \times 10^7$ (L/mol.s)	Primary radical termination rate constant
$k''_t$	$1.5 \times 10^9$ (L/mol.s)	Primary radical recombination rate constant
$E_a$	113.0 (kJ/mol)	Activation energy of decomposition reaction
$c$	3.3	BET constant
$h_{mt}$	$1.1755 \times 10^{-7}$ (cm)	Monolayer thickness

### **3.4.1.2. n-Butyl Acrylate Deposition Modeling**

Modeling of n-butyl acrylate (n-BA) polymerization in iCVD process is validated using the same geometrical and experimental conditions of the study reported by Lau and Gleason (2006b). Proposed cylindrical reactor geometry is constructed with a diameter of 25.4 cm (10 in.) and height of 3.175 cm (1.25 in) including an array of filaments consisting of 14 filaments with a diameter of 0.1 cm, spaced 1.5 cm apart and suspended over cooled surface at a distance of 2.5 cm. At the bottom of the reactor, a circular area with a diameter of 18 cm is cooled where the temperature is kept constant at 23 °C. A 100-mm-diameter of surface or wafer to be coated is placed upon the cooled substrate area and the model assumes that the wafer is in good thermal contact with the actively cooled surface. In the model, n-butyl acrylate (nBA) is used as a monomer together with tert-amyl peroxide (TAPO) initiator. Argon gas is used when patch flow is required. At filament temperature of 260 °C, ethyl radical is prescribed as a radical species as previously discussed in Chapter 2. Table 3.4 represents the process conditions and parameters applied to the model.

Table 3.4. Selected parameters and variables for nBA polymerization used in the model.

<b>Parameters</b>	<b>Value</b>	<b>Description</b>
F_monomer	3 (sccm)	Monomer flow rate
F_initiator	0.7 (sccm)	Initiator flow rate
F_argon	0.0 (sccm)	Inert gas flow rate
MW_monomer	128.17 (g/mol)	Molecular weight of monomer
MW_initiator	174.28 (g/mol)	Molecular weight of initiator
MW_argon	39.948 (g/mol)	Molecular weight of inert gas
MW_radical	29.062 (g/mol)	Molecular weight of radical
$\rho_{\text{monomer}}$	0.901 (g/cm <sup>3</sup> )	Monomer density
$\rho_{\text{polymer}}$	1.08 (g/cm <sup>3</sup> )	Polymer density
P_total	1 (Torr)	Reactor total pressure
P_sat	4.85 (Torr) @ 23 °C	Saturation pressure of monomer
T_substrate	23 °C	Substrate temperature
T_filament	260 °C	Filament temperature
T_inflow	80 °C	Inflow temperature
T_wall	40 °C	Reactor wall temperature
R_filament	0.05 (cm)	Radius of a filament
R_surface	5 (cm)	Radius of wafer

Flow rate of species was varied while keeping all other process parameters constant to evaluate the effect of monomer surface concentration on polymer deposition rate as represented in Table 3.5. Similar to experiments performed by Lau and Gleason (2006b), total gas flow rate was kept constant at 3.70 sccm, and reactor pressure was fixed at 1 Torr in the proposed model. Since kinetic data represented in Table 3.6 are available for the substrate temperature of 23 °C, all calculations were performed at a fixed substrate temperature for BA polymerization.

Table 3.5. Monomer (BA), initiator (TAPO) and carrier gas flow rates for nBA polymerization.

Run number	F_monomer (sccm)	F_initiator (sccm)	F_argon (sccm)
B1	3.00	0.70	0.00
B2	2.50	0.58	0.62
B3	2.00	0.47	1.23
B4	1.50	0.35	1.85
B5	1.00	0.23	2.47
B6	0.75	0.18	2.77
B7	0.50	0.12	3.08

Table 3.6. Kinetic parameters for nBA polymerization at 23°C.  
(Source: Lau and Gleason, 2006b)

Parameters	Value	Description
$k_i$	4990 (L/mol.s)	Initiation rate constant
$k_p$	15540 (L/mol.s)	Propagation rate constant
$k_t$	$0.98 \times 10^6$ (L/mol.s)	Termination rate constant
$k'_t$	$6.89 \times 10^7$ (L/mol.s)	Primary radical termination rate constant
$k''_t$	$7.41 \times 10^8$ (L/mol.s)	Primary radical recombination rate constant
$E_a$	74.6 kJ/mol	Activation energy of decomposition reaction
$c$	2.536	BET constant
$h_{ml}$	$1.31775 \times 10^{-7}$ (cm)	Monolayer thickness

### 3.4.2. Model Implementation in a Square Type Reactor Geometry

Model accuracy is also validated by experiments, at different process conditions, carried out using our custom-built, square type of iCVD reactor. This time iCVD polymerization is performed using Butyl acrylate (nBA) monomer with tert-butyl peroxide (TBPO) initiator. In order to use the same kinetic data exist for the BA polymerization (which is shown in Table 3.3), substrate temperature is kept constant at 23 °C. Details about the iCVD procedure for BA polymerization are given in the following section.

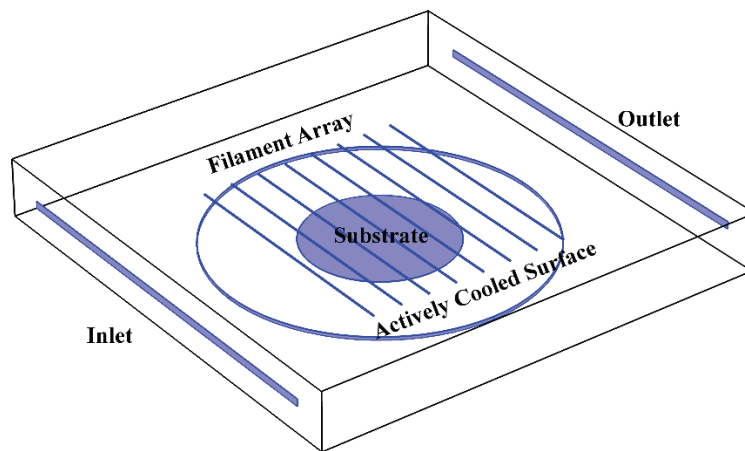


Figure 3.4. Square type iCVD reactor geometry used in the study.

The square type of reactor geometry with 31.6 cm width and 4 cm height was used in the computational model. The reactor geometry involves inlet and outlet slits 26.7 cm in width and 0.5 cm in height. At the bottom of the reactor, there is an actively cooled surface where a 100-mm- diameter of substrate is placed. The filament array, consists of 8 filaments with a diameter of 0.1 cm and spaced 2 cm apart, is suspended over substrate at a distance of 2.5 cm. Table 3.7 represents the process conditions and model parameters used in the computational simulations.

Table 3.7. Selected parameters and variables for nBA polymerization with TBPO initiator.

Parameters	Value	Description
F_monomer	3 (sccm)	Monomer flow rate
F_initiator	0.7 (sccm)	Initiator flow rate
MW_monomer	128.17 (g/mol)	Molecular weight of monomer
MW_initiator	146.23 (g/mol)	Molecular weight of initiator
MW_radical	76.115 (g/mol)	Molecular weight of radical
$\rho_{\text{monomer}}$	0.901 (g/cm <sup>3</sup> )	Monomer density
$\rho_{\text{polymer}}$	1.08 (g/cm <sup>3</sup> )	Polymer density
P_total	1 (Torr)	Reactor total pressure
P_sat	4.85 (Torr) @ 23 °C	Saturation pressure of monomer
T_substrate	23 °C	Substrate temperature
T_filament	300 °C	Filament temperature
T_inflow	80 °C	Inflow temperature
T_wall	40 °C	Reactor wall temperature
R_filament	0.05 (cm)	Radius of a filament
R_surface	5 (cm)	Radius of deposition area

Table 3.8 shows the flow rate combinations of monomer, initiator, and nitrogen species used in the model. Each run performed at 1 Torr reactor pressure, at 23 °C constant substrate temperature while keeping all other process parameters constant in order to compare the deposition rate results. Since depositions carried out at constant substrate temperature, kinetic data presented in Table 3.6 is used for BA film deposition in which activation energy of decomposition reaction is described as 113.0 kJ/mole for TBPO initiator.

Table 3.8. Flow rates of monomer and initiator for nBA polymerization.

<b>Run number</b>	<b>F_monomer (sccm)</b>	<b>F_initiator (sccm)</b>
E1	4.00	0.5
E2	3.50	0.5
E3	3.00	0.7
E4	3.80	1.1

### 3.4.2.1. iCVD Process

To perform the butyl acrylate iCVD polymerization, n-Butyl acrylate (nBA) monomer with >97% purity, and *tert*-butyl peroxide (TBPO) initiator with 97% purity were purchased from Sigma-Aldrich and used as received without further purification. Deposition studies carried out using our custom-built, square type of iCVD reactor, which has 31.6 cm width and 4 cm height dimensions, and has a removable transparent quartz top (2.5 cm thick) allowing visual inspection. At the bottom of the reactor, 100-mm-diameter of silicon wafers to be coated placed on a backside cooled stage, with a radius of 12 cm, and the stage temperature was kept constant at 23 °C using water from a recirculating chiller (WiseCircu WCR-P8). Besides, reactor surrounding walls was heated to 40 °C using heating tapes in order to promote adsorption of species only onto cooled substrate surface. Inside the reactor, an array of NiCr (80% Ni/20% Cr) filaments, consisting of 8 filaments spaced 2 cm apart and suspended over the silicon substrate at a distance of 2.5 cm, was resistively heated to the required filament temperature using an AC power supply in order to provide thermal energy for decomposition of initiator. The actual temperature of the filaments was measured by a K-type thermocouple (Omega Engineering) by carefully attaching it to the filament assembly, touching at one point. Both nBA monomer and TBPO initiator were fed into the reactor at room temperature, without further heating, through mass flow controllers, MKS Instrument-Model 1152C and Model 1479A, respectively. Precursor gases were mixed in a separate chamber before



entering the reactor. All gas lines and mixing chamber was kept at 75 °C via silicon based heating tapes controlled by PID controllers (TK4 series, Autonics). Reactor pressure was kept constant at 1 Torr which was controlled by using a downstream throttle valve (MKS-253B) together with a Baratron capacitance manometer (MKS- 627D) connected to a pressure controller (MKS- 651C), and reactor vacuum was provided by rotary vane pump (2XZ-Rotary Vacuum Pump). Figure 3.5 shows the setup of the custom-built iCVD reactor.

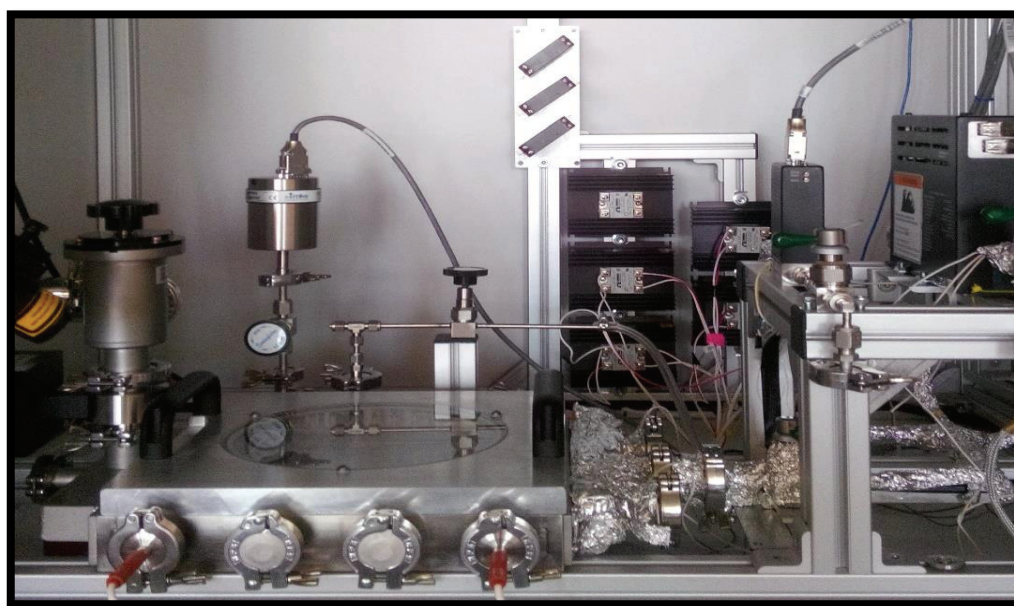


Figure 3.5. Custom-built square type of iCVD reactor used for polymerization of nBA with TBPO initiator.

## CHAPTER 4

### RESULTS AND DISCUSSION

In previous chapter, a mathematical model, which includes the governing transport equations with specified boundary conditions, is developed by making some assumptions in order to simplify and to describe the transport phenomena occurring in iCVD process. Here, in this chapter, by applying a computational program based on the finite element analysis, it is first aimed to check the accuracy of the developed model by comparing computational model predictions with the reported experimental results of deposition rate; then to analyze the governing transport phenomena inside the reactor geometry, and show the effects of process conditions on film deposition rate. To be able to do this, two reported studies both of which involve experimental conditions, deposition results, and confirmed kinetic data, which are presented in previous chapter, are used and computed in a software platform to validate the model accuracy. In addition to this, model applicability is also checked for different reactor shape and conditions of which experiments are carried out in our home-made square type of reactor.

In order to better understand of underlying transport phenomena of deposition process, in the representation of the figures; gas phase mixture velocity, heat, and species concentration distribution are shown in a three-dimensional reactor geometry. It is worth to note that in the figures, flow direction is from left to right unless otherwise indicated. In addition, simulation results of deposition rates, which are given in tables in following sections, represent the average film growth rate of a 100-mm-diameter of wafer.

#### **4.1. Model Implementation in Cylindrical Type of Reactor Geometry**

Since the two of reported studies, which were mentioned in previous chapter, carried out in a typical cylindrical iCVD reactor, the model validation is simulated using the reported dimensions of described reactor geometry for both 1H,1H,2H,2H-perfluorodecyl acrylate (PFDA) and n-butyl acrylate (BA) film depositions.

### 4.1.1. Model Validation for PFDA Polymerization

In order to obtain a reliable model describing transport phenomena and film deposition in iCVD process, it is first aimed to check the model accuracy for poly (1H,1H,2H,2H-perfluorodecyl acrylate) p(PFDA) film deposition with TBPO initiator, of which iCVD process conditions and kinetic data have already been given in previous chapter in detail. Table 4.1 shows the deposition rate for each of reported experimental run which are performed at constant reactor pressure ( $P_{\text{reactor}}$ : 0.10 Torr) and substrate temperature ( $T_{\text{substrate}}$ : 44 °C). Since deposition takes place on the substrate surface and all of the experiments carried out at constant substrate temperature, the same polymerization steps with the same rate of polymerization coefficients occur for the film depositions. Therefore, according to the rate of deposition results given in table below, at fixed process conditions, it can be concluded that the higher the monomer partial pressure yields to higher film deposition rate.

Table 4.1. Reported process conditions and experimental deposition rates of PFDA polymerization in iCVD process at constant initiator flow rate of 0.82 sccm. (Source: Gupta and Gleason, 2006)

Experimental Run	F_monomer (sccm)	$P_M/P_{\text{sat}}$	DR_measured (nm/min)
P1	0.67	0.28	375
P2	0.52	0.24	259
P3	0.42	0.21	150
P4	0.35	0.18	88
P5	0.31	0.17	72
P6	0.26	0.15	55
P7	0.13	0.08	22

The developed model involves reactor geometry with defined boundaries, general transport equations, prescribed process parameters, and kinetic data for describing the PFDA film deposition in iCVD process. Details about the model geometry and boundary conditions were explained in previous chapter. Using data given in Table 3.1-3.3, the

computational study was carried out in a cylindrical reactor geometry considering that steady-state conditions exist.

As stated before, the presented model employs detailed diffusion mechanism to describe the multicomponent gas phase diffusion. For multiple component systems, Maxwell-Stefan diffusivity matrix is described in which Maxwell-Stefan diffusivities of all component pairs are required to be known in the computational software to calculate the multicomponent Fick diffusivities. For a gas mixture involving  $Q$  species, for example, the Maxwell-Stefan diffusivity matrix is a  $Q$ -by- $Q$  symmetric matrix, where the diagonal components are unity. In the presented model, the gas mixture in the reactor consists of PFDA, TBPO, and tert-butoxy radical species. Since data are not available in literature for the diffusivities of gas pairs of prescribed species in the presented conditions, it is assumed that each species have the same diffusional behavior in other gas species environment. Therefore, in the Maxwell-Stefan diffusivity matrix, all species diffusivities are taken as a constant value. It is obvious that this is not an accurate approach for diffusivity predictions, but, it is preferred since it requires much less computational effort and reduces the total number of iterations required to obtain a converged solution.

Since diffusion coefficient of a gas molecules is typically in the range of  $1e-6$  and  $1e-5$   $m^2/s$  (Web1), predicted deposition rates of PFDA polymerization with TBPO initiator are represented at  $D_{ik}$  value of  $1e-5$ ,  $5e-5$ , and  $1e-6$   $m^2/s$  at given experimental conditions of iCVD process, as shown in Table 4.2. In the table, at given process conditions, DR values, which were experimentally found and reported in literature, are labeled as 'DR\_measured', while of those obtained from simulation outputs labeled as 'DR\_predicted'. In addition, predicted value of deposition rates represent the average film growth rate over a 100-mm-diameter of substrate.

Table 4.2. Comparison of experimental results of deposition rates with model predictions at different Maxwell-Stefan diffusivities.

Run number	$P_M/P_{sat}$	DR_measured (nm/min)	DR_predicted (nm/min)		
			$D_{ik} 1e-5$ ( $m^2/s$ )	$D_{ik} 5e-5$ ( $m^2/s$ )	$D_{ik} 1e-6$ ( $m^2/s$ )
P1	0.28	375	457.20	423.27	955.23
P2	0.24	259	282.89	266.75	568.17
P3	0.21	150	188.31	179.48	363.89
P4	0.18	88	132.79	127.41	248.16
P5	0.17	72	105.13	101.23	192.28
P6	0.15	55	74.84	72.364	132.91
P7	0.08	22	19.34	18.877	31.43

As experimental and predicted values of deposition rate are compared for each deposition conditions, close prediction is obtained for predicted deposition rate at  $D_{ik}$  value of  $5e-5 m^2/s$  rather than  $1e-6 m^2/s$ . Thus, for further analysis of the model simulation outputs, the value of  $5e-5 m^2/s$  is selected and used for describing the diffusivities of species pairs in the comparison of model predictions with experimental results. Figure 4.1 shows the deposition rates obtained from simulation at  $D_{ik}$  value of  $5e-5 m^2/s$  as well as reported DR values at various  $P_M/P_{sat}$ .

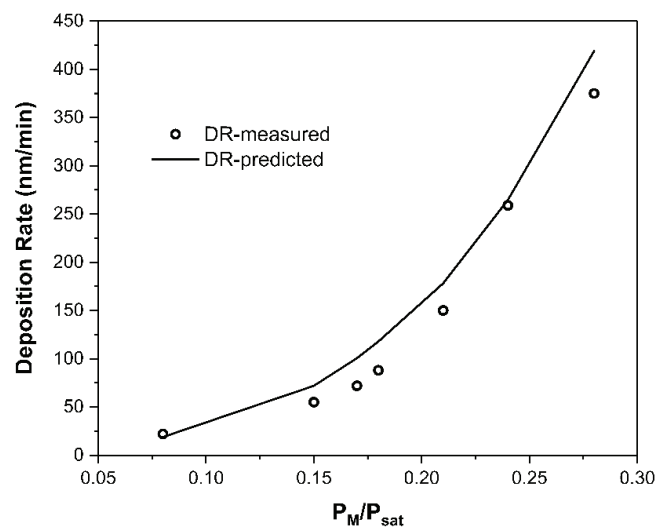


Figure 4.1. Comparison of experimental and predicted deposition rates at  $D_{ik}: 5e-5 m^2/s$  with respect to  $P_M/P_{sat}$ .

As model predictions and experimental results are compared in detail, it can be seen that model over-predicts the growth rate which may be possibly resulted from small errors caused by the approaches and/or assumptions through the calculation of gas phase mixture properties, such as assuming that all component pairs having equal mass diffusivities to describe gas diffusion behavior. In addition, it is worth to note that in the figure given above, fixed values of  $P_M/P_{sat}$ , which are given in Table 4.1, are used to compare the predicted and measured deposition rates. However, in the study of Gupta and Gleason (2006), these ratio are calculated according to the Eq. (1.7) assuming that monomer flow rate is constant at every point of the reactor geometry. This approach can be assumed to be practical; but not realistic, due to the bulk motion existence during the film deposition which is also the reason of observed thickness variation on the substrate in deposition experiments. For this reason, model prediction of  $P_M/P_{sat}$  is not expected to be fixed as employed in the literature due to the change of precursor flow along the reactor. This assumption, therefore, makes a difference in the calculation of experimental and prediction values of DR. In the explanation of the differences, it is also worth to note that no information exists for the substrate location and thickness measurement. It is obvious that film thickness, and also deposition rate, strongly depend on substrate size and location, and how the thickness measurements are taken i.e., number of measurement points, calculation method etc. As a result, lack of knowledge about these issues will bring some uncertainty in the comparison of deposition rates. In the model, to minimize the uncertainty resulted from substrate location inside the geometry, a circular wafer which has the maximum substrate size of  $78.5 \text{ cm}^2$  is assumed to be located at the center of the reactor. Therefore, a reliable prediction of experimental thickness measurement can be predicted more precisely by assuming that film thickness measurement could be taken at any point of described surface area. In simulation results, deposition rate is averaged for the entire substrate surface instead of a single location reading. It is obvious that averaging deposition rate value for the substrate size of  $78.5 \text{ cm}^2$  leads to significant differences instead of a single location measurement in the comparison of deposition rate. Although some differences are present between model prediction and experimental results, the trend of film growth rate is similar and the qualitative aspects are reflecting the process correctly.

For a 100-mm-diameter of wafer, the simulation result of film deposition rate is represented in Figure 4.2 for the process conditions of P4 of which deposition condition was described in Table 4.1.

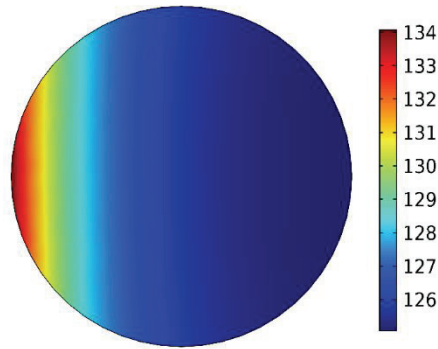


Figure 4.2. Predicted film deposition rate (nm/min) on substrate surface at process conditions of P4.

It can be seen that, while the deposition rate (or film thickness) decreases on the substrate surface along the flow direction (x-axis). Although there is a slight change in DR at the region of the wafer close to the inlet boundary, for the right half of the substrate surface, almost uniform film is achieved. It should also be mentioned that, for a given process conditions, the figure below shows the rate of deposition at steady-state conditions. However, for the long-lasting depositions, such as for a deposition longer than 30 minutes, thickness variation along the flow direction can be significant since final film thickness is determined by deposition time. Rate of film deposition variation through the midline of substrate surface is demonstrated in Figure 4.3 for all experimental runs of which deposition conditions represented in Table 4.1.

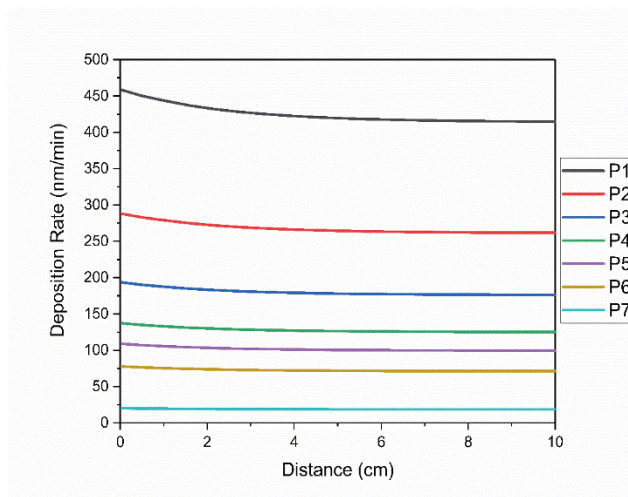


Figure 4.3. Predicted deposition rates at midline of the substrate surface.

It is apparent from figure that deposition rate is almost constant along the flow direction for experimental conditions of P4-P7 while it is slightly higher for P1-P3 at the regions of substrate close to the inlet boundary. The decreasing on average deposition rate

from P1 to P7 follows the trend of  $P_M/P_{sat}$ , i.e, monomer flow rate, since initiator flow rate is fixed as indicated in Table 4.1. Both of Figures 4.2 and 4.3 indicate that for an industrial standard of substrate, right half of the reactor will be appropriate for substrate location to obtain uniform film thickness.

As described in previous chapter, deposition rate is a function of rate of polymerization,  $R_p$ , which is directly related to monomer surface concentration,  $[M]$ , and the polymer radical concentration,  $[M\cdot]$ , on the surface. In order to calculate  $R_p$  value, both  $[M\cdot]$  and the primary radical concentration,  $[R\cdot]$ , are needed to be defined by solving Eq. (3.37) and Eq. (3.38) together according to pseudo-steady state assumption on the surface. Figure 4.4 shows the rate of polymerization ( $R_p$ ), which is determined by calculating those of non-linear equations applying finite element procedure, as well as rate of deposition (DR). Since simulated results are represented for the average value of whole substrate surface,  $R_p$  is not directly proportional with DR.

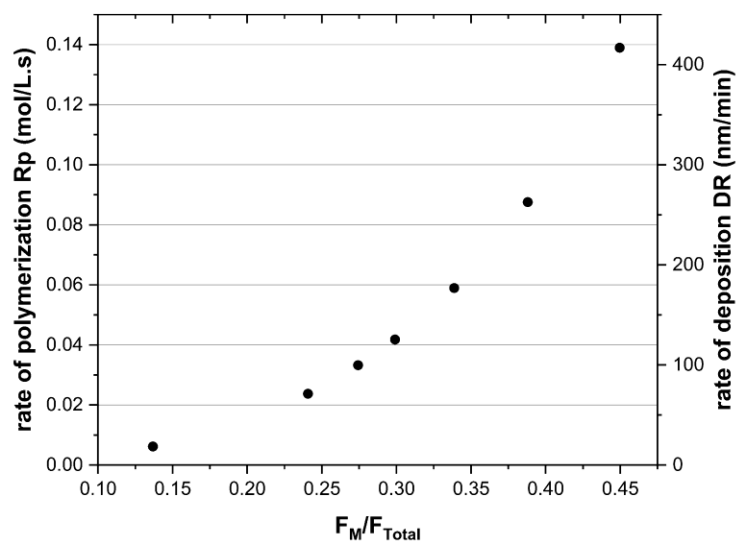


Figure 4.4. Predicted surface average rate of polymerization ( $R_p$ ), and deposition rate (DR) at process conditions given in Table 4.1.

Figure 4.5 shows the surface monomer  $[M]$ , surface radical  $[R\cdot]$ , and active polymer  $[M\cdot]$ , concentrations through the midline of substrate surface. In the figure adsorbed radical concentration increases along the midline of the substrate which may possibly resulted from gas phase convective diffusion of the radical species present right above the substrate surface. On the other hand, active polymer concentration slightly decreases along the midline of the substrate due to its consumption in propagation and termination steps during the polymerization.



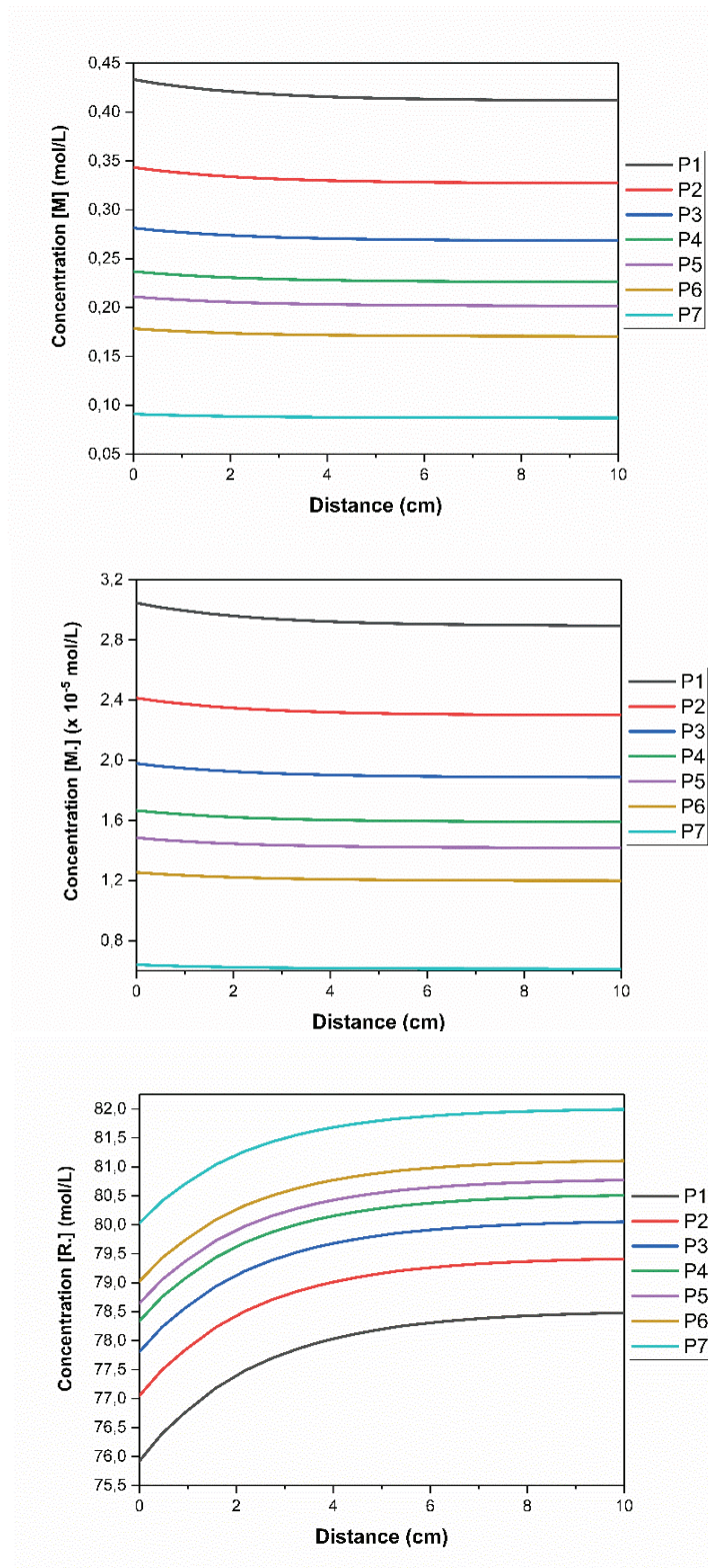


Figure 4.5. From top to bottom: surface monomer  $[M]$ , active polymer  $[M.]$ , and surface radical  $[R.]$  concentrations at midline on substrate surface for all deposition conditions given in Table 4.1.

It is obvious that obtaining a reasonable prediction of film thickness is strongly related to the successful coupling of transport phenomena in the reactor as well as making appropriate simplifications or assumptions to reduce the complexity of the model. Because of the good agreement between model predictions and experimental thickness measurements, underlying transport phenomena (gas phase fluid flow, heat and concentration distributions) will be explained in detail.

Figure 4.6 shows the velocity profile in a three-dimensional cylindrical type of iCVD geometry for the process conditions of P2 given in Table 4.1. In the figure, for the entire volume of reactor, slices placed apart at a distance of 1.4 cm in y-axis. The mixture of monomer (PFDA) and initiator (TBPO) species are delivered into the reactor through an array of circular inlet openings, and leave the reactor at a semi-circular opening which is placed at the bottom of the reactor. Apart from the inlet openings and outlet boundary, as flow moves along the reactor, the mixture velocity does not change significantly at given flow rates and vacuum conditions, and velocity is zero at the walls of the reactor due to the no-slip condition.

As stated before, two-different temperature regions present in iCVD reactor. One of which is heated filaments where the initiator molecules decompose to form radical species, and the other one is the substrate surface of which temperature is kept cooled in order to promote the adsorption of the species. Figure 4.7 shows the temperature distribution for the deposition conditions of P2 given in Table 4.1. In the model, inlet temperature of precursor mixture is described as 80 °C (353.15 K). Inside the reactor, filament temperature is fixed at 300 °C (573 K) while the substrate surface is at 44 °C (317 K). As expected, maximum temperature is seen at the top of the reactor which is close to the heated filament array, and minimum temperature is observed at the cooled surface. As flow moves between those regions, temperature varies as a result of bulk motion and diffusion of the molecules. Since total flow rates are almost the same in the experimental runs, and temperatures which are described for the boundaries are fixed, similar temperature profiles are observed for other experimental conditions.

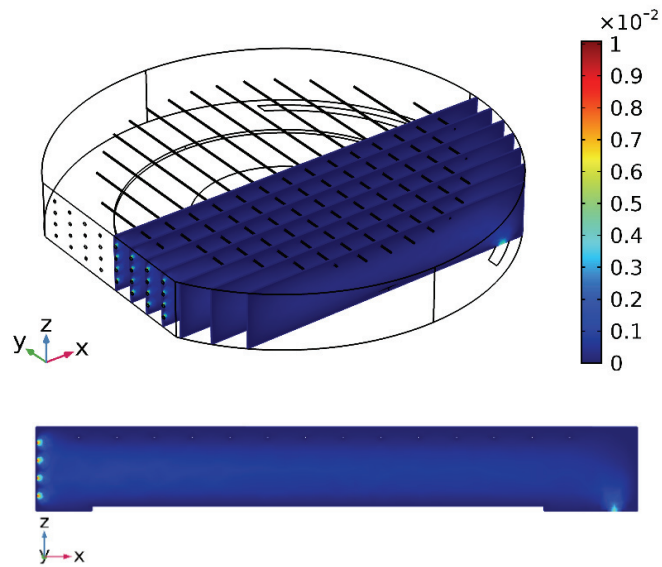


Figure 4.6. Model prediction of velocity distribution (SI unit: m/s) for P2 inside iCVD reactor (top), and detailed view of velocity distribution at the midline of the reactor (bottom).

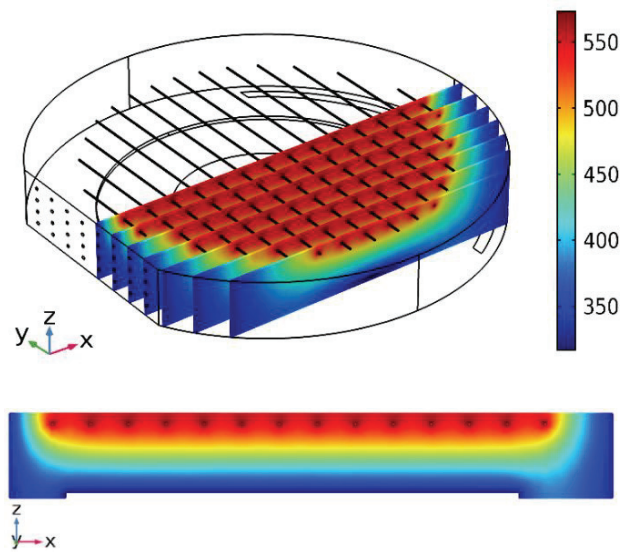


Figure 4.7. Model prediction of temperature distribution (SI unit: K) for P2 in iCVD reactor (top), and detailed view of temperature distribution at the midline of the reactor (bottom).

Accurate predictions and/or well-coupling of flow, heat, and mass transport of all species calculated through the governing equations will lead to better control of the process, and final film properties. Inside the reactor geometry, chemical species movement is not only resulted from the convection applied by fluid flow, but also resulted from the diffusion caused by the uneven concentrations as stated by the Fick's Law

represented in Eq. (3.6). For the Cartesian coordinate system, as flow moves along the reactor, concentration of species will change in x, y, z directions with respect to species flow rate, pressure, temperature, and reactions. Inside the reactor geometry, it is assumed that one mole of initiator molecule decomposes to form two moles of radical species at the vicinity of the filaments while monomer species do not involve in any chemical reactions in the gas phase. It is important to highlight that at described filament temperature, the primary radical that was formed by the decomposition of TBPO initiator is *t*-butoxy radical addition to methyl radical existence as previously stated in Chapter 2.2. Since methyl radicals have high volatility, it was observed that methyl radical did not involve in film deposition (Ozaydin-Ince, 2009). Therefore, in the presented study, TBPO initiator is assumed to thermally decompose to form only *t*-butoxy radicals.

Figure 4.8 shows the concentration distribution of monomer (top), initiator (middle), and primary radical (bottom) species as mole fractions for the deposition conditions of P2 given in Table 4.1. In the figures, mole fraction distribution is shown by multiple slices for the half of reactor geometry in which slices placed 3 cm apart from each other in *y*-axis, and as a cross-sectional area which is placed at *y*=0.3 axis. Visualizing the species concentration distribution in a three dimensional reactor geometry enables to understand how introduced and formed species distribution change in reactor chamber. Since deposition rate strongly depends on the gas phase monomer and radical concentration and/or partial pressures of species right above the substrate surface, species' concentration distribution also affect the film uniformity on the substrate surface. It is expected that monomer species do not involve in any chemical reaction in the gas phase, and its mole fraction is controlled by the mole fraction of other species inside the vacuum chamber since sum of all species mole fraction should be equal to one. According to the Figure 4.8 (a), gas phase monomer mole fraction is 0.12 at the inlet boundary and slightly changes to 0.09 above the top of filament array and close to the outlet boundary due to the fraction changes resulted from the thermal decomposition of initiator species. In addition, as represented in Figure 4.8 (b), mole fraction of the initiator species is 0.5 and maximum at the inlet boundary, and goes to zero at the vicinity of filament array due to fast thermal decomposition reaction. On the other hand, radical mole fraction, which is shown in Figure 4.8 (c), follows the inverse trend of thermal decomposition of initiator, and reaches maximum value on the filaments as expected. It is worth to note that, although radical formation is zero at the inlet openings, presence of radical species is observed at

the inlet boundary wall as shown in the Figure 4.8 (c) which may possibly resulted from fast decomposition reaction of TBPO.

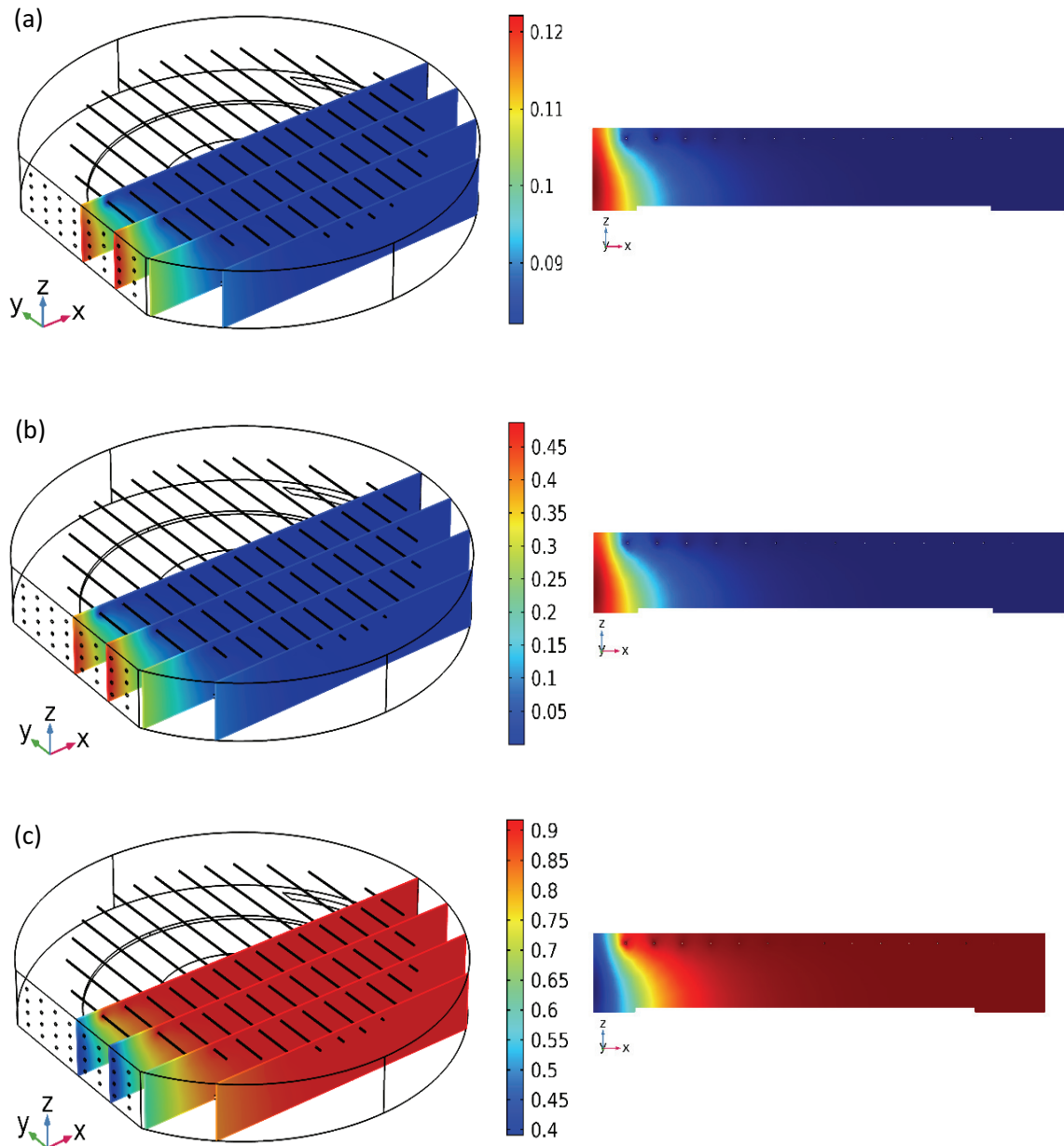


Figure 4.8. Predicted mole fraction variations of (a) monomer, (b) initiator, and (c) radical species along the flow direction for P2.

For the experiments given in Table 4.1, inlet monomer flow rates are changed while initiator flow rates are fixed. In addition, due to the decomposition reaction of the initiator, species mole fractions inside the reactor are expected to change along the flow direction as a result of convective and diffusive transport of species. Figure 4.10 shows

the mole fraction distribution of species for all experimental runs, of which deposition conditions are given in Table 4.1, through the midline at a distance of 1.5 cm above the surface as represented in Figure 4.9.

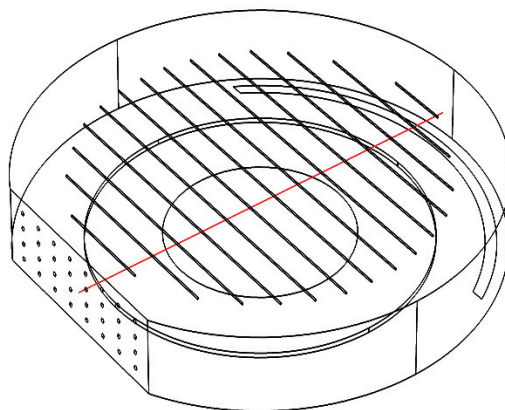


Figure 4.9. Representation of midline at a distance of 1.5 cm above the surface.

As shown in the plots in Figure 4.10, inlet initiator mole fraction is fixed and almost value of 0.5 while the monomer inlet mole fraction changes. Simulated mole fractions are given for the midline from inlet to outlet boundary as represented in Figure 4.9. However, it is worth to note that starting point of the midline is not from inlet opening, it is from a point of inlet wall. As a result of this, mole fractions of primary radical species are determined as close to value of 0.4 for all experimental conditions, which may be due to the diffusion of initiator species and fast decomposition reaction of molecules at heated region. On the other hand, at outlet boundary of the geometry, outlet stream does not involve significant amount of initiator species since almost all of them are converted to radicals.

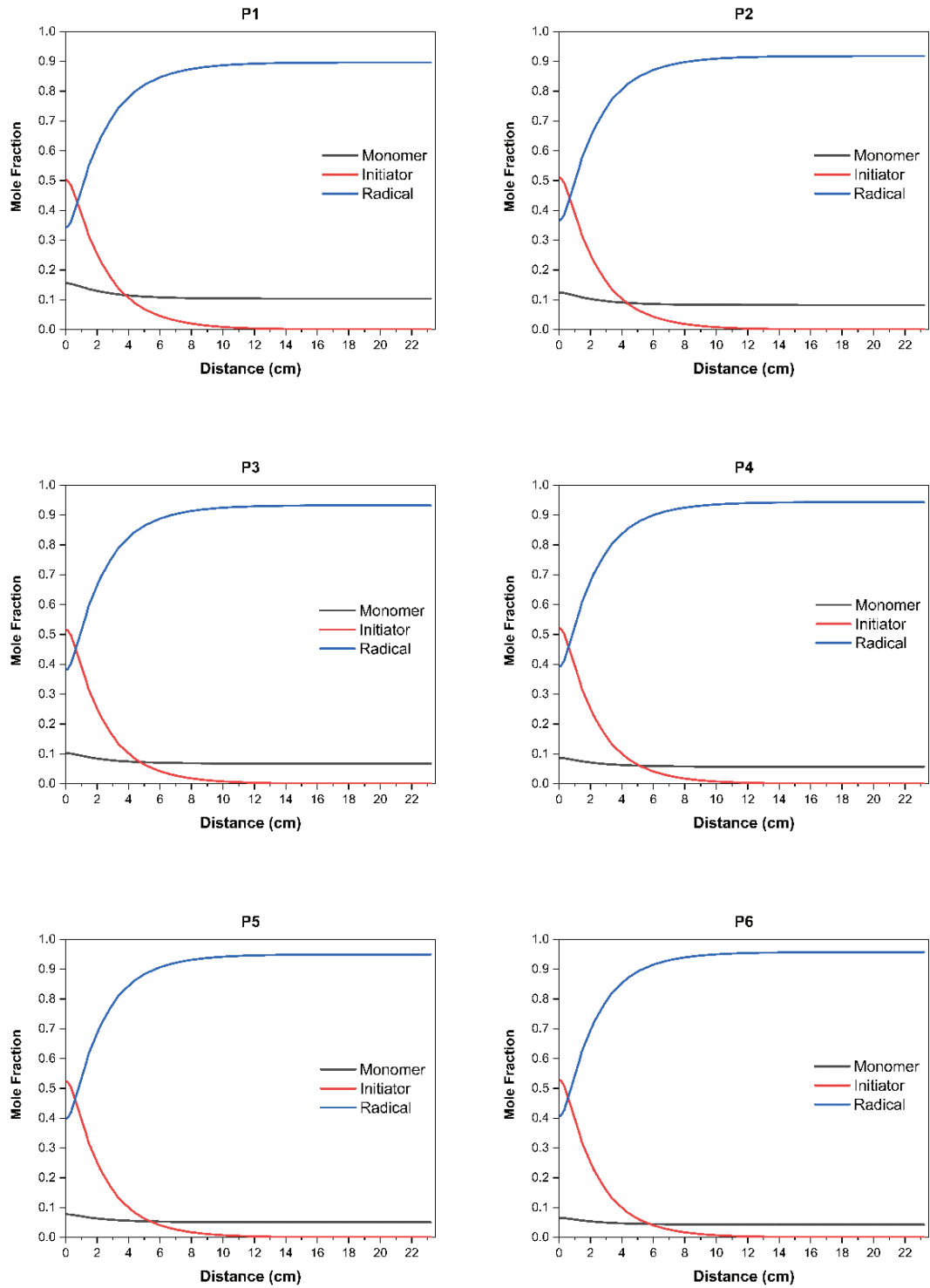


Figure 4.10. Predicted mole fractions of the species through the midline at a distance of 1.5 cm above the surface for P1-P6.

All that has been mentioned so far provides that predictions of developed model are in good agreement with reported experimental results for PFDA film deposition which means that fluid flow, heat transfer, transport of species, and chemistry are successfully coupled in simulation study of iCVD process. In order to validate the model applicability, this time; different precursors having different thermodynamic and kinetic properties, are used in the following section, and their polymerization kinetics employed to the computational program to investigate film deposition aspects for a variety of experimental conditions.

#### 4.1.2. Model Validation for nBA Polymerization

Apart from successful computational modeling of PFDA, developed model is also validated for different precursor type and iCVD process conditions based on the study reported by Lau and Gleason (2006b). Using the same computational software program, at steady-state conditions, iCVD polymerization of n-butyl acrylate monomer (BA) with tert-amyl peroxide (TAPO) initiator is simulated in a cylindrical shape of iCVD reactor at a given set of experimental data shown in Table 4.3.

Table 4.3. Reported process conditions of nBA polymerization in iCVD process.  
(Source: Lau and Gleason, 2006b)

Run Number	F_monomer (sccm)	F_initiator (sccm)	F_argon (sccm)	$P_M/P_{sat}$	DR_measured (nm/min)	DR_predicted (nm/min)
B1	3.0	0.7	0.0	0.1673	46.8	35.0
B2	2.5	0.58	0.62	0.1394	36.6	25.2
B3	2.0	0.47	1.23	0.1115	26.1	19.8
B4	1.5	0.35	1.85	0.0837	15.3	14.2
B5	1.0	0.23	2.47	0.0558	7.9	8.2
B6	0.75	0.18	2.77	0.0418	4.0	5.2
B7	0.5	0.12	3.08	0.0279	1.7	2.6

Table given above shows the experimental deposition rates at different monomer, initiator, and carrier gas flow ratios, each of which are carried out at 1 Torr reactor



pressure and 23 °C substrate temperature. Argon is employed when patch flow is required and total flow rate is fixed at 3.7 sccm to show the monomer partial pressure effect on deposition rate as stated in the reported study. Process parameters, deposition conditions, and kinetic parameters which were given in Table 3.4-3.6 are used in the simulation, and solved in a described three-dimensional reactor for each of experimental conditions, separately. As previously mentioned surface polymerization kinetics strongly depends on the substrate temperature where the adsorption takes place. Because of the fixed substrate temperature, for each of experimental run given in Table 4.3, the same kinetic data are applied in the simulation studies. In the presented model, the gas mixture in the reactor consists of BA monomer, TAPO initiator, Argon as carrier gas, and radical species. Since data are not available for the diffusivities of gas pairs of prescribed species in the presented conditions, it is assumed that each species have the same diffusional behavior in other gas species environment. Therefore, in the Maxwell-Stefan diffusivity matrix, all species diffusivities are taken as a constant value of  $1e-5 \text{ m}^2/\text{s}$  in order to lessen the computational effort and to reduce the total number of iterations in the solution.

Figure 4.11 shows the comparison of reported and predicted deposition rates, for each of experimental runs and conditions given in Table 4.3.

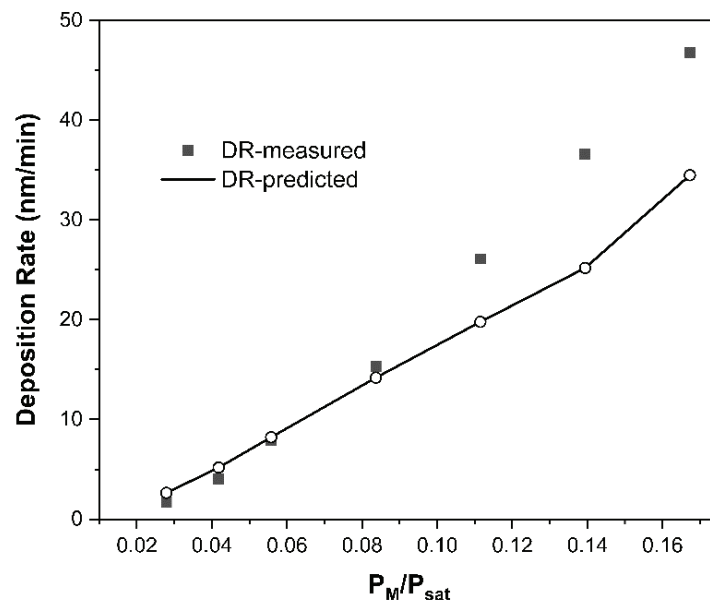


Figure 4.11. Comparison of reported and calculated deposition rates for nBA polymerization at different  $P_M/P_{sat}$ .

It is obvious from the figure that model deposition rate predictions are in good agreement with the experimental data at low  $P_M/P_{sat}$ , i.e., surface monomer concentration. Since total flow rate is constant and saturation pressure is fixed at surface temperature of 23 °C, the figure also indicates the effect of monomer flow rate on film deposition rate and/or thickness. As early mentioned for the modeling of PFDA deposition, the differences may result from assumptions, ignored process conditions, and also from finite element solver used in the computational model. But, the main reason between the differences is assumed to be resulted from the undefined substrate placement and data collection as film thickness measurement in the reported study.

Although simulation results of deposition rates which are plotted in Figure 4.11 represent the surface-averaged film growth rate, for the entire surface area of a 100-mm-diameter of wafer, simulation result of deposition rate is shown for the process conditions of experimental run number of B4 in Figure 4.12.

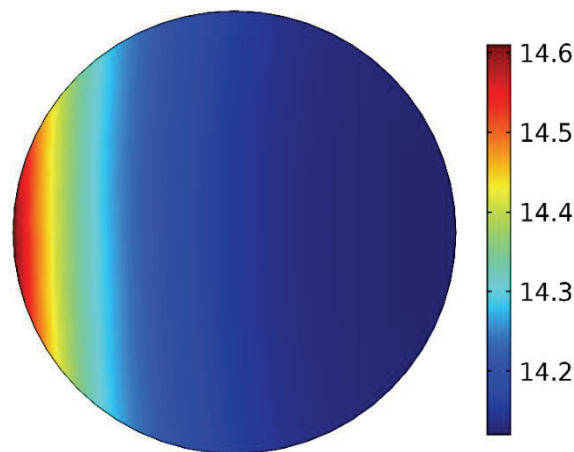


Figure 4.12. Model prediction of deposition rate (SI unit: nm/min) on substrate surface for B4.

According to the figure above, deposition rate slightly decreases on the substrate surface along the flow direction (x-axis). It should also be mentioned that, for a given process conditions, the figure above shows the rate of deposition at steady state conditions. However, for the long-lasting depositions, thickness variation along the flow direction can be significant since final film thickness is determined by deposition time. Variation in the predicted film deposition rate through the midline of substrate surface is shown in Figure 4.13 for all experimental runs of which deposition conditions represented in Table 4.3.

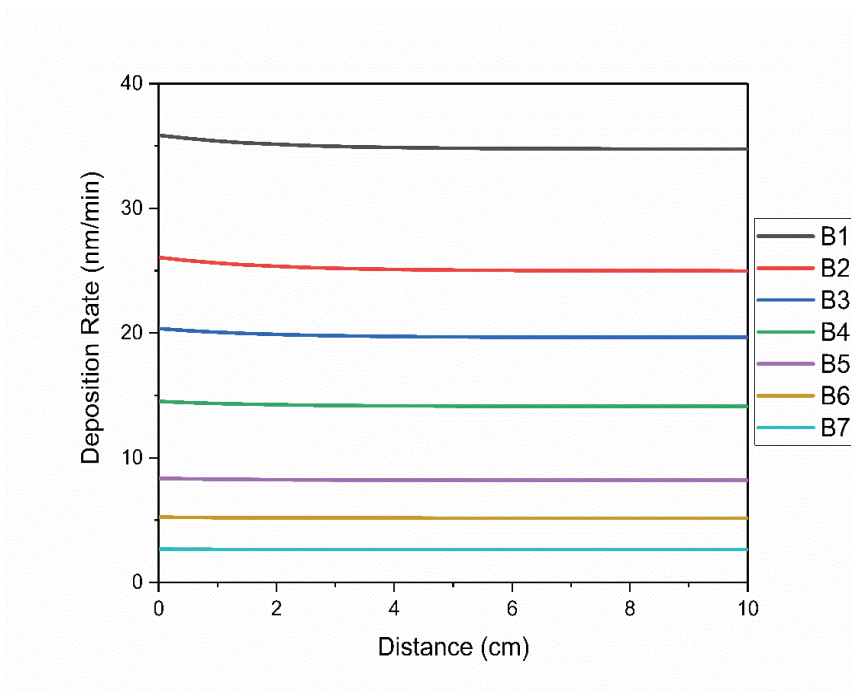


Figure 4.13. Predicted deposition rates for B1-B7 through at midline on substrate surface.

It can be seen from the figure that the deposition rate is slightly higher for B1-B3 at the region closer to the reactor inlet boundary while it is almost constant along the flow direction for experimental conditions of B4-B7. Therefore, it can be deduced from the figure that to obtain uniform film, where the film thickness variation is almost constant at any point of the surface, can be achieved at lower  $P_M/P_{sat}$ , i.e., monomer flow rates as in the conditions of B5-B7. Deposition rate is a direct function of rate of polymerization which is calculated by determining surface monomer concentration and polymer radical concentration on the surface. Figure 4.14 shows the averaged values of DR and  $R_p$  vs.  $F_M/F_{Total}$ , while Figure 4.15 represents the calculated surface monomer  $[M]$ , polymer radical  $[M]$ , and primary radical  $[R.]$  concentrations through the midline of substrate surface, respectively.

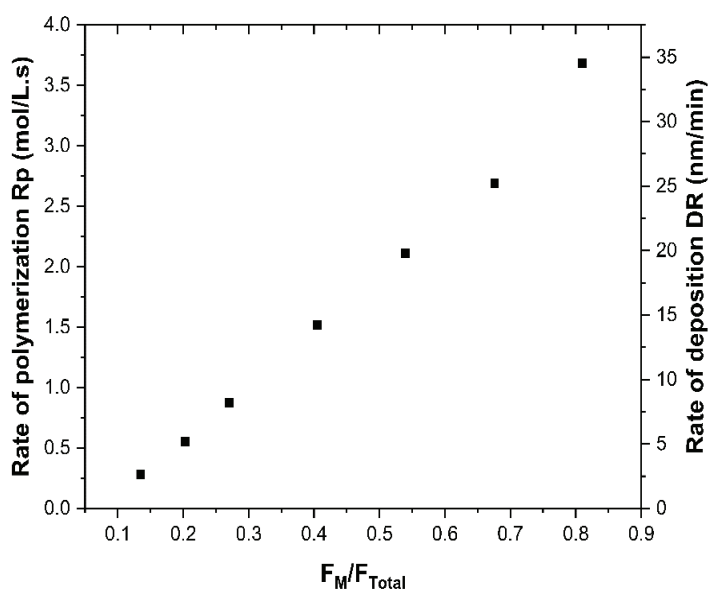


Figure 4.14. Surface-averaged values of predicted  $R_p$  and  $DR$  at different  $F_M/F_{Total}$  for nBA polymerization.

As shown in the figure above, there is an increasing trend line for both of deposition rate ( $DR$ ) and rate of polymerization ( $R_p$ ) versus  $F_M/F_{Total}$ . Since total flow rate is fixed at 3.7 sccm, Figure 4.14 also shows the same trend at increasing monomer flow rates. As monomer flow rate increases, surface adsorbed monomer concentration also increases as shown in Figure 4.15. Adsorbed radical concentration slightly increases along the midline of the substrate due to the convective diffusion of the radical species present right above the substrate surface while the polymer active concentration slightly decreases due to its consumption during the polymerization.

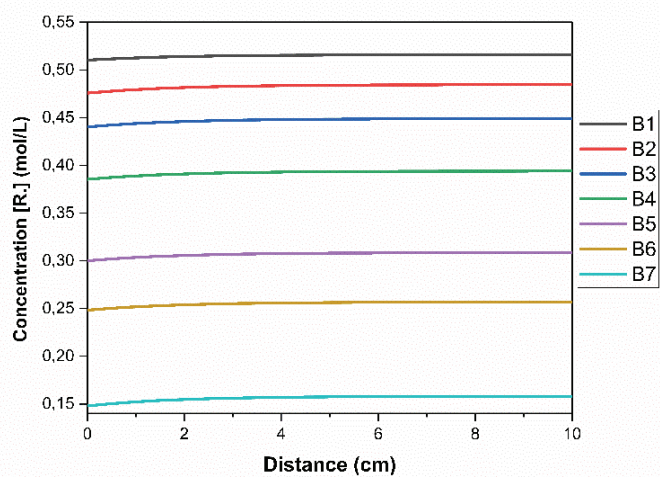
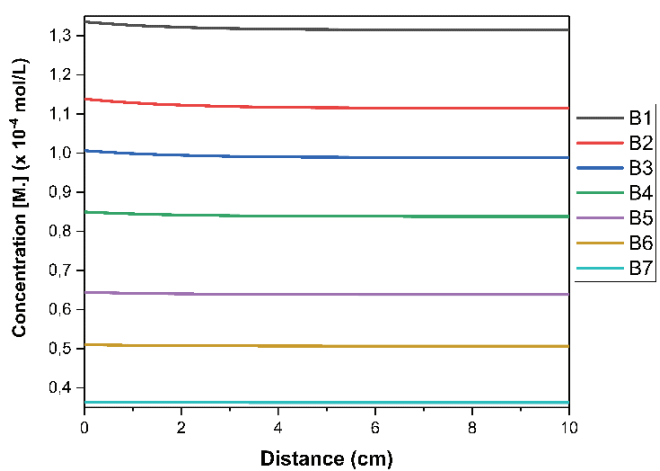
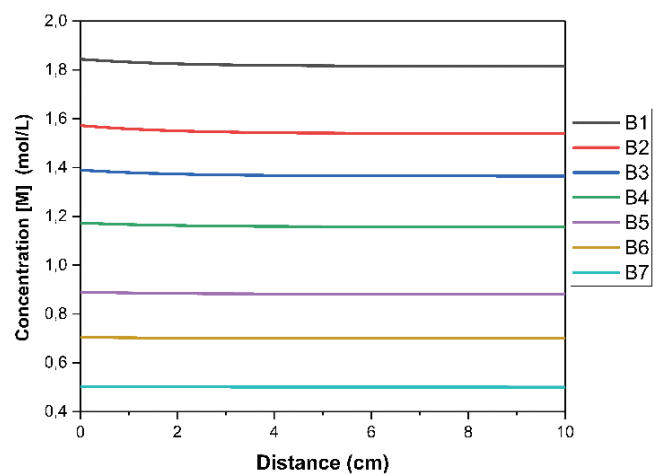


Figure 4.15. From top to bottom: adsorbed monomer concentration  $[M]$ , polymer radical concentration,  $[M.]$ , and primary radical concentration,  $[R.]$ , on substrate surface for B1-B7.

Since successful prediction of deposition rate on the surface is mainly resulted from successful coupling of transport phenomena occurring inside the iCVD geometry, simulation graphs of flow velocity and temperature distribution inside the vacuum chamber are represented in Figure 4.14 (a) and (b), respectively, for the deposition conditions of B4.

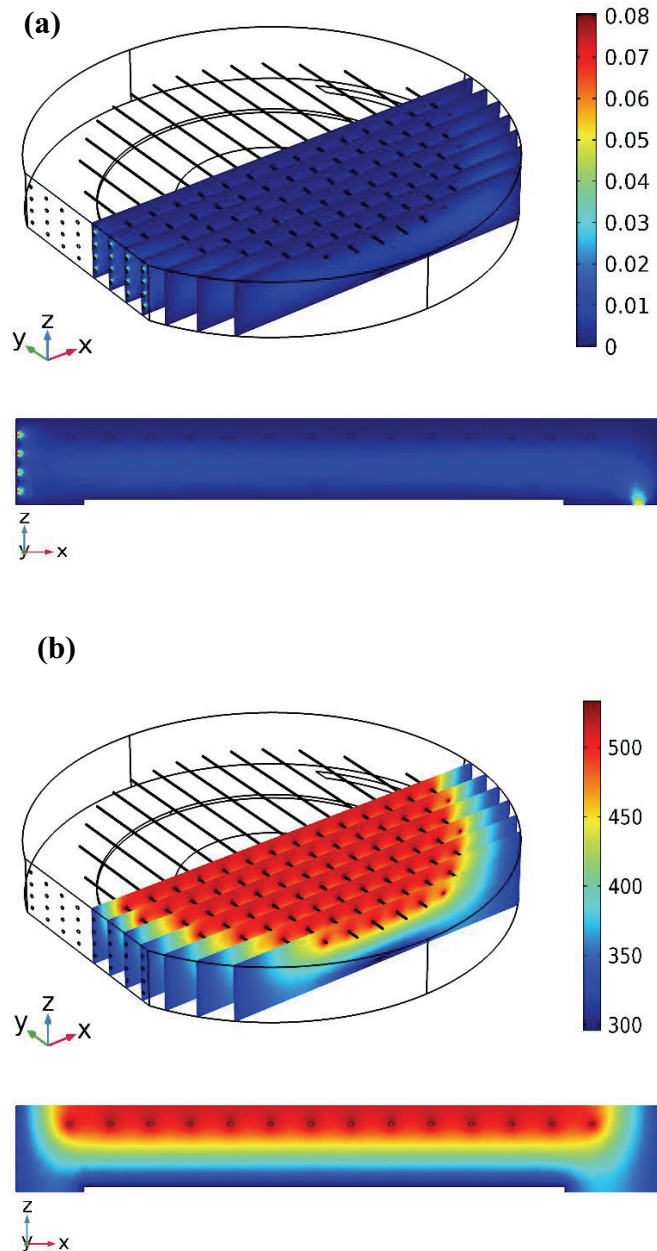


Figure 4.16. (a) Velocity (SI unit: m/s), and (b) temperature (SI unit: K) profiles along the flow direction for B4 with bottom profiles representing the midline of the reactor geometry.

At a given process conditions, inlet mixture includes BA monomer, TAPO initiator and argon carrier gas species, and delivered into the system at 80 °C. Inside the reactor box, flow is laminar for the entire volume. When a symmetrical substrate is placed at the center of the reactor, velocity profile can also be assumed as symmetrical through the midline in the flow direction. However, in most cases several substrates with different geometries are placed on the reactor disrupting otherwise symmetrical flow profile. Between the substrate and filament boundaries, where the temperatures are fixed at 23 °C and 260 °C, respectively, the mixture velocity does not change significantly along z-direction, and velocity is assumed to zero at the walls of the reactor due to boundary layer formation.

Inside the reactor geometry, it is expected that gas concentration of species change with respect to flow rate ratios of species, pressure and temperature. At the vicinity of heated filaments, one mole of initiator molecule decomposes to form two moles of radical gas species, at a rate of reaction kinetics. For the TAPO decomposition, mean activation energy is prescribed as -74.6 kJ/mole based on the study carried out by Lau and Gleason (2006a) to show concentration distribution of decomposed species of initiator as well as the formation of radical species. It is worth to note that, in literature, it is observed that decomposition reaction of TAPO yields to form peroxy radical which rapidly undergoes  $\beta$ -scission to yield acetone and ethyl radicals (Lau and Gleason, 2006b). For the filament temperature of 260 °C, ethyl radical is determined as a primary radical which involves in polymerization reactions. Therefore, in the simulation of BA polymerization, to satisfy the mass conservation, by-product generation is taken into the consideration since initiator does not effectively decomposed to radical.

Figure 4.17 shows the mole fraction of the species along the flow direction for the deposition conditions of B4. In the computational solving of the model, mole fractions of each defined species are simulated using the idea of sum of mass fractions of species is equal to 1. Therefore, mole fraction of species is expected to change inside the reactor depending on the species flow ratio, gas phase mixture properties, and decomposition reactions at the vicinity of the heated filaments. As shown in Figure 4.17, monomer and carrier gas mole fractions, although they do not involve any chemical reaction, vary along the flow direction due to by-product generation from thermal decomposition of initiator. In addition, radical mole fraction increases at the vicinity of the first filament in the array as a result of thermal decomposition of TAPO.

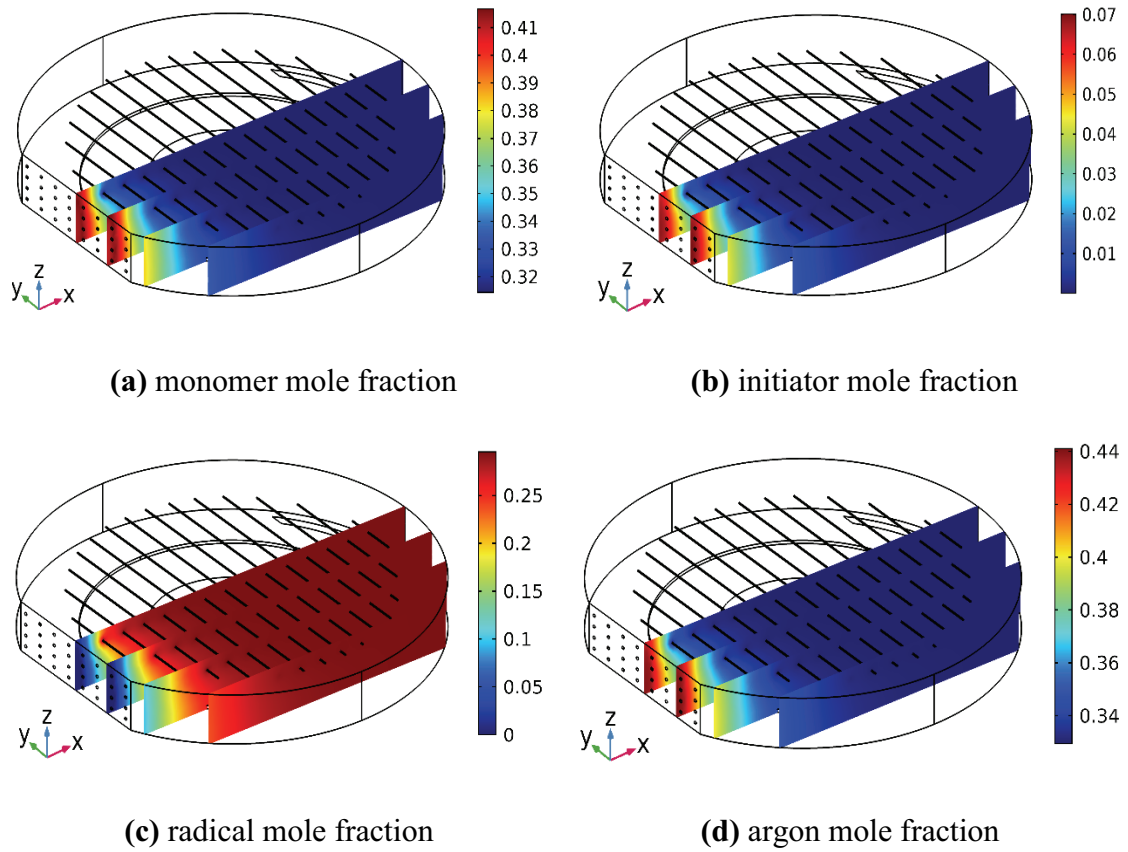


Figure 4.17. Predicted mole fraction distributions of (a) monomer, (b) initiator, (c) radical, and (d) carrier gas along the flow direction for B4.

At different flow rate ratio of the precursors, gas phase concentration distribution may be changed as a result of the convective and diffusive transport of species. Figure 4.18 shows the flow rate effect of precursors on the decomposition of initiator molecule.

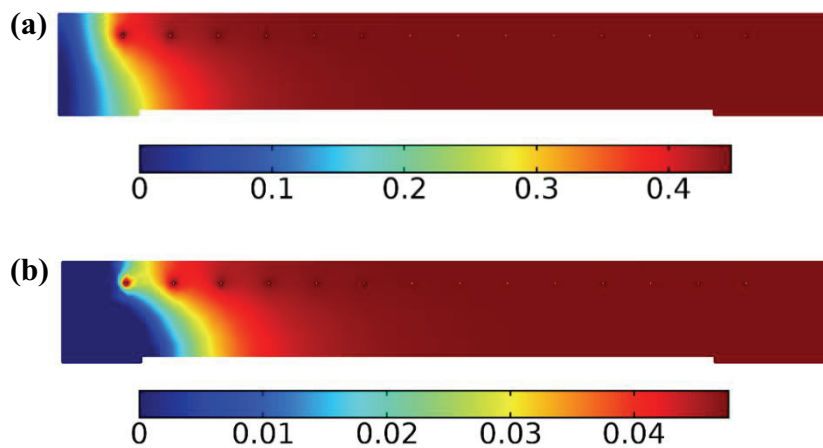


Figure 4.18. Radical mole fraction distributions at midline for (a) B2 (b) B7.



Since total flow rate is constant for the experimental run of B1-B7, the differences in decomposition may result from flow rate ratio of monomer: initiator: argon gases. In Figure 4.18 (a) radical mole fraction at experimental conditions of B2 is simulated where the  $F_{\text{monomer}}$ : 2.5 sccm,  $F_{\text{initiator}}$ : 0.58 sccm, and  $F_{\text{argon}}$ = 0.62 sccm. On the other hand, in Figure 4.18 (b), radical mole fraction at experimental conditions of B7 is simulated where,  $F_{\text{monomer}}$ : 0.5 sccm,  $F_{\text{initiator}}$ : 0.12 sccm, and  $F_{\text{argon}}$ = 3.08 sccm. Since initiator flow rate is high at the conditions of (a), radical concentration is higher than that of (b). Additionally, at higher initiator mole fraction, initiator decomposition is observed around the inlet boundary close to the first filament, as radical formation takes place right above the filament surface for the low initiator mole fraction.

In order to better understand of flow rate effect on species gas phase distribution, Figure 4.19 shows the mole fraction change of species through the midline of reactor geometry, above the surface at a distance of 1.5 cm for the conditions of B1-B6. Since sum of mole fractions of species equals to 1, species mole fraction varies at different flow conditions according to simulation results.

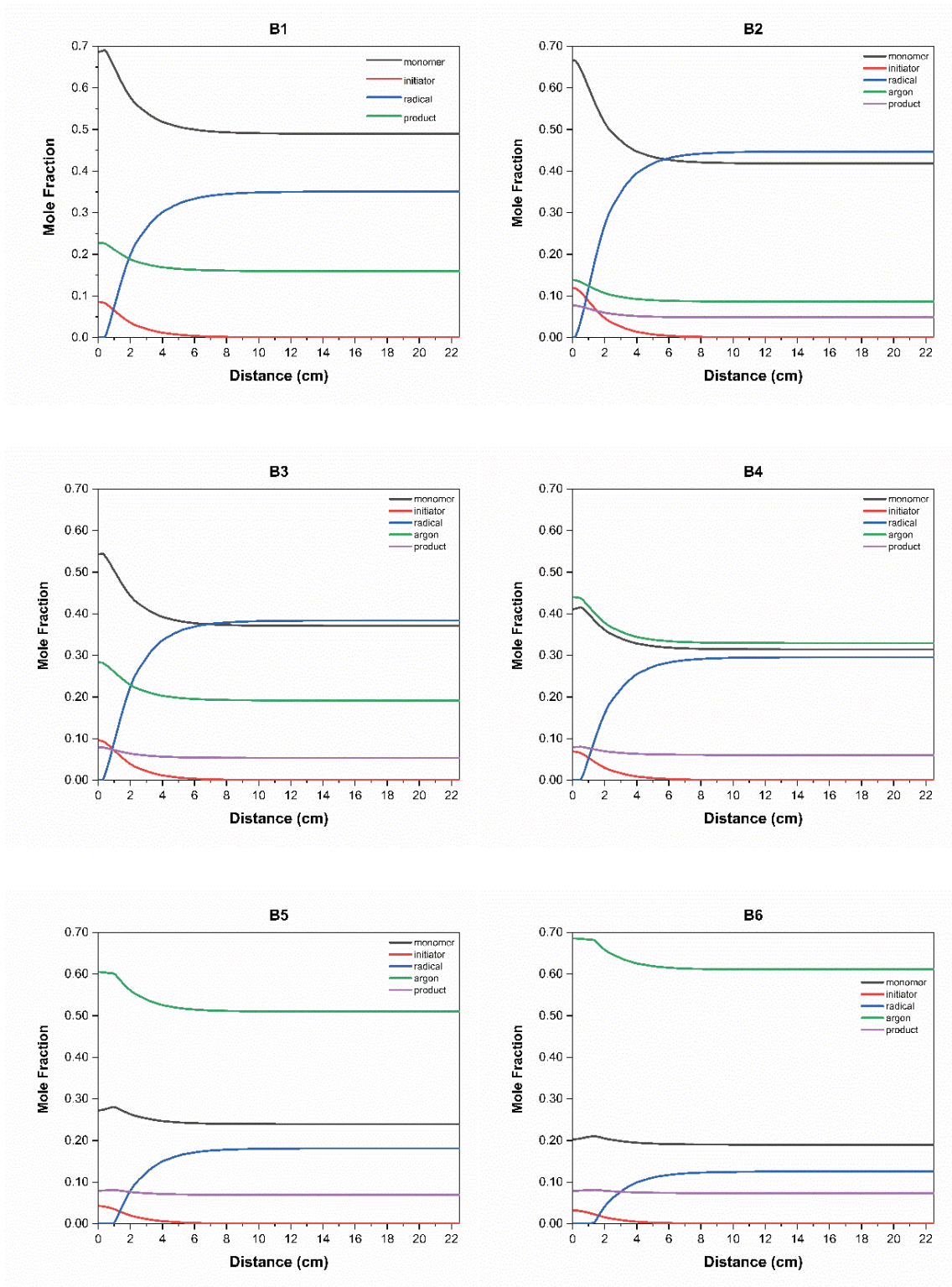


Figure 4.19. Predicted mole fractions of the species 1.5 cm above the substrate at the midline for deposition conditions listed in Table 4.3.

## 4.2. Model Implementation in Square Type of Reactor Geometry

To further validate the accuracy of the model, polymer thin film depositions were carried out for nBA monomer with TBPO initiator in a custom-built iCVD reactor. The details of the reactor geometry and the deposition conditions were given in Chapter 3. In each depositions, a 100-mm-diameter silicon wafer substrate which is positioned in the middle of actively cooled surface area was used. Substrate and filament temperatures were kept constant at 23 °C and 300 °C, respectively. Table 4.4 shows the deposition conditions of experiments carried out at 1 Torr in a square type of reactor, and comparison with the predicted deposition rates.

Table 4.4. Comparison of experimentally found deposition rates with the model predictions for nBA.

Run Number	F_monomer (sccm)	F_initiator (sccm)	$P_M/P_{sat}$	DR_measured (nm/min)	DR_predicted (nm/min)
E1	4.00	0.5	0.183	55.2	102
E2	3.50	0.5	0.180	57	96
E3	3.00	0.7	0.167	36	75
E4	3.80	1.1	0.160	46	67

According to the results shown in Table 4.4, rates of deposition observed in experiments are slightly different from model predictions due to the uncertain deposition conditions present during the deposition. Although the difference between the predicted and measured deposition rates is significant at given process conditions, model predictions will be shown for the deposition condition of E3.

Figure 4.20 shows the simulation result of deposition rate on a 100-mm-diameter of substrate surface for the process conditions of E3. Although there is a slight change in DR at the region of the wafer close to the inlet boundary, film DR does not vary significantly for the rest of the surface. It is important to note that for the long-lasting depositions, thickness variation along the flow direction can be significant since final film thickness is determined by deposition time.

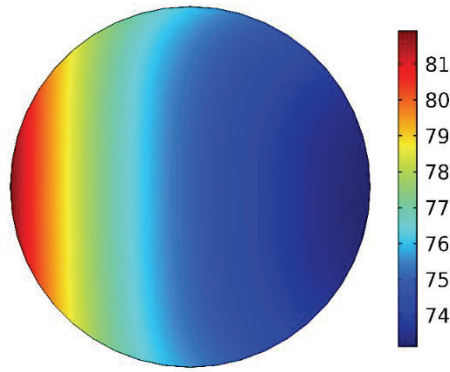


Figure 4.20. Model prediction of film deposition rate (nm/min) on substrate surface for E3.

Underlying reason of good prediction of film thickness is related with the successful coupling of gas phase momentum, heat and mass transfer of species with polymerization reactions which takes place on the substrate surface. Therefore, presented computational model not only predicts the deposition rate for a substrate of a particular size and shape, but also give valuable insight about flow, heat and mass transport process in the gas phase depending on the reactor geometry and process conditions. For square reactor geometry and filament array, gas phase fluid flow and temperature distributions are given in Figure 4.21. Due to no slip boundary, velocity is zero at reactor walls and velocity does not change significantly inside the reactor. In addition, maximum temperature is simulated above the filament array due to the very slow motion of the fluid flow which is also observed experimentally as well.

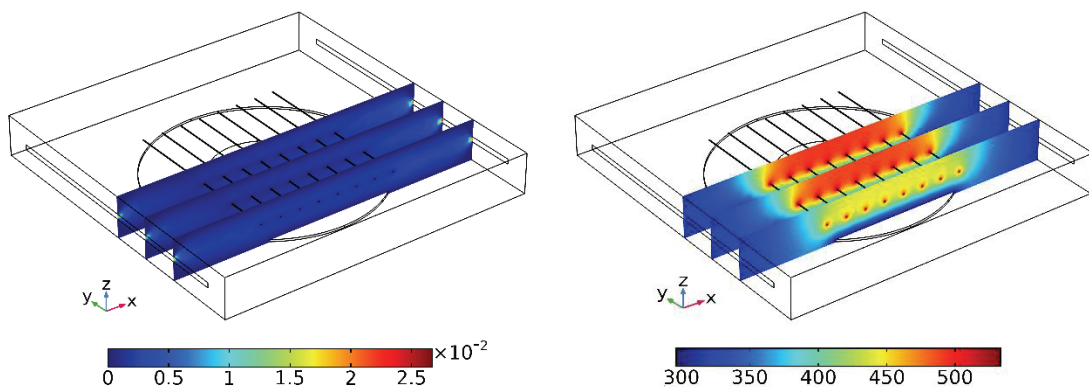


Figure 4.21. From left to right, velocity (SI unit: m/s) and temperature (SI unit: K) profiles along flow direction for E3.

Similarly, the model also couples heat, mass, and momentum transport with gas phase chemical reactions and predicts concentration of species inside the reactor. Figure 4.22 shows the mole fractions of monomer (top), initiator (middle), and radical (bottom) species along the flow direction for experimental conditions of E3. As expected mole fraction of initiator decreases with thermal decomposition reaction over filament array, and for every mole of TBPO fed into the reactor, two moles of primary radicals are generated. Due to location of filament array, radical formation occurs at a distance away from the inlet boundary, at the vicinity of the heated filaments where the appropriate decomposition temperature exists. According to the simulation results, un-utilized monomer and initiator, and un-used radical molecules are observed at the outlet boundary.

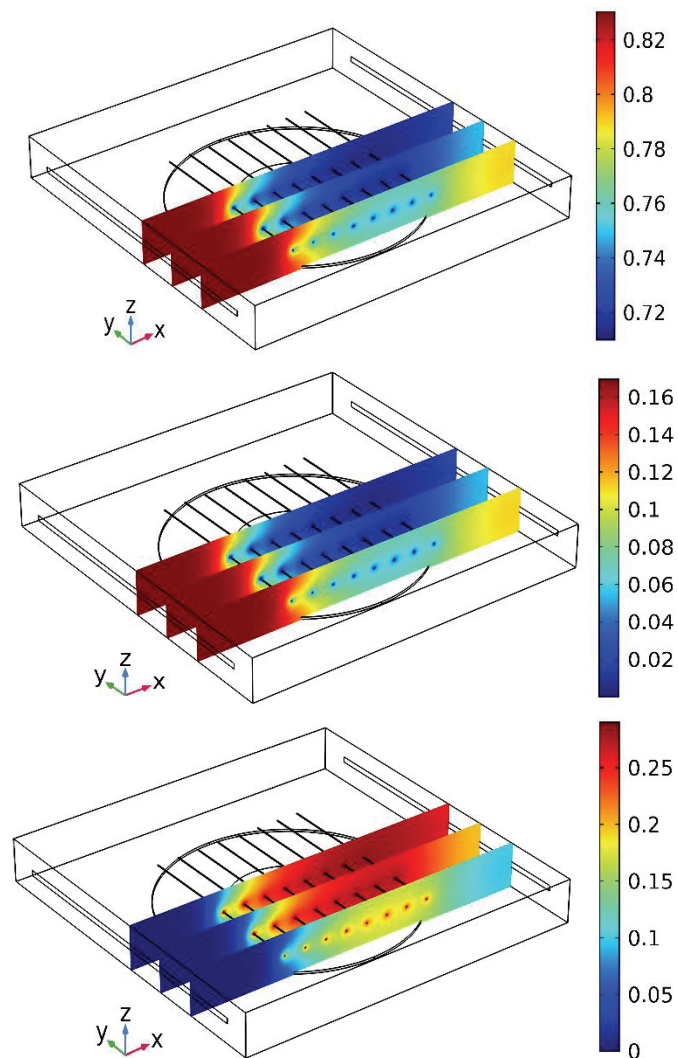


Figure 4.22. Predicted mole fractions of monomer (top), initiator (middle), and radical (bottom) species along the flow direction for E3.

### **4.3. The Effect of Process Parameters on Deposition Rate and Film Uniformity**

As discussed earlier, iCVD is a multi-parameter system involving specific variables which are needed to be defined and controlled such as precursor types, flow rates, substrate and filament temperature, reactor pressure, number of filaments, and filament-to-substrate distance. All of these factors are of crucial importance which affect the repeatability and uniformity of the growing polymer film in an experimental process. To predict the effect of these factors without carrying further experiments are also crucial due to the limited utilization of high-cost specialty chemicals particularly in a large-scale coating industries. For small-scale research applications and proof-of-concept demonstrations, on the other hand, such predictions provide better understanding of physics occurring inside the chamber as well as obtaining effective and faster solutions at lower cost.

Here, in this section the effect of selected iCVD process parameters on deposition rate and uniformity will be examined in detail applying butyl acrylate process parameters and polymerization rate constants to developed computational program.

#### **4.3.1. The Effect of $P_M/P_{sat}$**

Monomer surface concentration greatly affects the deposition rate, and is a direct function of monomer partial pressure ( $P_M$ ) to the saturation pressure of said monomer ( $P_{sat}$ ) at the temperature of the substrate. Representative plots of deposition rate versus  $P_M/P_{sat}$  for PFDA and BA depositions have already been shown in Figure 4.1 and Figure 4.11, respectively. From the figures, it can be seen that deposition rate increases as  $P_M/P_{sat}$  increases since surface monomer concentration increases as well. Therefore,  $P_M/P_{sat}$  is a convenient way of assuming surface monomer concentration on the substrate before doing experiment. It is important to note that at the reported studies, for both of PFDA and BA depositions, monomer partial pressure is determined according to the below relation by assuming that precursors flow rates are constant or not changed along the reactor.

$$P_M = \frac{F_M}{F_{total}} P_{total} \quad (4.1)$$

However,  $P_M/P_{sat}$  is not expected to be fixed as stated in literature because during the film deposition experiments, as a result of flow distribution of precursors thickness variation is commonly observed situation on the wafer. Since saturation pressure depends on the substrate temperature, it does not change on the surface but monomer partial pressure changes spatially through the reactor. Therefore, this can be the one of the reason of differences between experimental and prediction values of  $P_M/P_{sat}$  as shown in Figure 4.23.

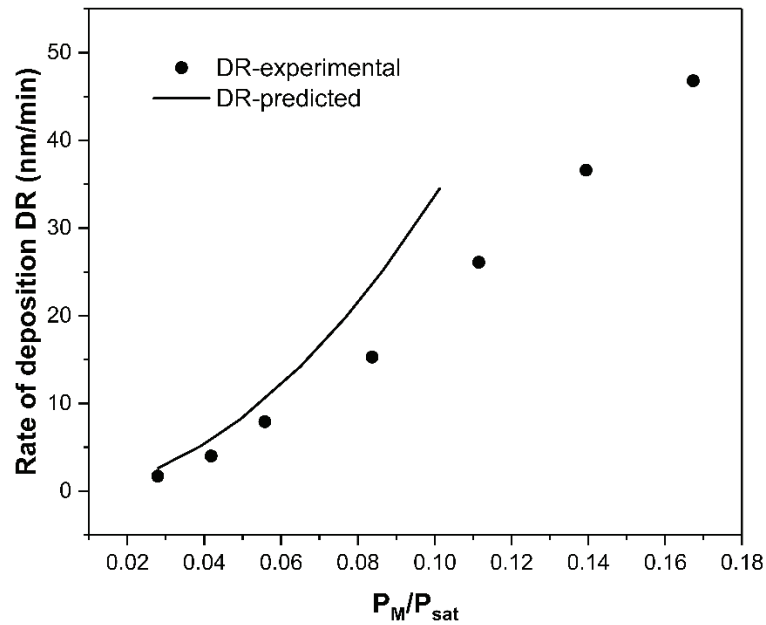


Figure 4.23. Comparison of experimentally measured and predicted deposition rates with respect to  $P_M/P_{sat}$ .

### 4.3.2. The Effect of Reactor Pressure

To show the effect of pressure inside the cylindrical reactor chamber, process conditions of experimental run of B4 in which  $F_{monomer}$ : 1.5 sccm,  $F_{initiator}$ : 0.35 sccm,  $F_{argon}$ : 1.85 sccm,  $T_{filament}$ = 260 °C, and  $T_{substrate}$ = 23 °C, is simulated at reactor pressure of 0.5, 0.75, 1, 1.25, 1.5 Torr. The results are represented for the five points which are placed at the midline of the surface as shown in Figure 4.24.



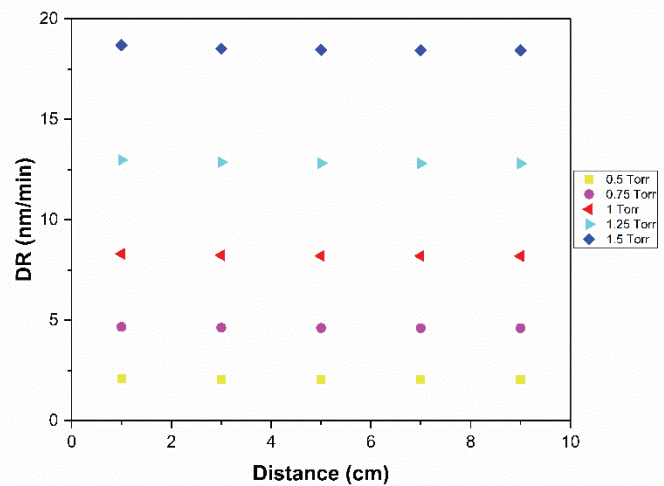
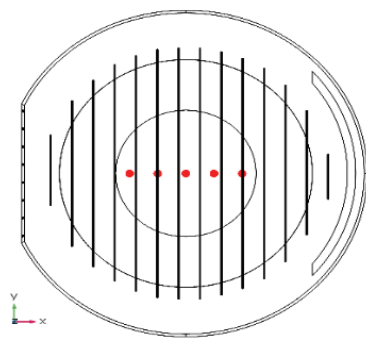


Figure 4.24. Change of deposition rate in flow direction with respect to total pressure for B4.

It can be seen from the figure that as reactor total pressure is increased from 0.5 Torr to 1.5 Torr, rate of deposition also increases from 2.4 nm/min to 18 nm/min, respectively. Simulation results obtained are not experimentally proved due to the absence of reactor type, but, model simulation shows an approach that how the increment in reactor pressure affects the deposition rate on the substrate surface. However, it should be noted that accurate prediction of diffusion coefficient contribute to accurate prediction of deposition rates. Although species diffusion coefficient inversely proportional to pressure, in the model it is not taken into the consideration since diffusion coefficients for coupled species are given as a constant value at described process conditions. Thus, describing diffusion coefficients in terms of pressure and temperature leads to obtain closer prediction of model with experimental results.

Although species diffusion are taken as a constant value, increasing reactor total pressure changes the partial pressure of the species inside the reactor geometry. Figure 4.25 shows the changes in partial pressure of species at different reactor pressure.



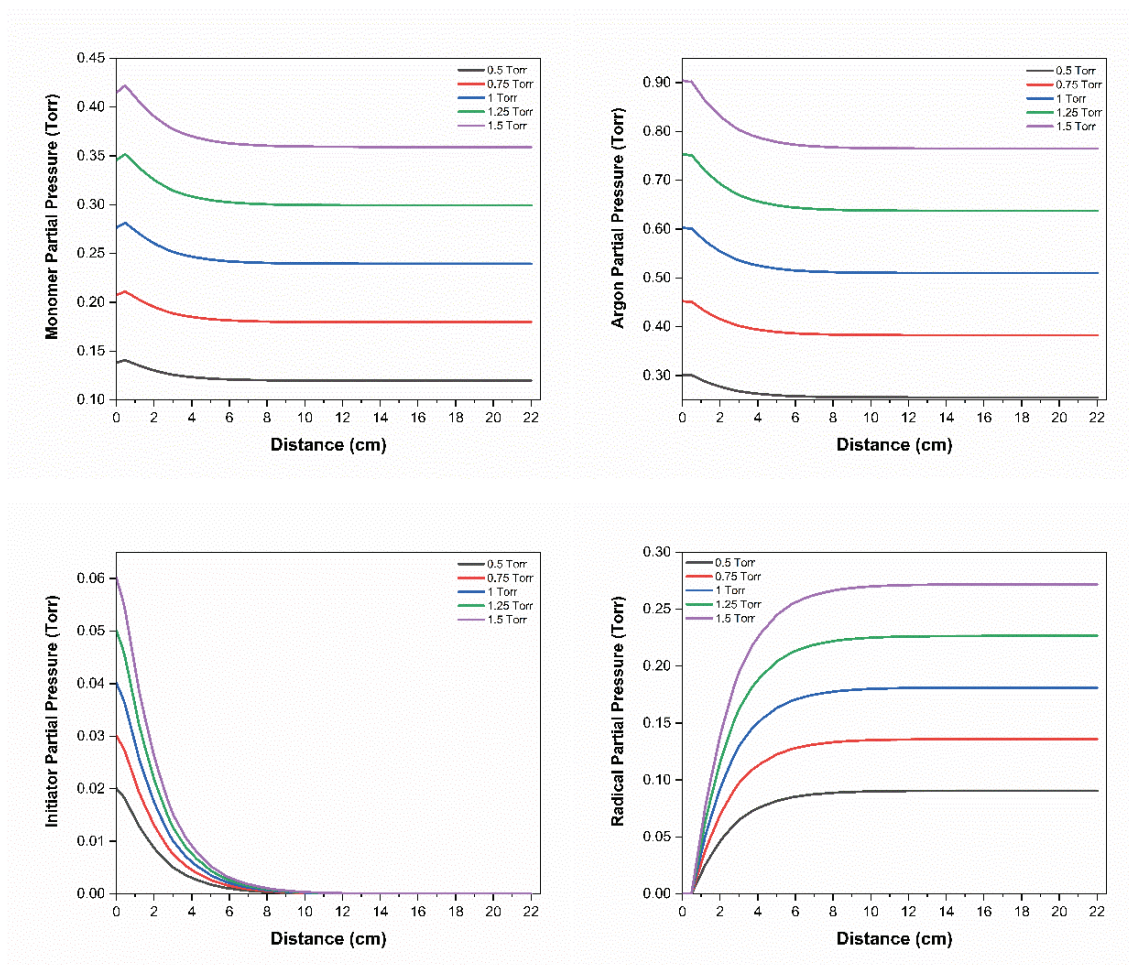


Figure 4.25. Partial pressures of monomer, initiator, radical, and argon through the midline 1 cm above the substrate surface.

As shown in the Figure 4.25, partial pressures of species vary with changing reactor total pressure. In particular, increase in total pressure increases the monomer partial pressure, therefore, it leads to increase in adsorbed monomer concentration on the surface which also result in increasing of film thickness.

### 4.3.3. The Effect of Initiator Type

To explore the influence of initiator type, commonly used thermally decomposing initiators, which are tert-butyl peroxide (TBPO), and tert-amyl peroxide (TAPO) are employed to iCVD polymerization of n-butyl acrylate model. The previously described cylindrical reactor geometry are used for the process conditions of B1 in which  $F_{\text{monomer}}$ : 3.0 sccm,  $F_{\text{initiator}}$ : 0.70 sccm. Inside the reactor, total pressure is kept

constant at 1 Torr, filament and substrate temperature are fixed at 260 °C and 23 °C, respectively. Therefore, the effect of initiator type, i.e., radical, is to be investigated for different types of initiators at the same deposition conditions and the same iCVD reactor geometry by using activation energies of decomposition reactions of each initiator species. Since primary radical types as well as the rate of decomposition are different for each type of initiator, it affects the mole fractions of species inside the reactor. Table 4.5 shows the types of initiator used in the model, and their formed primary radicals at filament temperature of 260 °C.

Table 4.5. Initiator species and primary radicals.

<b>Initiator Type</b>	<b>MW_initiator (g/mole)</b>	<b>Primary Radical</b>	<b>MW_radical (g/mole)</b>	<b>Ea_logarithmic (kJ/mole)</b>	<b>Reference</b>
TBPO	146.23	t-butoxy radical	76.115	113.0	Ozaydin-Ince and Gleason (2006)
TAPO	174.28	ethyl radical	29.06	74.6	Lau and Gleason (2006)

Considering the data given above table, each type of initiator performed in the computational model, separately. Figure 4.26 shows the volumetric distribution of radical species which are formed by the decomposition of the initiator. In the figure, the top represents the radical formation for the conditions of TAPO, while the bottom is of TBPO. As seen from the figure, mole fractions of radical species are different for both of the reactor volumes. For the TBPO-employed study, radical formation increases sharply and reaches maximum while slow increment is observed for TAPO-employed study. For both of the case, efficient decomposition of the initiator species, therefore formation of radicals, is observed with the first filament and distribute to whole reactor volume along the flow direction.

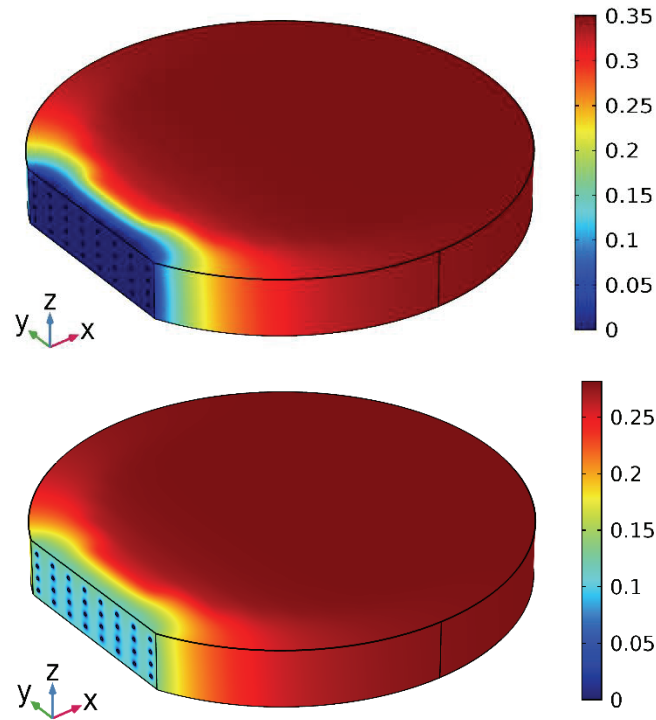


Figure 4.26. Mole fraction distributions of radical species when a) TAPO, and b) TBPO initiators are used.

Figure 4.27 shows the mole fraction distribution of species through the midline which is above the surface at a distance of 1.5 cm.

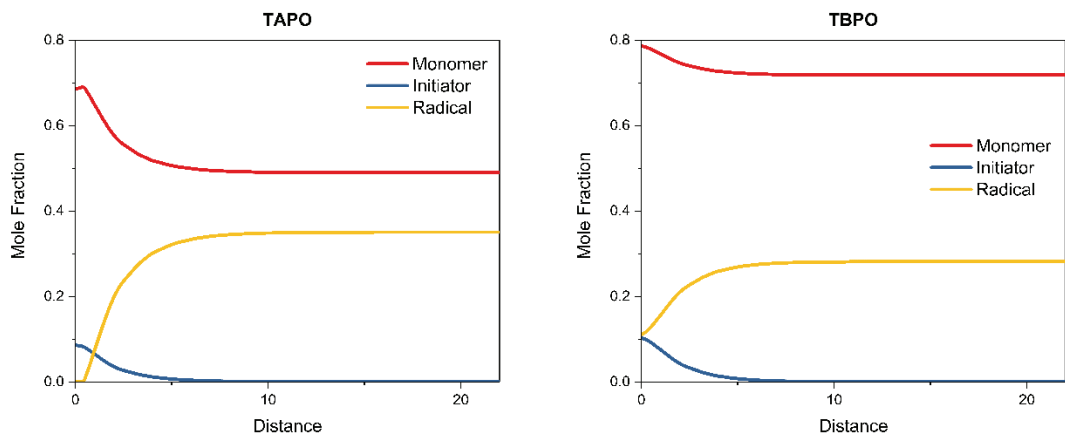


Figure 4.27. Species mole fractions 1.5 cm above the bottom surface of the reactor when a) TAPO b) TBPO initiators are used.

Since radical mole fraction therefore; partial pressures are changed in the implementation of different type of initiator, it also affects the rate of deposition on the substrate. Figure

4.28 shows the rate of depositions for the 100-mm-diameter of substrate length. Although the same deposition conditions (precursor flow rates, reactor pressure, temperature, etc.) exist for both of the situations, using TBPO is almost doubled the deposition rate instead of using TAPO due the initiator decomposition behavior and primary radical material properties.

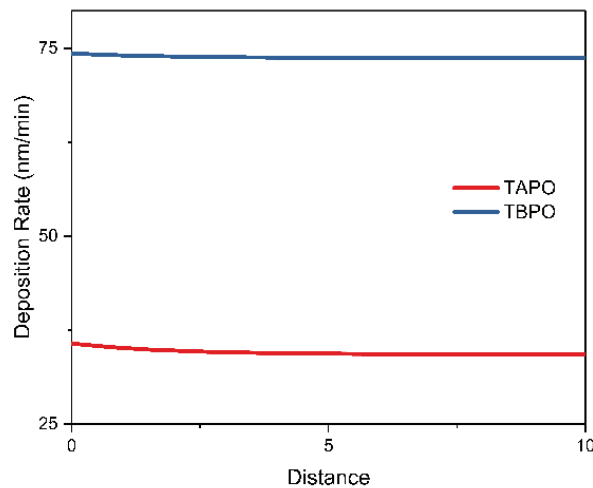


Figure 4.28. Comparison of deposition rate for nBA polymerization with different initiator species.

#### 4.3.4. The Effect of Filament Array

Heated filaments have an important role in the thermal decomposition of initiator in iCVD process. To explore the effect of filament array configuration on precursor distribution, the computational model of polymerization with TAPO initiator at process conditions of B6 in which  $F_{\text{monomer}}$ : 0.75 sccm,  $F_{\text{initiator}}$ : 0.18 sccm, and  $F_{\text{argon}}$ : 2.77 sccm is used. Inside the reactor, total pressure is kept constant at 1 Torr, filament and substrate temperature are fixed at 260 °C and 23 °C, respectively.

Addition to circular filament array which involves 14 filaments, two different filament arrays, which are placed at a distance of 2.5 cm above the surface are also used in the computational model as represented in Figure 4.29, and distribution of formed radical species at given deposition conditions are represented for the entire reactor geometry.

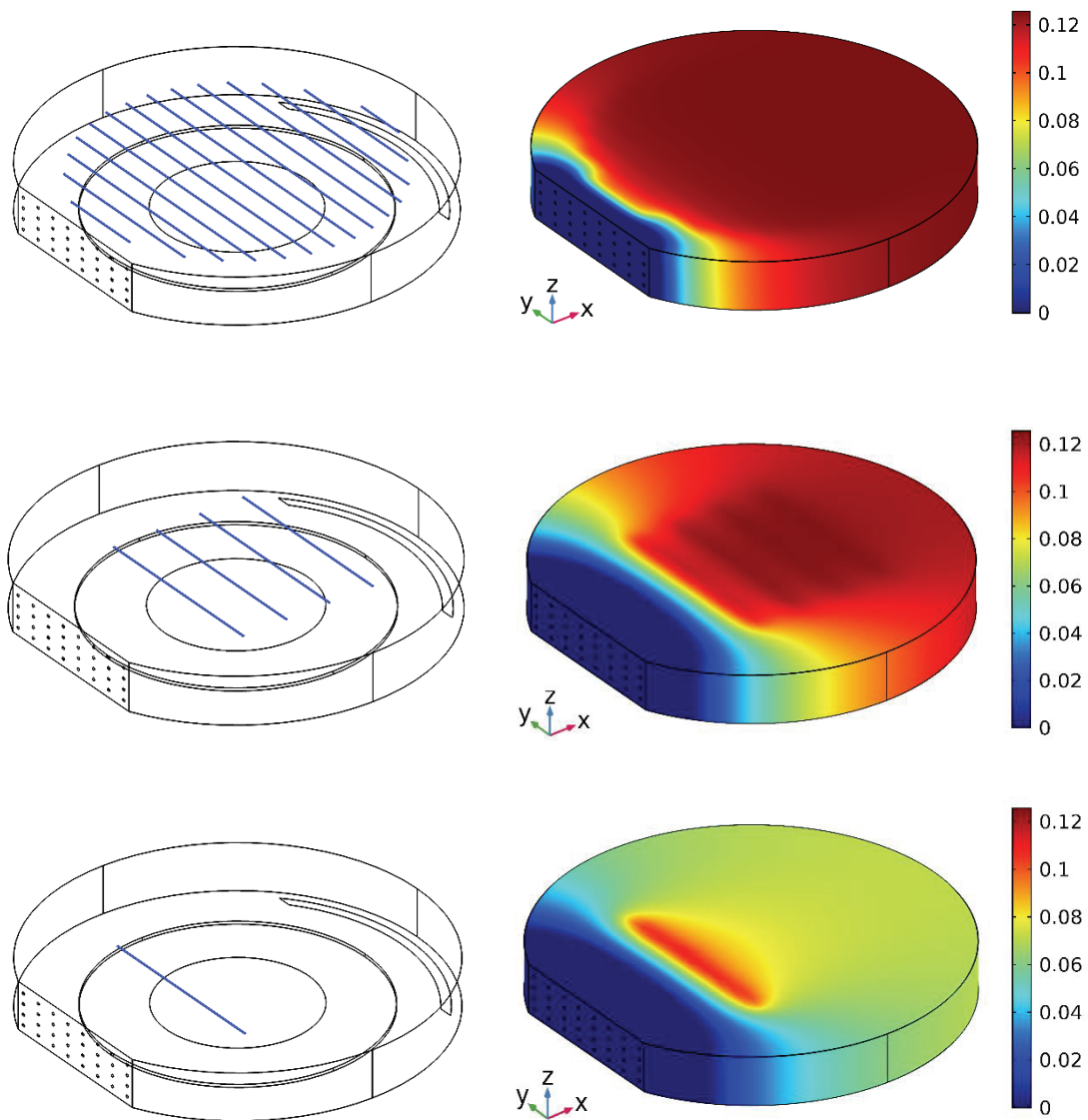


Figure 4.29. Predicted mole fraction variation of radical species for 14 filaments (top), 4 filaments (middle) and 1 filament (bottom).

According to the figure, radical formation starts with the gas precursor's arrival to the heated filament surface where the initiator decomposition takes place. Since initiation reaction is very fast and relatively low concentrations of radical are needed for the polymerization, deposition rates should not change much with decreasing number of filaments. One can argue that the presented model can be improved by taking into account the energy per length of filament or number of filament in an array. However, it should also be taken into account that due to filament aging, higher power is needed to achieve the same filament temperature, so this approach is only valid if a new filament is used for each deposition. Filament number and/or the distance between each filament affect the

species distribution inside the reactor, therefore, it affects the partial pressures and gas phase concentration of species, and leads to different film depositions on the substrate.

Figure 4.30 shows the deposition rates at the midline of 100-mm-diameter of substrate length for the filament arrays given in Figure 4.29. It is obvious that increase in filament number leads to obtain more uniform film thickness on the surface due to the presence of regular distribution of radical species.

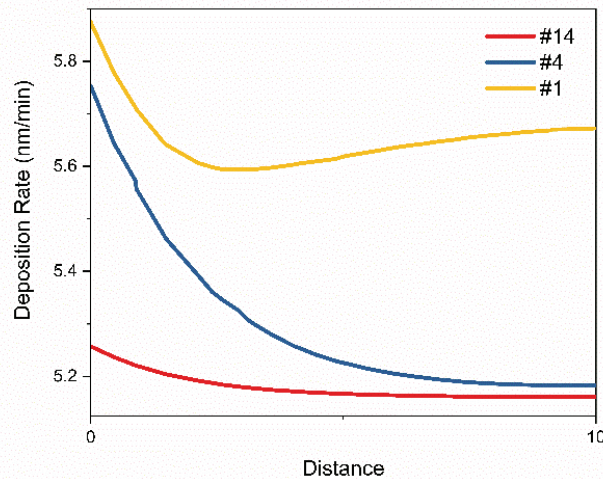


Figure 4.30. Comparison of deposition rates for nBA polymerization at different filament numbers.

### 4.3.5. The Effect of Substrate Geometry

The iCVD process is capable of depositing polymer films on various substrates such as micro- and nanostructured surfaces, trenches, curves, fibers, etc. This capability results from vapor phase precursors that can easily achieve all angles of the non-planar geometries. To show the polymer film deposition on different substrate surfaces, model of BA polymerization is run for the process conditions of experimental run of B4 in which  $F_{\text{monomer}}$ : 1.5 sccm,  $F_{\text{initiator}}$ : 0.35 sccm,  $F_{\text{argon}}$ : 1.85 sccm,  $T_{\text{filament}}$ = 260 °C, and  $T_{\text{substrate}}$ = 23 °C. As three dimensional substrates, a substrate with a dimensions of 3 cm of width, 4 cm of depth, and 2 cm of height, and a substrate with ellipsoidal geometry (with  $a=4$  cm,  $b= 2.5$  cm and  $c=1$  cm) positioned with 45° angle in the middle of reactor bottom were used as shown in Figure 4.31 (a) and (b), respectively. Since deposition is a strong function of substrate temperature, it is assumed that those three dimensional substrates, which are placed in the middle of cooled surface area, thermally



contact-well with actively cooled surface area that all the lateral surfaces of geometries have the same temperature with that of fixed surface area.

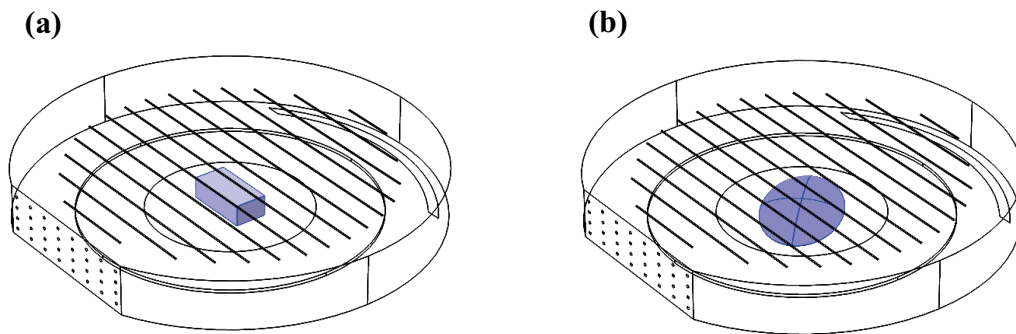


Figure 4.31. Three dimensional substrate geometries. a) rectangular shape b) ellipsoid shape.

Figure 4.32 shows the simulation results of deposition rate (nm/min) on 3-dimensional substrate surface. Thanks to successful coupling of gas phase transport phenomena with surface polymerization events, one can able to predict the deposition rate or polymer film thickness at different substrate geometries provided that uniform temperature distribution is achieved at every point of the surface.

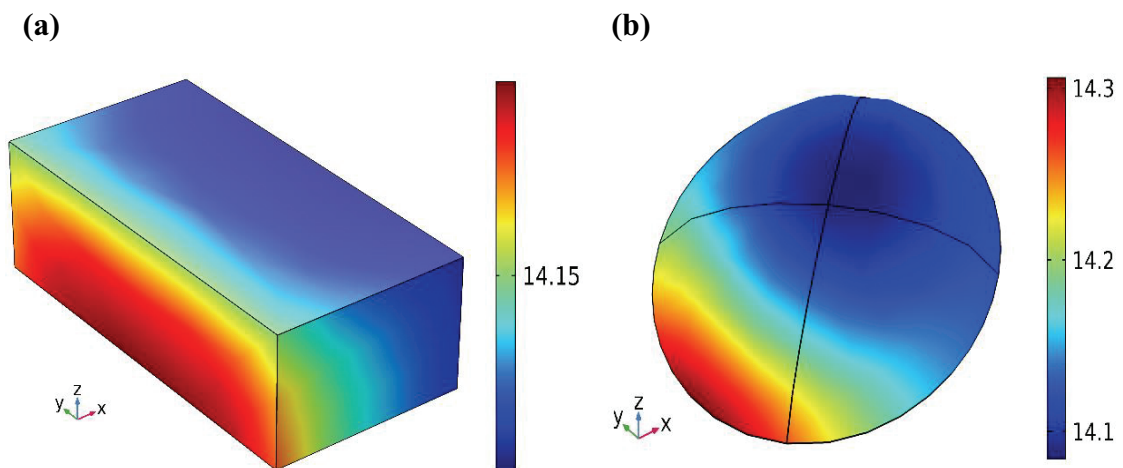


Figure 4.32. Deposition rates (nm/min) on substrates with (a) rectangular prism, and (b) ellipsoidal geometries showing uniform film thickness can be achieved for complex geometries.

According to the deposition rate results which are shown in Figure 4.32, the differences in film thicknesses are not significant and almost the same at different sides of geometries. However, at different deposition conditions and long-lasting depositions, the spatial differences can be significant. Therefore, using computational analysis, one can easily predict film deposition rate and the substrate position to obtain desired film thickness.



## CHAPTER 5

### CONCLUSION

In this study, all relevant transport phenomena which describes the iCVD process, and effect of process parameters on deposition rate were investigated by developing a three-dimensional computational model based on the Finite Element Analysis (FEA) approach.

In order to validate the model, reported experimental studies of BA and PFDA depositions, of which process conditions and polymerization kinetics are known, were simulated in a three dimensional cylindrical type of iCVD reactor. It was found that rate of deposition results predicted in the model coincide well with that of results obtained from the experiments reported in literature. Model captures good consistence with experiments at lower  $P_m/P_{sat}$  although small differences were observed between predicted and measured deposition rates. The differences between experimental and predicted value of deposition rate may resulted from approaches and/or assumptions made through the calculation of gas mixture properties. In the explanation of the differences, lack of data for the mass diffusivities of gas species, thickness measurement, and wafer placement were assumed to be affect the DR. These are all having importance in the determination of accurate and uniform film thickness predictions. Although some differences are present between model prediction and experimental results, the trend of film growth rate is similar and the qualitative aspects are reflecting the process correctly.

Additional iCVD deposition were also performed to validate model output for a variety of process conditions in a custom-built square type of iCVD reactor. However, due to the presence of uncertain conditions during the film depositions, film thickness results for the square type of geometry did not show good agreement with those of predicted. In order to make a reliable comparison of deposited film thickness with prediction results, repeatability tests of the produced films and QCM adsorption measurements are required to be considered.

Although not experimentally proved, model successfully predicts the effect of process parameters, describes the rate of deposition (or film thickness) and species surface concentration at different reactor geometries, filament assembly, and various film deposition conditions for a polymerization reaction with known kinetics data.

This study is of importance in terms of describing all relevant phenomena for different iCVD reactor geometries, prediction of film thickness with high precision on complex substrate surface geometries, and also successful combining of gas phase and surface deposition phenomena in a model simulation environment. The accurate prediction of the effect of process parameters, in turn, leads to utilization of high-cost specialty chemicals, save time and money. Additionally, it enables to extract polymerization kinetic data for various substrate temperatures provided that a sufficient number of experiments are performed, and process parameters and measured final film thicknesses are entered to the model.

## REFERENCES

- Alf, M. E., Asatekin, A., Barr, M. C., Baxamusa, S. H., Chelawat, H., Ozaydin, G., Petruczok, C. D., Sreenivasan, R., Tenhaeff, W. E., Trujillo, N. J., Vaddiraju, S., Xu, J., Gleason, K. K. (2010). Chemical Vapor Deposition of Conformal, Functional, and Responsive Polymer Films. *Advanced Materials*, 22 (18), 1993-2027.
- Allen, B. M. (2014). Finite Element Analysis Modeling of Chemical Vapor Deposition of Silicon Carbide. The Degree of Master of Science Thesis, Department of the Air Force Air University, Ohio, USA.
- Asatekin, A., A., Barr, M. C., Baxamusa, S. H., Lau, K. K. S., Tenhaeff, W. E., Xu, J., Gleason, K. K. (2010). Designing polymer surfaces via vapor deposition. *Materials Today*, 13(5): 26-33.
- Baxamusa, S. H., Montero, L., Dubach, J. M., Clark, H. A., Borros, S., Gleason, K. K. (2008). Protection of sensors for biological applications by photoinitiated chemical vapor deposition of hydrogel thin films. *Biomacromolecules*, 9, 2857.
- Bird, R.B., Stewart, W. E., Lightfoot, E. N. (2007). *Transport Phenomena*. Revised Second Edition. WILEY
- Brcka, J. (2009). Model of a filament assisted CVD reactor. Paper presented at COMSOL Conference, Boston, MA.
- Chan, K., Gleason, K. K. (2006). A Mechanistic Study of Initiated Chemical Vapor Deposition of Polymers: Analyses of Deposition Rate and Molecular Weight. *Macromolecules*, 39(11): 3890-3894.
- Coclite, A. M., Howden, R. M., Borelli, D. C., Petruczok, C. D., Yang, R., Yagüe, J. L., Ugur, A., Chen, N., Lee, S., Jo, W. J., Liu, A., Wang, X., Gleason, K. K. (2013). 25th Anniversary Article: CVD Polymers: A New Paradigm for Surface Modification and Device Fabrication. *Advanced Materials*, 25 (38), 5392-5423.
- Cruden, B. A., Gleason, K. K., Sawin, H. H. (2002). Relationship of CF<sub>2</sub> concentration to deposition rates in the pyrolytic chemical vapor deposition process. *Journal of Vacuum Science & Technology B: Microelectronics and Nanometer Structures Processing, Measurement, and Phenomena*, 20 (2): 690-695.
- Curtiss, C. F., Bird, R. B. (1999). Multicomponent Diffusion. *Industrial and Engineering Chemistry Research*, 38 (7), 2515-2522.
- Dorschner, D. (2010). Multicomponent Free Radical Polymerization Model Refinements and Extensions with Depropagation. The Degree of Master of Science Thesis, University of Waterloo, Waterloo, Ontario, Canada.

- Gupta, M., Gleason, K. K. (2006). Initiated Chemical Vapor Deposition of Poly(1H,1H,2H,2H-perfluorodecyl Acrylate) Thin Films. *Langmuir*, 22 (24), 10047-10052.
- Im, S. G., Gleason, K. K. (2011). Solvent-free modification of surfaces with polymers: The case for initiated and oxidative chemical vapor deposition (CVD). *AIChE Journal*, 57(2): 276-285.
- Janakiraman, S., Farrell, S. L., Hsieh, C. Y., Smolin, Y. Y., Soroush, M., Lau, K. K. S. (2015). Kinetic analysis of the initiated chemical vapor deposition of poly(vinylpyrrolidone) and poly(4-vinylpyridine). *Thin Solid Films*, 595, Part B: 244-250.
- Kleijn, C. R., Werner, C. (1993). *Modeling of Chemical Vapor Deposition of Tungsten Films*. Springer Basel AG.
- Lau, K. K. S., Gleason, K. K. (2006a). Initiated Chemical Vapor Deposition (iCVD) of Poly(alkyl acrylates): An Experimental Study. *Macromolecules* 39 (10), 3688-3694.
- Lau, K. K. S., Gleason, K. K. (2006b). Initiated Chemical Vapor Deposition (iCVD) of Poly(alkyl acrylates): A Kinetic Model. *Macromolecules*, 39 (10), 3695-3703.
- Li, Z., Liu, X., Zhang, M., Zhai, M. (2015). Simulation study on the influence of distribution of temperature, gas flow rate and gas component on SiC nanowires grew in self-designed CVD reaction chamber. *Computational Materials Science*, 96 (Part A): 63-68.
- Nakamura, T., Busfield, W. K., Jenkins, I. D., Rizzardo, E., Thang, S. H., Suyama, S. (1996). Initiation Mechanisms for Radical Polymerization of Methyl Methacrylate with tert-Butyl Peroxypivalate. *Journal of the American Chemical Society*. 118(44): 10824-10828.
- Odian, G. (2004). In *Principles of Polymerization*. 4th ed.; John Wiley and Sons: Hoboken, NJ, pp 198-349.
- Olivas-Martinez, M., Perez-Tello, M., Cabanillas-Lopez, R., Contreras-Lopez, O., Soto-Herrera, G., Castillon-Barraza, F. (2007). A computational model for the hot-filament chemical vapour deposition process to produce diamond films. *Modelling and Simulation in Materials Science and Engineering*, 15 (3), 237.
- O'Shaughnessy, W. S., Gao, M., Gleason, K. K. (2006). Initiated Chemical Vapor Deposition of Trivinyltrimethylcyclotrisiloxane for Biomaterial Coatings. *Langmuir*. 22(16): 7021-7026.
- Ozaydin-Ince, G., Gleason, K. K. (2009). Transition between kinetic and mass transfer regimes in the initiated chemical vapor deposition from ethylene glycol diacrylate. *Journal of Vacuum Science & Technology A: Vacuum, Surfaces, and Films*, 27 (5), 1135-1143.

- Ozaydin-Ince, G., Coclite, A.M., Gleason, K.K. (2012). CVD of polymeric thin films: applications in sensors, biotechnology, microelectronics/organic electronics, microfluidics, MEMS, composites and membranes. *Reports on Progress in Physics*, 75 (1), 016501.
- Sreenivasan, R., Gleason, K. K. (2009). Overview of Strategies for the CVD of Organic Films and Functional Polymer Layers. *Chemical Vapor Deposition*, 15(4-6): 77-90.
- Tenhaeff, W. E., Gleason, K. K. (2008). Initiated and Oxidative Chemical Vapor Deposition of Polymeric Thin Films: iCVD and oCVD, *Advanced Functional Materials*, 18 (7), 979-992.
- Uzuafa, F., Lin, S., Gabitto J., Shuckla K. (1999). Modeling and Simulation of Photo-CVD Reactors. *Industrial & Engineering Chemistry Research*, 38 (12), 4579-4584.
- Vanka, S. P., Luo, G., Glumac, N. G. (2004). Parametric effects on thin film growth and uniformity in an atmospheric pressure impinging jet CVD reactor. *Journal of Crystal Growth*, 267(1): 22-34.
- Veneroni, A., Omarini, F., Moscatelli, D., Masi, M., Leone, S., Mauceri, M., Pistone, G., Abbondanza, G. (2005). Modeling of epitaxial silicon carbide deposition. *Journal of Crystal Growth*, 275(1): e295-e300.
- Web1, <https://www.comsol.com/multiphysics/diffusion-coefficient>, Understanding the Diffusion Coefficient. Retrieved: 15.11.2017.
- Xu, J., Gleason, K. K. (2011). Conformal Polymeric Thin Films by Low-Temperature Rapid Initiated Chemical Vapor Deposition (iCVD) Using tert-Butyl Peroxybenzoate as an Initiator. *ACS Applied Materials and Interfaces*, 3 (7): 2410-2416.
- Yagüe, J. L., Coclite, A. M., Petruczuk, C., Gleason, K. K. (2013). Chemical Vapor Deposition for Solvent-Free Polymerization at Surfaces. *Macromolecular Chemistry and Physics*, 214 (3), 302-312.

# APPENDIX A

## MODEL DETAILS

This part involves a brief report of model, which is obtained from computational program, for nBA polymerization with TAPO initiator.

### 1. PARAMETERS

Name	Expression	Value	Description
MW_monomer	128[g/mol]	0.128 kg/mol	molecular weight of BA monomer
MW_initiator	174.28[g/mol]	0.17428 kg/mol	molecular weight of TAPO initiator
MW_radical	29.06[g/mol]	0.02906 kg/mol	molecular weight of radical
MW_argon	39.948[g/mol]	0.039948 kg/mol	molecular weight of Ar carrier gas
MW_product	116.16[g/mol]	0.11616 kg/mol	molecular weight of product
F_monomer	2.5[cm <sup>3</sup> /min]	4.1667E-8 m <sup>3</sup> /s	monomer flow rate
F_initiator	0.58[cm <sup>3</sup> /min]	9.6667E-9 m <sup>3</sup> /s	initiator flow rate
F_argon	0.62[cm <sup>3</sup> /min]	1.0333E-8 m <sup>3</sup> /s	inert gas flow rate
P_total	1[Torr]	133.32 Pa	total pressure
P_sat	4.85[Torr]	646.61 Pa	saturation pressure
rho_monomer	0.901[g/cm <sup>3</sup> ]	901 kg/m <sup>3</sup>	monomer density
rho_polymer	1.08[g/cm <sup>3</sup> ]	1080 kg/m <sup>3</sup>	polymer density
ki	4990[L/(mol*s)]	4.99 m <sup>3</sup> /(s·mol)	rate coefficient of initiation
kp	15540[L/(mol*s)]	15.54 m <sup>3</sup> /(s·mol)	rate coefficient of propagation
kt	0.98*10 <sup>6</sup> [L/(mol*s)]	980 m <sup>3</sup> /(s·mol)	rate coefficient of termination
kt_x	6.89*10 <sup>7</sup> [L/(mol*s)]	68900 m <sup>3</sup> /(s·mol)	rate coefficient of primary radical termination
kt_xx	7.41*10 <sup>8</sup> [L/(mol*s)]	7.41E5 m <sup>3</sup> /(s·mol)	rate coefficient of primary radical recombination
bet_constant	2.536	2.536	BET constant
h_ml	1.31775*10 <sup>-7</sup> [cm]	1.3178E-9 m	monolayer thickness
T_heater	533.15[K]	533.15 K	Filament temperature
T_inlet	353.15[K]	353.15 K	Inlet temperature
T_surface	296.15[K]	296.15 K	Surface temperature
T_wall	313.15[K]	313.15 K	Wall temperature

### 2. COMPONENT 1

#### 2.1. DEFINITIONS

##### Variables 1

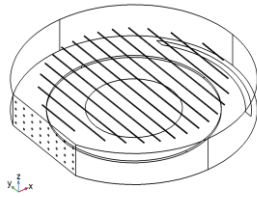
Name	Expression	Unit
F_total	F_monomer + F_initiator + F_argon	m <sup>3</sup> /s
P_monomer	tcs.x_w_monomer*P_total	Pa
P_initiator	tcs.x_w_initiator*P_total	Pa
P_radical	tcs.x_w_radical*P_total	Pa
P_argon	tcs.x_w_argon*P_total	Pa

Name	Expression	Unit
P_product	tcs.x_w_product*P_total	Pa

## Variables 2

Name	Expression	Unit
c_monomer	$(\rho_{\text{monomer}}/\text{MW}_{\text{monomer}}) \cdot \beta_{\text{c}} \cdot \text{constant} \cdot (P_{\text{monomer}}/P_{\text{sat}})$	mol/m <sup>3</sup>
Rp	$k_p \cdot c_{\text{monomer}} \cdot c_{\text{Mactive}}$	mol/(m <sup>3</sup> ·s)
Ri	$k_i \cdot c_{\text{monomer}} \cdot c_{\text{radical}}$	mol/(m <sup>3</sup> ·s)
DR	$R_p \cdot h_{\text{ml}} \cdot \text{MW}_{\text{monomer}} / (\rho_{\text{polymer}})$	m/s
R_initiation	$k_i \cdot c_{\text{monomer}} \cdot c_{\text{radical}}$	mol/(m <sup>3</sup> ·s)
R_primary_radical_termination	$k_{t_x} \cdot c_{\text{Mactive}} \cdot c_{\text{radical}}$	mol/(m <sup>3</sup> ·s)
R_primary_radical_recombination	$2 \cdot k_{t_{xx}} \cdot (c_{\text{radical}})^2$	mol/(m <sup>3</sup> ·s)
R_termination	$2 \cdot k_t \cdot (c_{\text{Mactive}})^2$	mol/(m <sup>3</sup> ·s)

## 2.2. GEOMETRY

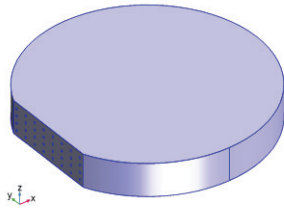


Length unit	cm
Angular unit	deg

## GEOMETRY STATISTICS

Description	Value
Space dimension	3
Number of domains	15
Number of boundaries	130
Number of edges	333
Number of vertices	268

### 2.3. LAMINAR FLOW



#### SELECTION

Geometric entity level	Domain
Selection	Domain 1

#### EQUATIONS

$$\rho(\mathbf{u} \cdot \nabla)\mathbf{u} =$$

$$\nabla \cdot \left[ -p\mathbf{I} + \mu(\nabla\mathbf{u} + (\nabla\mathbf{u})^T) - \frac{2}{3}\mu(\nabla \cdot \mathbf{u})\mathbf{I} \right] + \mathbf{F}$$

$$\nabla \cdot (\rho\mathbf{u}) = 0$$

#### FEATURES

Fluid Properties 1
Initial Values 1
Wall 1
Inlet 1
Outlet 1

#### 2.3.1. FLUID PROPERTIES

##### EQUATIONS

$$\rho(\mathbf{u} \cdot \nabla)\mathbf{u} =$$

$$\nabla \cdot \left[ -p\mathbf{I} + \mu(\nabla\mathbf{u} + (\nabla\mathbf{u})^T) - \frac{2}{3}\mu(\nabla \cdot \mathbf{u})\mathbf{I} \right] + \mathbf{F}$$

$$\nabla \cdot (\rho\mathbf{u}) = 0$$

#### 2.3.2. WALL

$$\mathbf{u} = \mathbf{0}$$

#### 2.3.3. INLET 1

$$-\int_{\partial\Omega} \frac{\rho}{\rho_{st}} (\mathbf{u} \cdot \mathbf{n}) d_{bc} dS = Q_{sv}, \quad \rho_{st} = \frac{P_{st} M_n}{RT_{st}}$$

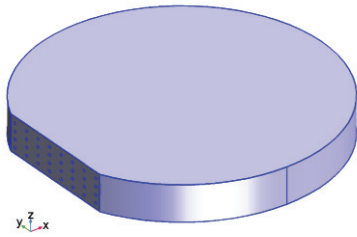


### 2.3.4. OUTLET

$$\mathbf{n} \cdot \left[ -p\mathbf{I} + \mu(\nabla\mathbf{u} + (\nabla\mathbf{u})^T) - \frac{2}{3}\mu(\nabla \cdot \mathbf{u})\mathbf{I} \right] \mathbf{n} = -\hat{p}_0$$

$$\hat{p}_0 \leq p_0, \quad \mathbf{u} \cdot \mathbf{t} = 0$$

### 2.4. HEAT TRANSFER IN FLUIDS



#### EQUATIONS

$$\rho c_p \mathbf{u} \cdot \nabla T + \nabla \cdot \mathbf{q} = Q + Q_p + Q_{vd}$$

$$\mathbf{q} = -k \nabla T$$

#### FEATURES

Heat Transfer in Fluids 1
Initial Values 1
Thermal Insulation 1

Temperature 2
Temperature 3
Temperature 4
Temperature 5
Outflow

#### 2.4.1. HEAT TRANSFER IN FLUIDS

$$\rho c_p \mathbf{u} \cdot \nabla T + \nabla \cdot \mathbf{q} = Q + Q_p + Q_{vd}$$

$$\mathbf{q} = -k \nabla T$$

$$\rho = \frac{M_n \rho_A}{RT}$$

$$c_p = \frac{\gamma R_g}{M_n(\gamma - 1)}$$

#### 2.4.2. THERMAL INSULATION

$$-\mathbf{n} \cdot \mathbf{q} = 0$$

### 2.4.3. TEMPERATURE 2

$$T = T_0$$

### 2.4.4. TEMPERATURE 3

$$T = T_0$$

### 2.4.5. TEMPERATURE 4

$$T = T_0$$

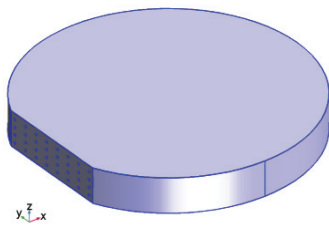
### 2.4.6. TEMPERATURE 5

$$T = T_0$$

### 2.4.6. OUTFLOW

$$-\mathbf{n} \cdot \mathbf{q} = 0$$

## 2.5. TRANSPORT OF CONCENTRATED SPECIES



### EQUATIONS

$$\nabla \cdot \mathbf{j}_i + \rho(\mathbf{u} \cdot \nabla)\omega_i = R_i$$

$$\mathbf{N}_i = \mathbf{j}_i + \rho\mathbf{u}\omega_i$$

### FEATURES

Transport Properties 1
Initial Values 1
No Flux 1
Inflow 1
Outflow 1
Flux 1

### 2.5.1. TRANSPORT PROPERTIES

$$\nabla \cdot \mathbf{j}_i + \rho(\mathbf{u} \cdot \nabla)\omega_i = R_i$$

$$\mathbf{N}_i = \mathbf{j}_i + \rho\mathbf{u}\omega_i$$

$$\mathbf{j}_i = - \left( \rho \omega_i \sum_k \bar{D}_{ik} \mathbf{d}_k + D_i^T \frac{\nabla T}{T} \right)$$

$$\mathbf{d}_k = \nabla x_k + \frac{1}{\rho_A} [(x_k - w_k) \nabla \rho_A]$$

$$x_k = \frac{\omega_k M_n}{M_k}, \quad M_n = \left( \sum_i \frac{\omega_i}{M_i} \right)^{-1}$$

### 2.5.2. INITIAL VALUES

$$\omega_{0j} = \frac{x_{0j} M_i}{M_n}$$

### 2.5.3. NO FLUX

$$-\mathbf{n} \cdot \mathbf{N}_i = 0$$

### 2.5.3. INFLOW

$$\omega_i = \omega_{0j}, \quad \omega_{0j} = \frac{x_{0j} M_i}{M_n}$$

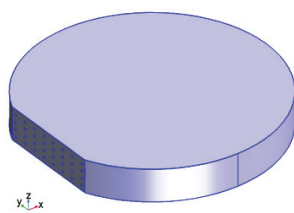
### 2.5.4. OUTFLOW

$$-\mathbf{n} \cdot \rho \omega_i \sum_k \bar{D}_{ik} \mathbf{d}_k = 0$$

### 2.5.5. FLUX

$$-\mathbf{n} \cdot \mathbf{N}_i = N_{0j}$$

### 2.5.6. CHEMISTRY

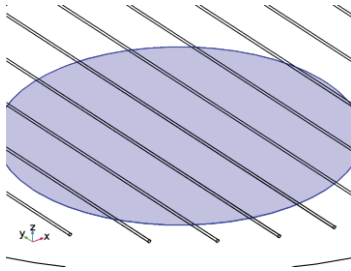


$$R_i = \sum_j R_{ij}$$

### FEATURES

1: I=>2R+P
Species: I
Species: R
Species: P

## 2.7. BOUNDARY ODES AND DAES



Distributed ODE 1
Initial Values 1

### DISTRIBUTED ODE

#### EQUATIONS

$$e_a \frac{\partial^2 \mathbf{u}}{\partial t^2} + d_a \frac{\partial \mathbf{u}}{\partial t} = f$$

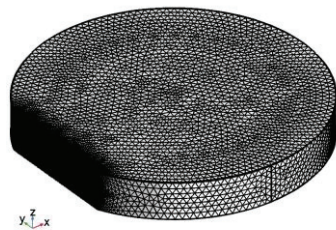
$$\mathbf{u} = [c_{M,active}, c_{r,adical}]^T$$

## 2.8. MULTIPHYSICS

### 2.8.1. TEMPERATURE COUPLING

### 2.8.2. FLOW COUPLING

## 2.9. MESHES



## COMPUTATIONAL INFORMATION

Computation time	3 h 57 min 26 s
CPU	Intel(R) Core(TM) i7-6700HQ CPU @ 2.60GHz, 4 cores
Operating system	Windows 10

## 2.10. PARAMETRIC SWEEP

Parameter name	Parameter value list	Parameter unit
F_monomer	2.5,2,1.5,1,0.75,0.5	cm <sup>3</sup> /min
F_initiator	0.58,0.47,0.35,0.23,0.18,0.12	cm <sup>3</sup> /min
F_argon	0.62,1.23,1.85,2.47,2.77,3.08	cm <sup>3</sup> /min

## STUDY SETTINGS

Description	Value
Sweep type	Specified combinations
Parameter name	{F_monomer, F_initiator, F_argon}
Parameter value list	{2.5, 2, 1.5, 1, 0.75, 0.5, 0.58, 0.47, 0.35, 0.23, 0.18, 0.12, 0.62, 1.23, 1.85, 2.47, 2.77, 3.08}
Unit	{cm <sup>3</sup> /min, cm <sup>3</sup> /min, cm <sup>3</sup> /min}

## 2.11. STATIONARY

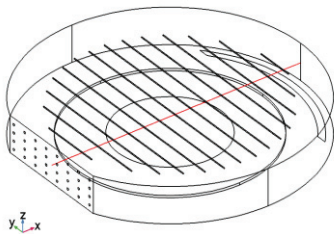
### PHYSICS AND VARIABLES SELECTION

Physics interface	Discretization
Laminar Flow (spf)	physics
Heat Transfer in Fluids (ht)	physics
Transport of Concentrated Species (tcs)	physics
Chemistry (chem)	physics
Boundary ODEs and DAEs (bode)	physics

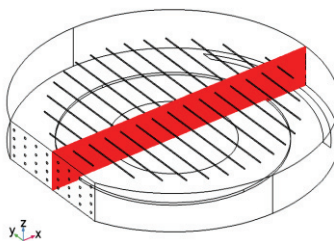
## RESULTS

### STUDY 1/ SOLUTION 1

#### Cutline 3D 1



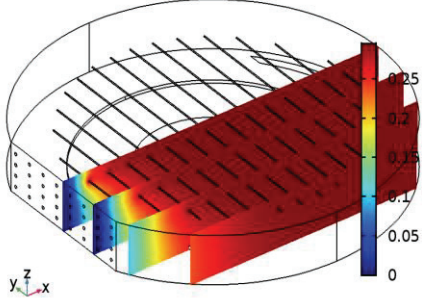
#### Cut Plane 1



## PLOT GROUPS

### 3D Plot

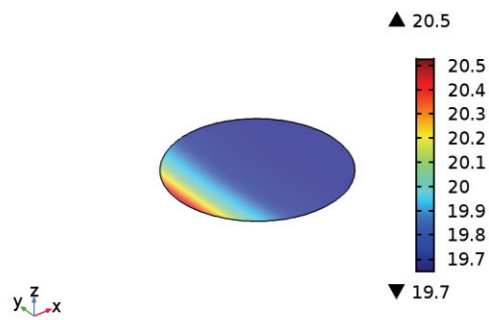
$F_{\text{monomer}}=1.5 \text{ cm}^3/\text{min}$ ,  $F_{\text{initiator}}=0.35 \text{ cm}^3/\text{min}$ ,  $F_{\text{argon}}=1.85$   
Slice: Mole fraction (1)



$F_{\text{monomer}}=1.5 \text{ cm}^3/\text{min}$ ,  $F_{\text{initiator}}=0.35 \text{ cm}^3/\text{min}$ ,  $F_{\text{argon}}=1.85 \text{ cm}^3/\text{min}$  Slice: Mole fraction

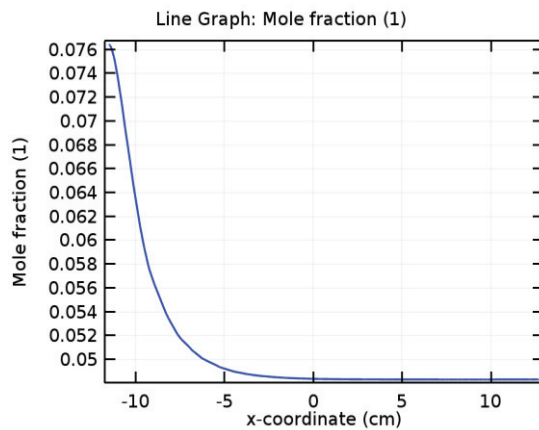
### Surface Plot

$F_{\text{monomer}}=2.5 \text{ cm}^3/\text{min}$ ,  $F_{\text{initiator}}=0.58 \text{ cm}^3/\text{min}$ ,  $F_{\text{argon}}=0.62$   
Surface: DR (nm/min)



$F_{\text{monomer}}=2.5 \text{ cm}^3/\text{min}$ ,  $F_{\text{initiator}}=0.58 \text{ cm}^3/\text{min}$ ,  $F_{\text{argon}}=0.62 \text{ cm}^3/\text{min}$  Surface: DR (nm/min)

### 1D Plot



# SELCAN ATEŞ

## RESEARCH EXPERIENCE

**Doctor of Philosophy** in Chemical Engineering, İzmir Institute of Technology, İzmir/Turkey, 2017.

**Master of Science** in Chemical Engineering, İzmir Institute of Technology, İzmir/Turkey, 2011.

**Bachelor of Science** in Chemical Engineering, Atatürk University, Erzurum/ Turkey, 2008.

**PhD Dissertation** 2012-2017  
“Experimental and Computational Investigation of Transport Phenomena in Initiated Chemical Vapor Deposition (iCVD) Process”. Supervisor: Assist. Prof. Dr. Özgenç Ebil

**MSc Dissertation** 2009-2011  
“Oxidation of Ethanol and Carbon Monoxide on Alumina-Supported Metal/Metal Oxide Xerogel Catalysts”. Supervisor: Prof. Dr. Erol Şeker

## CONFERENCE PRESENTATIONS

**S. Ates, O. Ebil.** “Modeling of Initiated Chemical Vapor Deposition (iCVD) for Polymeric Thin-Film Fabrication”, Material Research Society (MRS), November 30-December 5, Boston, USA, 2014.

**S. Ates, S. Alsoy Altinkaya, E. Şeker.** “Antibacterial efficacy of silver on Titania xerogels made using a sol-gel method against Escherichia coli and Staphylococcus aureus bacteria”, Nanomemwater Conference, October 8-10, İzmir, 2013.